University of Minho
School of Engineering

School of Engineering

Mariana Araújo Pires

# Study of Phase Separated Food-inks by Oral Tribology Assessment and Molecular Dynamics Modelling

Master Dissertation in Biomedical Engineering

Thesis performed under the supervision of,

Professor Doctor Cristiano Simões de Abreu and

Doctor Sara Maria Marques Oliveira

January of 2020

# DIREITOS DE AUTOR E CONDIÇÕES DE UTILIZAÇÃO DO TRABALHO POR TERCEIROS

# Acknowledgments

First of all I would like to thank my supervisor, Prof. Dr. Cristiano Abreu, for all the help and availability. Thank you for always being willing to help me and answer my questions.

To Dr. Sara Oliveira for all the support and opportunities you gave me. Thank you for all the shared knowledge and for being permanently available.

To Sérgio Carvalho for the technical assistance and encouraging words.

To all the Food Processing Group, from INL, thank you for the opportunity of working alongside you, I learned a lot with all of you, it was a remarkable experience.

All this work would not be possible without my perfect family, the family that saw me grow and the family that I chose.

To my parents, I am very grateful for all the unconditional support you have given me, thank you for never letting me give up at the most disheartening moments. You are the most important people in my life.

To Raquel, Kiko and Miguel, you are the greatest examples of the hard work that pays off, thank you for the strength and trust you place in me, you are the best friends/siblings our parents could have given me.

To Didi, my life mate, one of the smartest people I know, I'm very blessed to have had you to share this great journey with.

Finally, and not least, to the friends of my heart: Nocas, Lipa, Sarinha, Ricardo, Rui e Carina. I don't know anyone as happy, dedicated, hardworking and available to each other as you. I carry you for the rest of your life, this was not possible without you.

# STATEMENT OF INTEGRITY

I hereby declare having conducted this academic work with integrity. I confirm that I have not used plagiarism or any form of undue use of information or falsification of results along the process leading to its elaboration. I further declare that I have fully acknowledged the Code of Ethical Conduct of the University of Minho.

# Estudos de Tribologia Oral e Dinâmica Molecular de Pastas Edíveis com Separação de Fase

**Resumo:** A incorporação de produtos lacticínios nos alimentos é amplamente utilizada em todo o mundo como fonte de nutrientes importantes na alimentação humana. Esta tem acompanhado ao longo dos anos o desenvolvimento tecnológico, à medida que o seu consumo aumenta. As proteínas do leite e as proteínas do soro de leite, em particular, exibem altos valores nutricionais, contribuindo para muitas propriedades funcionais das formulações alimentares. Apesar destas propriedades, com a incorporação destas proteínas surge uma preocupação relacionada com a perceção de adstringência, a qual se caracteriza, *grosso modo*, por uma sensação oral desagradável (de boca seca), embora constitua um fenómeno mais complexo.

Neste estudo, pretendemos destacar os mecanismos responsáveis pelo fenómeno de adstringência oral, conduzindo testes tribológicos e posteriormente validação experimental por simulações computacionais atomísticas (dinâmica molecular), para caracterizar o comportamento de atrito e lubrificação de 3 sistemas: alimento (proteínas do soro do leite), polissacarídeos (goma de gelana) e mucinas.

Os testes tribológicos foram realizados numa configuração bola sobre disco, lubrificados por saliva artificial e mucinas, submetidos a uma força de 1N. Para planear as amostras a serem testadas, quantificar a influência das variáveis estudadas e correlação entre estas, no comportamento ao atrito e lubrificação, foi utilizado uma ferramenta estatística de desenho experimental (DOE). Todos os ensaios foram acompanhados com técnicas de microscopia (SEM, AFM, CLSM).

Relativamente à simulação, recorreu-se à dinâmica molecular (MD) com o código LAMMPS e à visualização das trajetórias atómicas com o OVITO. A simulação por MD foi utilizada para modelar o tribo-sistema estudado, de modo a observar os mecanismos subjacentes à escala nanométrica em condições equivalentes aos ensaios macroscópicos.

No que concerne aos resultados obtidos, as amostras de WPI, GG e mucinas produzidas revelaram que é possível estabelecer uma correlação entre as várias ferramentas utilizadas. A informação obtida por estas ferramentas, fornece dados relevantes para aferir quanto à adstringência e, subsequentemente, possibilita que futuramente seja possível a produção de alimentos (produtos lácteos) que possam reduzir essa sensação na boca.

**Palavras-chave: Adstringência, atrito, desenho experimental, dinâmica molecular, perceção**

# Study of Phase Separated Food-inks by Oral Tribology Assessment and Molecular Dynamics Modelling

**Abstract:** The incorporation of dairy products in food is widely used worldwide as a source of important nutrients in human food. It has kept pace with technological development over the years as its consumption increases. Milk proteins and whey proteins, in particular, exhibit high nutritional values, contributing to many functional properties of food formulations. Despite these properties, with the incorporation of these proteins there is a concern related to the perception of astringency, which is roughly characterized by an unpleasant oral sensation (dry mouth), although it is a more complex phenomenon.

In this study, we intend to highlight the mechanisms responsible for the oral astringency phenomenon, conducting tribological tests and later experimental validation by atomistic computational simulations (molecular dynamics), to characterize the friction and lubrication behaviour of 3 systems: food (whey proteins), polysaccharides (gellan gum) and mucins.

Tribological tests were performed in a ball-on-disk configuration, lubricated by artificial saliva and mucins, subjected to a 1N force. To plan the samples to be tested, to quantify the influence of the studied variables and their correlation on friction and lubrication behaviour, a statistical design tool (DOE) was used. All assays were followed with microscopy techniques (SEM, AFM, CLSM).

For simulation, we used molecular dynamics (MD) with the code LAMMPS and the visualization of atomic trajectories with OVITO. MD simulation was used to model the system tribe studied, in order to observe the mechanisms underlying the nanometer scale under conditions equivalent to macroscopic assays.

Regarding the results obtained, samples of WPI, GG and mucins produced revealed that it is possible to establish a correlation between the various techniques used. The information obtained from these tools provides relevant data for astringency measurement and subsequently enables the production of foods (dairy products) that may reduce this mouthfeel, in the future.

**Keywords: Astringency, friction, molecular dynamics, perception, statistical design tool**

# Table of contents

# List of Figures

# List of Tables

# List of Symbols

β-LG - Beta-Lactoglobulin

α-LA - Alpha Lactalbumin

$F_x$ - Foad Force on the x axis

$F_y$ - Load Force on the y axis

$F_z$ - Load Force on the z axis

μ - Friction coefficient

$\vec{F}_i$- Load force on a particle i

$\vec{v}_i$- Velocity applied to a particle i

$\vec{r}_i$- Position of a particle i

$\vec{a}_i$ - Acceleration of a particle

∇U- Total potential energy

$E_{Total}$ - Total energy of the interactions

$E_{bonded}$ - Energy of bonded interactions

$E_{non-bonded}$ - Energy of non-bonded interactions

$\delta t$ – Time-step

$K_\theta$ - Parameter that describes the stiffness of the angle θ

$\theta_0$ - Parameter that describes the equilibrium geometry of the angle θ

$K_b$ - Parameter that describes the stiffness of the bond

$b_0$ - Parameter that describes the equilibrium length of the bond

χ - Value of the dihedral

$K_\chi$ - Energetic parameter that determines barrier heights

$\varepsilon_{ij}$- Prefactor based on the types of the two interacting atoms i and j

$q_{ij}$ - Parameter that describe the effective charges on atoms i and j

$w_f$ - Final angular velocity

ε - Potential strength

σ - Zero-crossing distance

# List of Abreviations

AFM - Atomic Force Microscopy

AM - Additive Manufacturing

AMBER - Assisted Model Building with Energy Refinement

ANOVA – Analysis of Variance

ASTM - American Society for Testing and Materials

BSM - Bovine Submaxillary Mucin

CAD - Computer Aided Design

CCD - Central Composite Design

CETR - Center for Tribology

CHARMM – Chemistry At Harvard Macromolecular Mechanics

CMC – Carboxymethyl Cellulose

COMPASS – Condensed-Phase Optimized Molecular Potential For Atomistic Simulation Studies

DEO - Design of Experiments

EPFL - Extended Depth of Field

FAO - The Food and Agriculture Organization of the United Nations

GAFF - General Amber Force Field

GG - Gellan Gum

GPL - GNU Public License

GROMACS - Groningen Machine for Chemical Simulations

HPLC-DAD - High-Performance Liquid Chromatography with Diode-Array Detection

ISO - International Organization for Standardisation

ITC - Isothermal Tritation calorimetry

LAMMPS- Large-scale Atomic/Molecular Massively Parallel Simulator

LJ(12,6) - Lennard-Jones

MD - Molecular Dynamic

MEMS/NEMS - Micro- and Nano-Electromechanical Systems

MG - Mucin-glycoproteins

MIT - Massachusetts Institute of Technology

MMFF - Merck Molecular Force Field

MPI – Message Passing Interface

NAMD - Nanoscale Molecular Dynamics

NMR - Nuclear Magnetic Resonance

NVE - Fixed number of atoms, N, fixed volume, V, fixed energy, E

OPLS-AA – Optimized Potential for Liquid Simulation-All Atom

PBS – Phosphate-Buffered Saline

PDB - Protein Data Bank

PDMS – Polydimethylsiloxane

PRPs - Proline-rich proteins

Ra - Roughness average

RF - Radio Frequency

RMS - Root Mean Square

SBIR - Small Business Innovation Research

SEM - Scanning Electron Microscopy

SP - Salivary Proteins

STD-NMR - Nuclear Magnetic Resonance Spectroscopy

STI - Soybean Trypsin Inhibitor

TI - Time-intensity

UFF – Universal Force Field

UMT - Universal Tribometer

WCA - Water Contact Angle

WPI - Whey Protein Isolate

# CHAPTER I: Introduction

## 1.1 Motivation

The perception of food texture, especially at the oral cavity level, is a determining factor of food quality (Szczesniak, 2002).

Astringency is an important quality characteristic which strongly influences consumers' acceptability for many polyphenol-rich foods. This phenomenon has aroused huge scientific interest, considering its potential application in both food nutriology and pharmacology. The incorporation of whey proteins in foods tends to increase the perception of astringency in the oral cavity, degrading the sensation of food quality (Jianshe Chen, 2014). However to learn more about the reasons for astringency and the interaction between it and these proteins, it is necessary converge the amount of information given by diverse studies. Unfortunately, there is not a lot of research out there.

The motivation of this thesis is relate with the need to build substantial and relevant hypotheses about the phenomena (mainly molecular) and thus guide the astringency mechanism understanding in the right direction.

## 1.2 Contextualization and aim of the thesis

The understanding of how a person chooses to eat, his food choices, consumption and psychological processes involved in implementing one's intentions, are crucial to promote more mindful eating regulation. Food choices are determined by a range of factors that contribute to aversion or pleasure and guide to final intake (Teixeira, Patrick, & Mata, 2011).

Accordingly, features of food, trigger some sensory attributes that play a key role in food selections and intake. Aspects such as psychological and social factors, including beliefs, habits, values and past experiences, age, gender, individual's personality, different levels of knowledge and experience with regard to food related issues may induce different types of behaviours relative to food and will influence sensorial perception of that food (Lamy, Rodrigues, Louro, & Capela, 2017).

Based on literature, astringency demonstrates to be one issue that influences this food choices and intake constituting the main subject of this study. The aim of this thesis will be to

explore the mechanisms involved in this phenomenon, encompassing strategies that can circumvent astringency perception, including several disciplines capable of describing, evaluating and quantifying, taking into account that a few models have already been proposed for explaining of this phenomenon (Escribano-Bailon et al., 2015; Rodrigues et al., 2015).

We intend to highlight the mechanisms responsible for the oral astringency phenomenon, conducting atomistic computational simulations and subsequent experimental validation by oral tribological tests to characterize the friction behaviour related with sensory properties of food preparations. The final goal of this work intended to create food-inks for 3D Printing, both rich in microstructured proteins (e.g whey protein) with potential to reduce astringency.

In short, the key message is that eating is a dynamic process and, therefore, our sensation and perception of food texture is not instantaneous but is the result of an integrative process that includes the understanding of how oral perception (e.g. astringency perception), relates with food acceptance and choices.

## 1.3 Structure

The present dissertation is divided in six main chapters that will now be allowed. In Chapter I, the work of the dissertation is briefly presented, namely the motivation of the study, the contextualization of it and the aim and scope, is also presented the structure of dissertation and the references used in it.

After, in Chapter II will be held the literature review where the sensory perception of the texture of the food will be presented, as well as the astringency and the respective techniques that quantify it. This chapter will also present the 3D food printing, as well as the references used.

Posteriorly, in Chapter III the materials and methods will be described, following the chapter IV the article made developed during this dissertation will be introduced, where the presentation of the results obtained will be carried out and their respective discussion will be made, associating them with the analysed literature.

In turn, Chapter V will present the conclusions obtained through the realization of the experimental work of this research.

Lastly, in Chapter VI is presented complementary and detailed information of some parts of the present work.

## 1.4 References


Chen, J. (2014). Food oral processing: Some important underpinning principles of eating and sensory perception. *Food Structure*.

Escribano-Bailon, M. T., de Freitas, V., Ferrer-Gallego, R., Bras, N. F., Gomes, P., Quijada-Morin, N., & Rivas-Gonzalo, J. C. (2015). Characterization of Sensory Properties of Flavanols–A Molecular Dynamic Approach. *Chemical Senses*, *40*(6), 381–390. https://doi.org/10.1093/chemse/bjv018

Lamy, E., Rodrigues, L., Louro, T., & Capela, F. (2017). The role of saliva in food sensory perception : relevant knowledge to design healthy foods.

Rodrigues, R., Vicente, A. A., Ramos, O. L., Martins, A., Fuciños, C., Malcata, F. X., ... Teixeira, J. A. (2015). Design of whey protein nanostructures for incorporation and release of nutraceutical compounds in food. *Critical Reviews in Food Science and Nutrition*, *57*(7), 1377–1393. https://doi.org/10.1080/10408398.2014.993749

Teixeira, P. J., Patrick, H., & Mata, J. (2011). Why we eat what we eat: The role of autonomous motivation in eating behaviour regulation. *Nutrition Bulletin*, *36*(1), 102–107. https://doi.org/10.1111/j.1467-3010.2010.01876.x

Szczesniak, A. S. (2002). Texture is a sensory property, 13, 215–225.

# CHAPTER II: Literature Review

## 2.1 Overview: Sensory Perception of Food Texture

The human being interacts consciously with the universe that surrounds him through his five senses. The development of the sensory mechanisms is based on a slow evolutionary process, which involves its connection with the brain that is able to process and store the information. A better perception of the surrounding environment was a driving force for the progressive process, and an analogy could be made with the effort from man to create means to help him understand, overcome and improve his own sensory limitations.

Perception defined in the Oxford dictionary, is "*the awareness through the senses interpreted in the light of experience*". Perception can be consciousness that arises through a single sense or through a combination of many. The perception of food is the result of food characteristics which interact with the processes in the mouth and then are interpreted by the brain (Engelen & Bilt, 2007). Sensory responses to the taste, aroma, colour, and texture of foods help determine food preferences and eating habits.

"Food quality" englobes a range of criteria from sensory characteristics, such as visual appearance, nutritional benefit (the real benefit and the one perceived by the consumer), and consumer beliefs about the acceptability of production processes (Bhuiyan, Torab, & Rahim, 2015) in addition to the previously mentioned.

Consumer expects that food products provide pleasant sensory perceptions, healthy nutrition and at a reasonable cost. It is challenging to provide food products meeting the consumer demands for foods with functional or healthier compositions (reduction of salt, fat and calories and increase of bioactive compounds). For example, while a reduction of fat in cheddar cheese is desirable, consumers are not willing to sacrifice texture and flavour alterations in consequence of the fat reduction process. Texture is one of the most important factors determining food choice, especially for semi-solid or solid foods (Pascua, Koç, & Foegeding, 2013).

The implication of sensory texture on food quality was first recognised by Matz et al. (1962). A half century later, oral texture sensation has been attracting the interest of both academic and industrial researchers because of its critical role in influencing oral processing behaviour and ultimately consumer preference of a product.

According to the ISO (1994) standard, texture involves all the mechanical, geometrical and surface attributes of a product perceptible by means of mechanical, tactile and, where appropriate, visual and auditory cell receptors. Food texture monitoring is a crucial aspect in the food industry from raw materials and manufacturing process, and the quality of the finished product control, passing the development of new products or re-formulations.

In the late 1950s, a group of forward thinking technical research managers at the General Foods Corporation in the USA took a look more closely to this texture characteristic. Alina Szcesniak and her colleagues began to develop a scheme that described the characteristics of texture from a sensory point of view, naming it the General Foods Texture Profile. This Profile provide means to report the attributes of texture, classifying them into three groups (Szczesniak, 1963):

(a) Mechanical characteristics, which are perceived by the forces on teeth, tongue, and roof of the mouth when the food is stressed;

(b) Geometrical characteristics, which are related to size, shape, and the arrangements of particles in food;

(c) Other characteristics such as moisture and fat content of food and mouthfeel attributes

The definition of texture, given by Szczesniak (2002), points out that this characteristic can only be perceived and described by humans and some animals, being the sensory and functional manifestation of the multiscale structure of the food (molecular, microscopic or macroscopic), mechanical and surface properties of foods detected through the sense of vision, hearing, touch and kinesthesis.

Szcesniak adds that the so-called texture testing instruments can detect and quantify only certain physical aspects in terms of sensory perception, being the most important ones: touch and pressure(Szczesniak, 2002). Meanwhile diverse terminologies have been used to describe the textural characteristics and it is hence important that objective, standard methods be adopted for measuring the textural properties of food (J. Chen & Rosenthal, 2015).

Texture is connected to the two major variables considered in food oral processing and sensory perception. They're the individuality of human beings and the properties of food materials. The first is related with the oral physiology (because of age, gender, health status, etc.), while the second is based on the effects of food rheology and texture (such as hardness, softness, geometric dimensions). Both play an important role in influencing how a food is orally processed and sensorially perceived (Jianshe Chen, 2009; Pascua et al., 2013). Numerous factors, both product and individualy related, that can direct and indirectly influence the perceived texture (Figure 1).

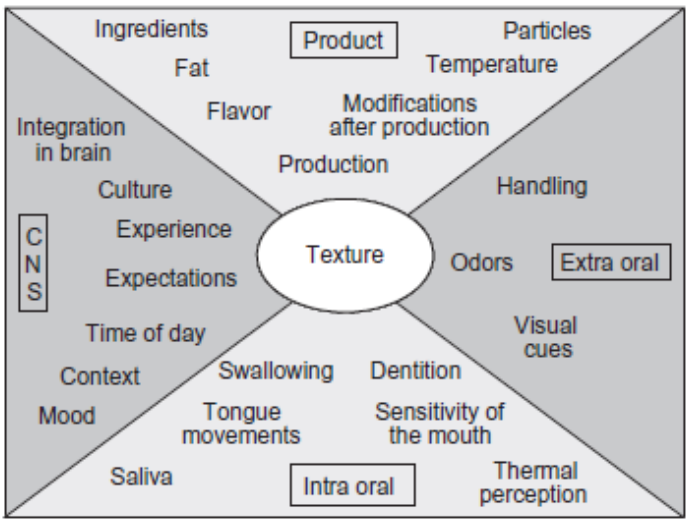


**Chapter II - Figure 1 -** Diagram of factors influencing food texture.

**Source:** (Engelen & Bilt, 2007)

From the oral perspective, food texture has been recently defined as the sensation resulting from the process of ingestion, mastication and swallowing of the food, which is influenced by the physical properties of the food being masticated (Kupirovič, Elmadfa, & Juillerat, 2017; Prakash, Dan, Tan, & Chen, 2013).

During the oral processing, the solid foods are subjected to a continuous particle size reduction via various oral actions (e.g., biting, chewing, tongue slapping, compression) ending up to submillimetre size before being swallowed (Figure 2). Another very important aspect of eating is the continuous evolving of other food properties, both in its length-scale and in physical properties. This length-scale reduction increase the contact area between the oral surfaces throughout the eating process, which certainly will have implications on the perceived sensation and bolus formation.

Therefore, the evaluation of food should considered this highly dynamic process. Although it is now agreed that the texture and mouthfeel are major determinants of consumer acceptance and preference for foods and beverages, there is limited understanding of which textural attributes are desirable, and whether preferences for textural and mouthfeel characteristics are innate or learned. (Jean-xavier Guinard & Mazzucchelli, 1996).

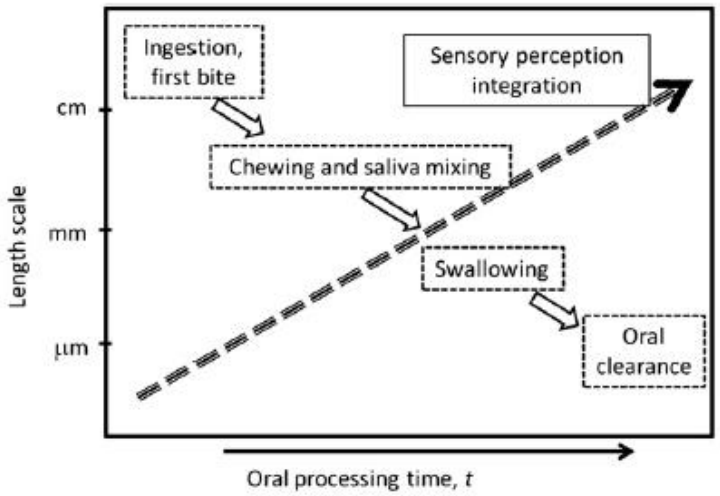


**Chapter II - Figure 2 -** Length scale of food particles and sensory features throughout eating process.

**Source:**(Jean-Xavier Guinard & Mazzucchelli, 1996)

## 2.2 Astringency

### 2.2.1 Definition

Astringency is commonly referred to the dry mouthfeel, although it is a very complex sensation whose definition has yet different and not consensual explanations. To understand this concept, its necessary to comprehend that astringency has gone through many studies and hypotheses over the years and any complex phenomenon like this has not only one definition.

Astringency originates from the Latin root *ad stringere*, meaning "to bind". In the earlier years, Bate-Smith (1954) first suggested that it was a feeling not a taste, and since then the postulated tactile nature of astringency has been accepted as a paradigm. On the other hand, from the perceptual view of Lawless and Corrigan (1996), astringency is a more physical event, referring to the tightening and drawing sensations felt in the buccal musculature, and to the sensations of drying and roughness when there is contact and movement in the mouth. This general concept view has been perpetuating, and actually later Peleg (1998) described that "*Astringency is a complex phenomenon: it elicits a range of sensations, different types of compounds evoke it, and several mechanisms have been suggested to explain it".*

Later, the American Society for Testing and Materials (ASTM) defined astringency as the *"the complex of sensations due to shrinking, drawing or puckering of the epithelium as a result of*

*exposure to substances such as alums or tannins"* (ASTM, 2004).

Overall astringency is discussed in the context of taste and sensations as it is an oral feeling usually caused by food. Given the recent trend towards fortifying consumables with ingredients with the propensity to be astringent and there is a major need to minimise their dryness, roughing, and puckering feelings. Therefore, understanding the development of astringency is of major interest for investigation (Bajec, Pickering, Bajec, & Pickering, 2008).

### 2.2.2 Influence of Astringency on Oral Perception

Astringency was once considered a basic taste modality in ancient Indian culture. But since then, the astringency was understood as a tactile sensation due to the mechanical effect of decreased salivary lubrication, as mentioned above (Jiang, Gong, & Matsunami, 2014). In fact, Bate-Smith (1954), opposed to the explanation of astringency as a distinct taste quality (such as sweet, sour, salty, bitter, and umami), reporting it as an event induced by tannin interaction and/or precipitation of salivary PRPs (Proline-rich proteins), in the oral cavity. Joslyn and Goldstein (1964), who advocated this theory at the time, promoted the tactile theory of astringency, stating that the "*precipitation of tissue proteins is accompanied by shrinkage of tissue due to water loss and a decrease in permeability of this tissue to water and solutes*". Besides this affirmation, the theory of astringency as a tactile sensation is based on characteristic differences between astringency and the five accepted gustatory sensations (sweetness, sourness, saltiness, bitterness, and umami). Years later, Lee and Lawless (1991) hypothesized that astringent and bitterness sensation could be confused since both can be induced by related compounds. Moreover, the nature of the response curves of bitterness of caffeine and quinine on a time-intensity procedure and the average time-intensity curve for astringency in white wine, are similar and both perceptions develop comparatively slowly and possess lingering aftertastes (Figure 3). This study showed that the time-courses of "dry", "rough", and astringent sensations are well matched, and the time-courses of bitterness, differ subtly from astringency when elicited by compounds commonly accepted as astringent. On top of that, the perception of astringency needs some time to fully develop (about 15 seconds) and may extend for far longer (about 5 minutes) (Guinard, Pangborn, & J. Lewis, 1986).

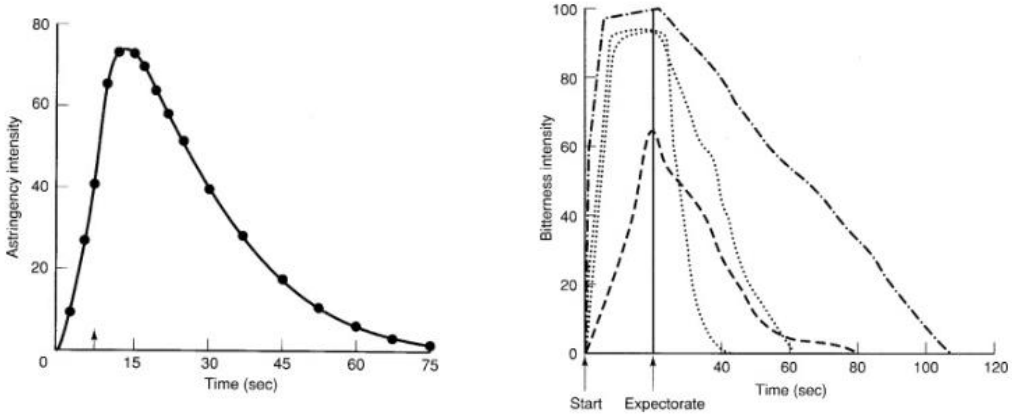


**Chapter II - Figure 3 -** Representative graphs comparing astringency and bitterness intensities.

**Source:** (R. S. Jackson, 2016)

Green (1993) suggested that this result implies that pucker, sourness and bitterness are not essential to the sensation of astringency, being highly recommend that future studies of astringency address, and account for the possibility of multiple sub-qualities.

Despite of being primarily perceived as a disagreeable oral sensation, especially when intense, astringency is under certain circumstances a desirable feature. For instance, it adds flavours to red wines and extends the finish; characteristic described as "smooth" (Jiang et al., 2014) .

Laaksonen (2011) detailed study on the relations of food sensory attributes (Figure 4), reported that several attributes are always simultaneouly perceived. Astringent compounds may themselves have other sensory characteristics or they may enhance or suppress other sensory properties. For example, astringent phenolic compounds are often linked to bitterness, although not all of them have bitter properties. The same happens to astringency of divalent salts that may be accompanied by metallic and bitter sensations; or sugars (sweetness) and fats (fattiness, creaminess) that are used to mask astringency; and even astringency of organic acids that can be directly linked to the perception of sourness as it increases with decreasing pH.

Repeated interaction, tasting and drinking with the perception of astringency are dependent on stimuli, which affect astringency, as pointed out by Kershaw and Running (2019), who maintained that the effects felt in sensory tests, i.e. when more than one of the sensory properties are felt, underpins consumers' indecisive attitude toward the sense of astringency and test compounds containing astringent compounds. If, on the one hand, some individuals who are more sensitive to different sensations may more clearly observe the differences between astringent

properties, in many cases the taste for astringent foods may need to be learned by repeated exposure.

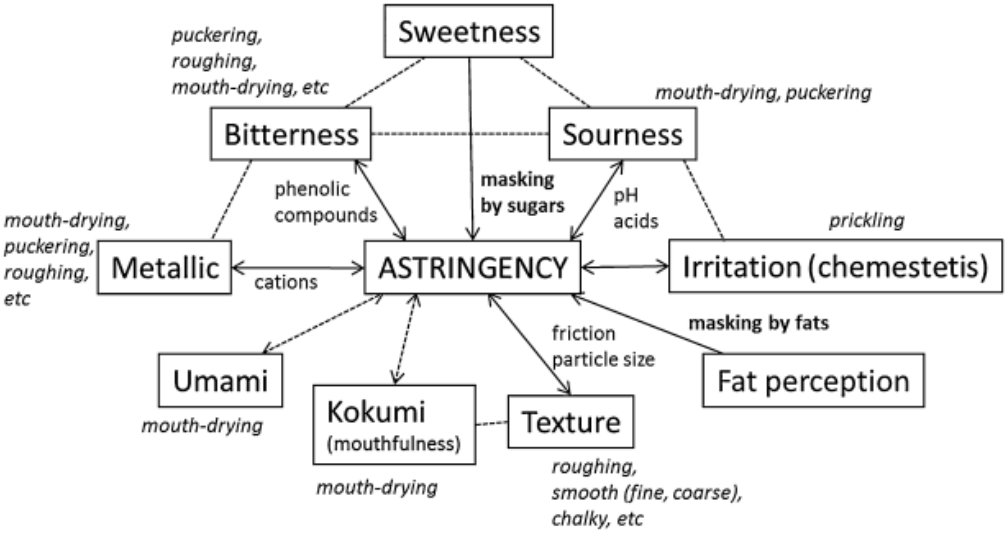


**Chapter II - Figure 4 -** Summary of the interactions between astringency and other oral sensory attributes. Some of the key factors are described next to the arrows and some sub-qualities are mentioned alongside the corresponding attributes.

**Source**: (LAAKSONEN, 2011)

Nowadays, astringency is not considered one of the five basic taste modalities. Those taste modalities are sensed by taste buds on the tongue, which relay sensory information to the brain through taste nerves, the chorda tympani and the glossopharyngeal nerve. However it was unclear whether astringents only trigger mechano-sensation, chemo-sensation, taste-sensation or a combination of both. (Jiang et al., 2014)

Many genetic factors influencing the perceptions of taste properties, such as variations in perceiving bitter taste or variations in saliva, may also affect perception of astringency. Moreover, Fleming et al. (2016) reported that the astringent stimuli come from various classes of chemical compounds, not being limited to tannins. He also pointed out that they are likely to differ on their relative astringent sub-qualities, side tastes, and on the physical and chemical mechanisms originating those sensations. Therefore, additional work should be done exploring both the quantitative and qualitative characterization of various types of astringent compounds and how these may contribute to the complexities of this integrated perception. Some *in vitro* methods to quantify astringency excluding the individual factors mechanisms have already been developed and will be discussed in the following sections.

Furthermore, confusion identifying astringency and its sub-qualities, especially among naive participants, presents additional challenges: similar ratings for sourness, astringency, puckering and bitterness (common astringency descriptors), by untrained assessors suggest possible confusion identifying and differentiating astringent sub-qualities and side-tastes.

- Compounds causing astringency: A sensory challenge

The astringent stimuli is many times associated with polyphenolic compounds, such as those found in red wine, tea, chocolate, and a variety of fruits and nuts ( Bajec, & Pickering, 2008). This sensory experience can also be brought about by a diverse range of foods and beverages. Numerous and potent health-promoting benefits of some astringent compounds (polyphenols) are reported. However, ingestion of polyphenol-rich foods and beverages is associated with a tactile dryness and roughness and constriction perceived throughout the oral cavity (Valentova & Panovska, 2003b). The most known polyphenols are tannins, which have been defined as having molecular weights between 500 and 3000 Da, that elicit astringency (smaller tannins compounds, including 5-0-caffeoylquinic acid, and flavan-3-ol, monomers, dimers and trimers can also provoke this phenomenon) (He, Tian, Luo, Qi, & Chen, 2015).

In fact, the astringency and bitterness of many nutrients containing vegetables and fruits is often cited as the reason consumers reject plant products for such health benefits. In addition to polyphenols, several other classes of compounds may cause oral astringency, including organic and inorganic acids (such as malic or hydrochloric acid), dehydrating agents (e.g. ethanol), multivalent salts (such as potassium ammonium sulphate) and proteins. These compounds exhibit a high isoelectric point and amine functionalized polymers, which carry positive charges at said physiological pH, causing a sensation on admission to the mouth (Biegler, Delius, Käsdorf, Hofmann, & Lieleg, 2016). In the case of fruits, astringency is mainly due to the fact that they are not sufficiently ripe. In the case of red wine, one of the most consumed beverages in the world, a balanced level of astringency in order to make it a desirable product is required. By wine writers, astringency adds flavours to red wines and extends the finish. Indeed, the renowned winemaker Emile Peynaud states that the harmony, balance and elegance of astringency are signs of great red wines (Brandão, 2018; Jiang et al., 2014).

## 2.2.3 Mechanisms responsible for Astringency

When Rosseti et al (2008) suggested that *"astringency is not a simple lubrication driven tactile percept, and that it may arise from a mechanosensation or chemosensation caused by the interaction of astringent compounds with components within the oral mucosa, including the oral tissue itself, the membrane-bound proteins and epithelial cells, as well as mechanoreceptors within the tongue and oral tissues"*, they lifted the veil that elucidates the variety of mechanisms that may be involved in astringency. Actually, this sensation is a very complex process mediated by physical, physiological and psychological factors.

The most studied mechanism related with astringency development is the interaction between salivary proteins and astringent compounds. Several works have shown good correlations between the perceived astringency and the interaction of the astringent with the proteins. This interaction can lead to precipitation of those salivary proteins, thus importantly affecting astringency in different ways. Different mechanisms can be involved in the phenol-protein interaction, which in turn may be affected by the kind of bonds implicated in the interaction. Thus, the cross-links established between phenols and proteins could involve mainly two kinds of bonds, hydrophobic interactions and hydrogen bonds (Ignacio García-Estévez, Alba María Ramos-Pineda, 2018).

How astringent molecules alter the physical properties of the salivary film and pellicle over time also seems to be important. The salivary film plays a major role in lubricating the oral cavity, and this can be significantly affected by the consumption of food and drinks (Jianshe Chen & Stokes, 2012). The salivary film is a layer of saliva coating all surfaces in the mouth, which can change on terms of its rheological and tribological properties. Indeed, Gibbins and Carpenter (2013) proposed which mechanisms of astringency occur simultaneously in the oral cavity:

i) Alterations in salivary film and pellicle;

ii) Changes in rheological and lubricating properties of the salivary film;

iii) The activation of transient protein channel receptor;

Rosseti et al (2009), proposed that the interaction of tannins causes a disruption of the lubricating salivary film which covers all oral surfaces causing friction in the oral cavity, leading to exposure of the oral mucosa allowing tannin protein aggregates to interact directly with oral tissue possibly through receptors. It is also possible that the free tannins alone interact directly with the mucosa/receptors after disruption of the pellicle by tannin–protein aggregates. These authors concluded, from their tribology experiments, that 3 catechin solutions, added to a saliva-lubricated

PDMS tribological contact, affects the variation of the friction coefficient with time, but that friction may not be the primary mechanism for the perception of astringency. Both compounds studied were perceived to be similarly astringent, but had different responses to the loss of salivary lubrication. From these statements was revealed that astringency mechanisms caused by such stimuli, combined by many complex sensations recognised by the neurological system, being a joint work of different physical alterations and perception signals happening in the mouth.

Clearly astringency is a complex sensation and it is likely that multiple mechanisms are occurring simultaneously as discussed in the previous sections. Figure 5 summarizes the hypothetical and basic mechanisms involved: protein precipitation, breakage of salivary pellicle, decrease on salivary lubrication, mechanical perception sensed by receptors (mechano and chemoreceptors) and shrinkage of tissues, mainly changes in oral epithelium. Further studies on the salivary pellicle, about the continuity and properties of the film are still needed, in order to validate this holistic point of view of the sensorial astringency (Rene A De Wijk & Prinz, 2006; Lee, Ismail, & Vickers, 2012).

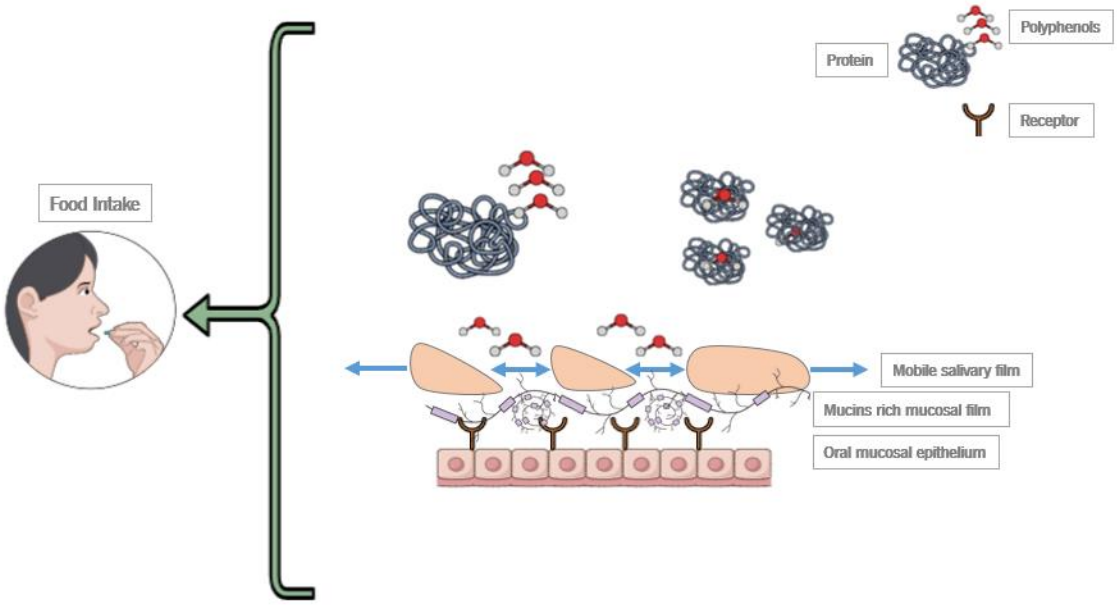


**Chapter II - Figure 5 -** Possible mechanisms of astringency occurring simultaneously in the oral cavity: aggregation of salivary proteins creating grittiness, salivary film disruption, reduced salivary lubrication and possible exposure of receptors.

**Source:** Adapted from (Gibbins & Carpenter, 2013)

The innumerable point of views always highlighted the interaction between tannins and some specific salivary proteins. It is generally accepted that in tannin-rich foods, astringency is directly correlated with the capacity of tannins to interact with salivary proteins, resulting in the formation of protein-tannin aggregates in the mouth (Bajec, 2010).

A proposed model by Charlton et al. (2002) demonstrated that such mechanism was responsible for astringency and showed a polyphenol-protein interaction preceding the binding of the complex to the epithelial proteins in 3 steps. In step 1, binding of multiple polyphenols to several sites on the protein results in the previously randomly coiled protein to coil around the polyphenol, thereby becoming more compact. In step 2, the polyphenol portions of the protein-phenol complex crosslink, forming polyphenol bridges and protein dimers. In the final step, the dimers aggregate, forming large complexes that precipitate. This salivary protein complexation by tannins in mouth could induce:

- a)salivary protein precipitation, reducing lubrication and increasing friction between the surface of the oral cavity, thereby stimulating mechanoreceptors
- b) the shrinkage of tissues due to the loss of water
- c) changes in oral epithelium and its constriction, causing it to feel rough

When it comes to the molecular phenomenon of astringency, this topic has becoming more popular, mainly on studying the interaction of different proteins present in saliva with polyphenols (Freitas & Mateus, 2012). However, food intake englobes several steps, comprising mechanical & chemical actions, interactions between food and receptors, signal transfer to the brain, cognition and feedback, until actually sensory perception (Boehm, Yakubov, Stokes, & Baier, 2019).

Since Yamamoto et al.(1984) pioneering study described the electrophysiological responses of rat chorda tympani and glossopharyngeal nerves to tannic acid (an astringent), that chemoreceptors of the taste and somatosensory systems were consider equipped with specialized receptors to detect a wide range of stimuli and sensations. Further along, Schobel et al.(2014) work sheds light and deepens on the neural correlate and cellular basis of astringency perception (Schöbel et al., 2014; Yamamoto, Yuyama, Kato, & Kawamura, 1985). According to the recent research of Canon et al. (2018), the molecular mechanisms by which tannins generate the astringency sensation remain unclear. It was suggested that it can result from the activation of either trigeminal chemoreceptors or trigeminal mechanoreceptors. These mechanoreceptors are both superficial slow adapting and rapidly adapting receptor units, which may be more likely to respond to the astringency mechanism than any gustatory receptors because of friction from

reduced lubrication (Prakash et al., 2013). With regard to the involvement of chemoreceptors, it has been speculated that astringency is not purely, if at all, mediated by mechanoreceptors but might involve chemosensory detection mechanisms.

### 2.2.4 Regulatory Factors

Astringency may be affected by a number of factors such as: saliva composition, oral pH, temperature, surface properties of oral cavity, and composition in the oral fluid (e.g. viscosity) (Table I).

**Chapter II - Table I -** Direct and indirect studies related with regulatory factors of astringency.

| Regulatory factors | Description | References |
|---|---|---|
| pH | - Sensory analyses and instrumental analyses at whey protein at pH 3,5 and 7<br>- Determine the effects of protein concentration on astringency and interactions between whey and salivary proteins<br>- Study of astringency in model solutions and wines varying in total acid and total phenols<br>- Study on different physical-chemical features influencing protein-polyphenol interactions.<br>- The effect of acid on the perception of astringency evaluated for sensory protocols in wines and model solutions<br>- Study of interactive effects of temperature, pH, viscosity and quinic acid in astringency of cranberry juice<br>- The effect of viscosity and pH on the astringency of a model beverage containing whey protein isolate.<br>- Astringency and sourness of lactic, acetic and citric acids, each adjusted to pH 3, 5 and 7<br>- Determine if the acidity of whey protein solutions was responsible for their astringency | -(Sano, Egashira, Kinekawa, & Kitabatake, 2005)<br>-(Kelly et al., 2010)<br>-(Jean - Xavier Guinard, Pangborn, & Lewis, 1986)<br>-(Freitas & Mateus, 2012)<br>-(Kallithraka, Bakker, & Clifford, 1997)<br>-(Peleg & Noble, 1998)<br>-(Beecher, Drake, Luck, & Foegeding, 2008)<br>-(Lawless, Horne, & Giasi, 1996)<br>-(Lee & Vickers, 2008) |
| Temperature | - Study of interactive effects of temperature, pH, viscosity and quinic acid in astringency of cranberry juice | -(Rawel, Meidtner, & Kroll, 2005) |

| | | |
|---|---|---|
| | - Study of the noncovalent binding of selected phenolic compounds, and factors which influenced binding parameters<br>- Changes in fruit constituents and other characteristics at various temperatures<br>- Temperature treatments, by water immersion, on 'Triumph' persimmons to remove astringency<br>- Determine the sensory impact of white wine serving temperature and red wine serving temperature on wine sensory attributes<br>- Persimmon fruits of Turkay variety having high tannin content with an astringent taste were sliced and dipped in water at different temperatures | -(Peleg & Noble, 1998)<br>-(KATO, 1987)<br>-(BEN - ARIE & SONEGO, 1993)<br>-(F. ROSS & WELLER, 2008)<br>-(Akyildiz, Aksay, Benli, Kiroğlu, & Fenercioğlu, 2004) |
| Saliva | - Factors influencing bitterness, astringency, for example variations in salivary flow rates<br>- Mechanisms leading to different responses for the same sensorial stimulus is particularly important to understand food choices: saliva has a relevant role in that taste recognition mechanisms<br>- Study of frictional conditions in the mouth between two mucosal surfaces using stimulated and unstimulated saliva<br>-Sensory assessment of two red wine samples and the salivary proteins in all samples indicating that the concentration of individual proteins in saliva might be more important for astringency than the total protein content<br>- Understanding astringency mechanisms, based on precipitation of salivary proline - rich proteins by polyphenols and/or altered salivary lubrication | -(Lesschaeve & Noble, 2005)<br>-(Lamy et al., 2017)<br>-(Prinz, Wijk, & Huntjens, 2007)<br>-(Kallithraka, Bakker, Clifford, & Vallis, 2001)<br>-(Gibbins & Carpenter, 2013) |
| Viscosity | - Study of interactive effects of temperature, pH, viscosity and quinic acid in astringency of cranberry juice<br>- Study of the effects of viscosity and sweetness on astringency, aqueous solutions of grape seed tannin<br>- Evaluate the effect of viscosity, sucrose and oil on perception of astringency during consumption of soymilk, a sequential sipping time–intensity procedure<br>- The effect of viscosity and pH on the astringency of a model beverage containing whey protein isolate | -(Peleg & Noble, 1998)<br>-(Smith, June, & Noble, 1996)<br>-(Courregelongue, Schlich, & Noble, 1999)<br>-(Beecher et al., 2008) |
| Polysaccharides | - Understand about the sensorial properties of tannins (astringency), and study the influence of polysaccharides, on the interaction between salivary proteins and tannins | -(Brandão, 2018)<br>-(G. Luck et al., 1994) |

| | | |
|---|---|---|
| | - The action of polysaccharides and caseins in the moderation of the astringent response, caused by polyphenols present in foodstuffs and beverages<br>- The role of substrates possessing the ability to disrupt polyphenol-protein complexation on the loss of astringency in ripening fruit<br>- The study consisted in determining the modification of the polysaccharide fraction present in wines and its possible effect on the intensity of astringency perception | -(Ozawa, Lilley, & Haslam, 1987)<br>-(VERGARA, 2014) |

- pH

Astringency of phenolic compounds has been generally shown to increase in the presence of added acid or lowered pH. (Lawless et al., 1996). In fact, the astringency of phenolic compounds generally increases at low pH. One explanation for the effect is the shift to the un-dissociated phenolic species increasing the affinity to bind salivary proteins via hydrogen bonding, as stated by Peleg *et al.* (1998). They also observed that the behaviour depends on the compound, being the opposite for the case of alum. The astringency of alum decreased with the addition of acid, suggesting that the mechanisms of alum and polyphenol astringency are different (Jean - Xavier Guinard et al., 1986).

The acid solutions increases the strength of the interaction between protein and polyphenol, resulting in precipitation of more salivary protein, and thus withdrawing its lubricity in the mouth (Siebert & Chassy, 2004).

Sano *et al.* (2005) studied the astringency of whey protein isolate (WPI) and gelatin by panel testing and test sensors. Sensory comparisons of whey protein, beverages containing WPI at 6% protein at pH 6.8 and 3.4 showed that the beverage at pH 3.4 was more astringent. Researchers proposed that this concentration caused astringency through aggregation and precipitation of protein molecules in the mouth (Sano et al., 2005). Moreover, Kelly et al. (2010) *in vitro* study of the interactions between Beta-Lactoglobulin (BLG) and saliva indicated that astringency of whey proteins is a function of protein concentration and pH. The oral mixture pH will further depend on the amounts and buffering capacities of saliva on the initial pH of the protein beverage. They suggest that, the model should adequately describe protein-based astringency and take into account: pH, concentration, buffering capacity, and pH-related aggregation and how that alters physiological processes occurring in the mouth.

- **Temperature**

Oral temperature after consumption of hot or cold food rapidly returns to normal due to richly vascularised mouth. The influence of temperature on measures of taste is complex.

Temperature can affect hydrogen bonds and trigger the formation of hydrophobic bonds and is, therefore, an important parameter in the protein–phenolic interactions. Indeed, polyphenol revealed a stronger binding to proteins at higher temperature according with a model protein systems reported by Ozdal, T., Capanoglu, E., & Altay, F. (2013).

Laaksonen (2011) studied two different cases where the astringency and temperature were related. While astringency of tannic acid or catechin in water did not appear to differ in intensity at 7°C or 18°C, the perceived astringency of cranberry juice decreased with decreasing temperature. Cranberry juice is a complex beverage, and the small, but significant, decrease described were coincident with the decrease in viscosity, a parameter known to affect astringency perception (Peleg & Noble, 1998).

Later, the influence of temperature on the perceived intensity of alum warm versus cold alum, was examined. Astringency from warm alum reached a higher intensity and lasted longer, that may be due to the formation of stronger, more enduring bonds between alum and salivary proteins (Bajec, Martha R. Pickering & DeCourville, 2012).

Similar to other parameters, the effect of temperature seems to be also dependent on the protein and tannins features and compounds.

- **Saliva**

Saliva is the most important component defining the surface chemistry of human mouth. It consists of approximately 98% water and a variety of electrolytes and proteins, such as proline-rich proteins (PRP's), statherin, P-B peptide, cystatins, mucins, histadins and urea, ammonia, uric acid, glucose, cholesterol and fatty acids (Brandão, 2018). PRPs overall comprising 70% of salivary protein composition, provide lubrication and prevent bacterial agglutination in the oral surfaces. Basic PRPs with 6–9 kDa have demonstrated anti-viral activity and a high affinity for binding tannins, that increase the sensation of astringency (Lamy et al., 2017). Mucin-glycoproteins, or mucins, are principally responsible for the viscoelastic properties of all mucosal secretions, including saliva. The submandibular and sublingual glands, along with some of the minor salivary

glands, secrete the two main salivary mucins, MG1 and MG2 (Çelebioğlu, Gudjónsdóttir, Chronakis, & Lee, 2016). The involvement of salivary proteins in the perception of food has been most studied in the context of its effect on the development of astringency. Although the mechanisms involved in astringency development are not fully elucidated, the participation of salivary proteins is well accepted. Salivary PRPs constitute the main family of salivary proteins that are associated with astringency. Salivary proteins are adsorbed onto all solid substrates as well as mucosa membranes exposed to oral environment, and then form the salivary pellicle within seconds (Almeida, Grégio, Machado, Lima, & Azevedo, 2008).

The influence and interaction of saliva and its components is addressed in several studies providing insightful information in perceiving astringency. Beecher et al. (2008) showed that electrostatic interaction between positively charged whey proteins and negatively charged saliva proteins caused astringency. Likewise, Jobstl et al. (2004) assumed that the complexation and precipitation of the astringent compounds with salivary PRPs, which increases friction in the mouth is, closely related with the perception of astringency.

Vardhanabhuti et al. (2011) investigated the perception of astringency in relation to the effect of BLG (whey protein) at pH 3.5 and 7.0, studying the lubrication properties of saliva using a tribological approach. They observed that the addition of non-astringent BLG at pH 7.0 slowly increased the friction of saliva films between tribo-pair surfaces and the addition of BLG at pH 3.5 rapidly increased the friction coefficients of saliva.

Mucins also play a role in astringency. The interactions of salivary mucins and saliva with several food proteins, as well as their functional properties is related to the food oral processing and the perception of sensory attributes. Yakubov et al. (2009) present evidence that mucins have a reduced lubrication effect when mixed with tannins.

- **Viscosity**

Sensory attributes such as creaminess, fattiness, smoothness, stickiness, and astringency are difficult to characterize using viscosity alone. In the case of astringency, it is often related with Bate-Smith's (1954) speculation that this feeling is caused by the increase in friction between the mucosal surfaces. Such increase, results from a reduction in lubrication as salivary proteins are bound by astringent compounds. Possibly the precipitation reduces the lubricative properties of the saliva and the viscosity drops changing the perceived astringency (De Wijk & Prinz, 2006).

The high viscoelasticity and fluid properties of the salivary film can play a large role in its response to consuming food and drink and lead to changes in lubrication (Coles, Zauscher, & Chang, 2010). Studies reported that the astringency intensity and the rate of increase upon repeated sips were decreased by addition of sucrose or by increasing soymilk viscosity with carboxymethyl cellulose (CMC). Addition of oil, which yielded only small increases viscosity, did not reduce astringency significantly (Courregelongue et al., 1999).

More recently, Li, Y et al. (2018) studied the impact of pasteurization method, storage time, and fat content on the bovine milk astringency, rheological and tribological behaviour. They concluded that saliva addition did not impact instrumentally friction and they did not observe a relationship between astringency, viscosity and friction behaviour (Joyner, Li, Lee, & Drake, 2018).

- **Polysaccharides**

Protein-tannin or protein interaction with other astringent can be influenced by the presence of other compounds, namely polysaccharides. There is a strong interest in polysaccharides because their addition to food may modify the perception of flavour and, consequently, determine the acceptance of food products.

Some conceptions talked about the presence of polysaccharides that inhibit the protein-tannin interaction and appeared to explain the phenomenon of fruit ripening (phenomenon related with the decrease of astringency sensation) (Mcrae & Kennedy, 2011). The texture change in fruit, has been explained by the enzymatic degradation of the polysaccharides cell wall (pectin, hemicellulose and cellulose) and by the presence of storage polysaccharides (Wakabayashi, 2000). Indeed, it seems that some polysaccharides have the proper structure to compete with salivary proteins (SP) in complexing with tannins in the mouth and that could be at the origin of the decrease of astringency perception.

Trozynska et al. (2010) determined the modification of the fraction of polysaccharides present in the wines and their possible effect on the intensity of the astringency perception. They observed a reduction in astringency by establishing that the mixtures (mixtures or assemblies are common winemaking processes in the cellar) modify the characteristics of the base wines to improve their organoleptic quality. That allow them to state that the ability of polysaccharides to reduce the astringency was differentiated and depended both on the concentration and the type of the polysaccharides used.

## 2.3 Techniques to Quantify Astringency

The astringency phenomenon has been addressed by several methodologies: direct or indirect measurements and by simulation, and will be further discussed in the following sections. In the study of Vidal et al. (2004), they commented that experiments are required to link processes with sensory perception. They expressed succinctly that *"constructing mouthfeel perception can be a highly complex process. This process depends on the presence of each component by itself but also depends on interactions between components and on the structure of the resulting molecular assemblies".* Currently, there is no technique able to replicate the whole complexity and accurately quantify such kind of sequence of events. Therefore a wide range of different techniques will be needed to cover the behavior of the individual components and its interactions.

### 2.3.1 Direct (Sensory Analysis)

Texture evaluation is often an important step in developing new food products and optimizing processing techniques. Currently, to evaluate the aforementioned attribute, sensory analysis is one of the most useful methods. Sensory analysis uses the human senses vision, smell, touch, taste and hearing to evaluate the characteristics or attributes of a product. In the food industry this technique comprises a variety of sensitive tools to measure this human responses to foods (Drake, 2007).

Sensory science is a relatively young discipline and has been in existence for roughly 60 years. Many attribute the conception of sensory science to the 1940s with the development of consumer or hedonic food acceptance methodologies by the US Army Corps of Engineers (Peryam & Pilgrim, 1957). By that time, Sjiistriim (1954) and Jellinek (1964), were among the first to quantify the sensory features by temporal response. They used Time-intensity (TI) sensory evaluation technique, which is an extension of the classical scaling method providing temporal information about perceived sensations. In this method, the perceived sensations are monitor by judges, from onset through extinction, to quantify the continuous perceptual changes that occur. It is believed that TI methodology is highly underutilized in the evaluation of textural and flavour characteristics, having limited application in the evaluation of persistent flavour and aftertastes relating to food quality. Even so, TI have some applications on the texture features like bitterness, sweetness, sourness, saltiness, astringency, irritation, flavour, and texture. Particularly for

astringency, this technique was firstly used by Guinard *et al.* (1986b) and Robichaud & Noble (1990) that studied tannic acid in wine and astringent compounds.

For sensory analysis, there is also the descriptive sensory models that are classified as the most sophisticated tools in the arsenal of the sensory scientist. They detect and describe the qualitative and quantitative sensory components of a consumer product by trained panels of judges (Heymann & Lawless, 2010). Descriptive sensory analysis is also used to compare product prototypes to understand consumer responses to sensory attributes on products and as a means for sensory mapping and matching with products, constituted as a method of control of quality.

This technique is divided into 3 distinct parts. The selection of a descriptive analysis panel is the first step: through that selection, it is important to motivate and understand how committed each panellist is. Intrinsic to this selection, it is important that inside the panel a series of factors are taken into account, such as: health status, allergies, personality, education, dietary habits, verbal creativity, previous experience, medication, sensitivity and user of products.

The next phase is the training stage that begins with the development of a mutual language which describes the product attributes reasonably and in accordance with what is expected. Accordingly to Piggott & Conaway (1981), a descriptive language should be precisely defined and contain enough terms to include all attributes that you want to have into account, but it shouldn't be very large. This phase allows the training panel to use a common *''frame of reference''* to describe sensory concepts and to achieve if possible, a common scale.

The system adopted during training will depend to a large part, on the approach of the method chosen, the time available and the products under test (complexity and range involved). This final step is the selection of a method of evaluation including several different methods of descriptive analysis, like:

- Flavour Profile Method
- Texture Profile Method
- Quantitative Descriptive Analysis
- Spectrum Method
- Quantitative Flavour Profiling
- Free-choice Profiling (Murray, Delahunty, & Baxter, 2001)

Among those methods it is possible to highlight some, like the Free-choice profiling that was used by Delarue, J., & Sieffermann, J. M. (2004), in combination with comparative evaluation for sensory profiling, to draw up the sensory ID of a set of products. They both selected several

attributes (e.g ‘‘sweet’’ and ‘‘cream’’, ‘‘floral’’, ‘‘apricot peel’’, ‘‘artificial”, ‘‘astringent,...) that were used for the conventional profile flavour attributes of the strawberry yoghurts and apricot ‘‘fromages frais’’, both from the French market. The advantage of this comparing with the evaluation performed by a single expert (e.g. an oenologist or a perfumer), is that descriptive methods aim to provide a description of the product, free of hedonic judgments given by a panel of people. Quantification performed on descriptive attributes identifies clearly the attributes, taking into account that human subjects are not equally sensitive to sensory stimuli nor equally discriminant regarding the attributes.

### 2.3.2 Indirect: Tribology and Biotribology

The concept of tribology was enunciated in 1966, by the Department of Education and Science in the UK (Jost, 1990). Tribology is an interdisciplinary science and technology of interacting surfaces in relative motion and associated subjects and practices. Tribology includes principles of physics, chemistry, solid and fluid mechanisms, heat transfer, materials science, lubricant rheology, reliability and performance. Although being highly interdisciplinary, tribology is widely known for being the friction, wear and lubrication science (Bhushan, 1999).

Since biological systems face tribological challenges, the field of tribology considers the tribological processes also occur after the introduction of an artificial device in the human body or in naturally occurring parts such as the joints, in the blinking of an eye, or a fetus moving in a mother’s womb (Scherge & Gorb, 2001).

For eating and sensory perception, the behaviour of interacting surfaces includes, as well, relative motions that play a critical role in the mouth. Of these interacting surfaces, tongue-palate and tongue-food are probably the two most important surface motions (Bhushan, 1999) (Upadhyay, Brossard, & Chen, 2016). Such actions generate a friction/lubrication sensation between palate and tongue with the food product (or food–saliva mixture) acting as the lubricant. These oral actions are also associated with rheology and tribology (Prakash et al., 2013). Thus arised the concept of Biotribology, that was first used by Dowson and Wright in 1973 describing *‘‘all aspects of tribology related to biological systems’’*. But friction, wear and lubrication of biosystems have been mentioned by many investigators, before the term biotribology was introduce. In 1967, a symposium on lubrication and wear in living and artificial human joints was

organized in London, between the Institution of Mechanical Engineers and the British Orthopaedic Association.

Zhou et al.(2015) with an attempt to be indicative and emphasize the current research in Biotribology, reunited the number of presentations and their topics from 2 conferences, shown in Figure 6. The Joint, Skin and Oral tribology were the topics with the most participations.

| | Number of presentations ICoBT 2011 | Number of presentations ICoBT 2013 |
|---|---|---|
| Joint tribology | 47 | 48 |
| Skin tribology | 26 | 13 |
| Oral tribology | 10 | 11 |
| Tribology of the other human bodies or tissues | 18 | 11 |
| Medical Devices | 4 | 2 |
| Animal Tribology | 0 | 4 |
| Others: review, etc | 10 | 16 |
| **Total number of oral presentations** | **115** | **105** |

**Chapter II - Figure 6 -** Number of oral presentations and different topics in ICoBT conferences in 2011 and 2013.

**Source** : (Zhou & Jin, 2015).

A better understanding of astringency development in the oral cavity may lead to advancements in the comprehension of the mechanisms that can be represented by the tribological characterization. Researches began to focus their studies on relating certain sensory texture perceptions such as smoothness, slipperiness, creaminess, and astringency (Figure 7) with friction coefficient of the product in order to predict and understand food texture and structure (Prakash et al., 2013).

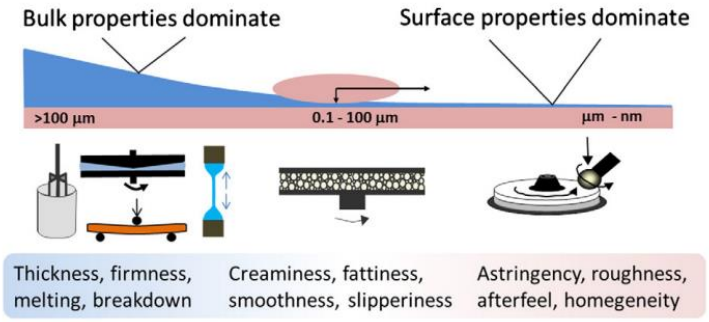


**Chapter II - Figure 7 -** Description of sensory texture perceptions after ingestion of the food and relations with the domains of tribology and rheology.

**Source:** (Stokes, Boehm, & Baier, 2013)

There is still some debate as whether astringency is a simple lubrication-driven tactile percept (physical stimulation) or a combination of physical and perception signals occurring in the mouth. For instance, Rossetti et al. (2009) stated that the measurements and the relationship between astringency and friction are neither sufficient conditions for the astringency perception and that friction measurement is not able, by itself, to predict astringency for all conditions they investigated (Upadhyay et al., 2016). On the other hand, Prakash et al. (2013) claimed that the sensation of astringency is believed to be closely related to the boundary lubrication of the Stribeck curve (Brossard, Cai, Osorio, Bordeu, & Chen, 2016). In agreement with that point-of-view, recently Brossard et al. (2016) quantified astringency using tribology techniques. The group evaluate the mixture of human saliva and typical astringent compounds such as tannins and red wines. In their work a higher friction coefficient corresponded linearly to a more pronounced astringency perception. From those observations, it was evident that synergizing sensory evaluation with oral tribology has great potential and that it can produce more reliable conclusions. Although very limited studies are available on application of oral tribology to astringency perception, the outcomes of their work have shown great potential of the approach, establishing relationships between tribology parameters and the perceived texture and mouthfeel attributes, explained later. Indeed, some authors have explored sensory astringency using tribology tools, taking into account at least two critical factors in the design of a tribometer to mimic oral processing, involving: (1) the control of the sliding and or rotating between the two surfaces and (2) the surface properties of the substrate materials (Goh, Versluis, Appelqvist, & Bialek, 2010; Prakash et al., 2013; Terpstra et al., 2005).

The tribometer is an instrument that measures tribological quantities and includes a cell that can be used to test conditions such as the nature of tribo-pairs surfaces, behaviour and speed of the sliding or rotating support plate, lubrication regimes (boundary, mixed and hydrodynamic) and solvent composition (e.g. saliva) (Upadhyay et al., 2016).

When it comes to instruments used to measure the lubrication properties of food since the advent of tribology, there has not been much progress from the food perspective, due to both the lack of appropriate techniques for food studies and the lack of fundamental understanding of its relevance to food oral sensation. This led to huge efforts among food scientists in seeking appropriate experimental techniques to conduct reliable food tribology and lubrication studies. Therefore, for measuring tribological parameters, either a commercially available tribometer system or a custom-made system is utilised. Types of systems used include plate or pin-on-disk

tribometers or traction measurement systems, and even adaptation of equipments such as tribometers and rheometers coupled with oral performance instruments (Prakash et al., 2013).

### 2.3.2 Oral Tribology: Role on Food Sensory Perception

The recent work of oral tribology point out that it can be an effective tool to analyse lubrication-based textural features, such as the sensation of astringency. Since food oral processing involves transforming solid food to small particle sizes, mixed with saliva, and forming a bolus that is then swallowed and transferred to the stomach, oral tribology believes that astringency is related to the presence of an immobile layer of saliva and food on the tongue and palate surfaces (Brossard et al., 2016).

- **Oral Physiology and Processing**

Oral physiology is the part of physiology that specifically studies the function of the mouth/oral cavity and the related craniofacial structures. In particular, studies of physical, chemical and mechanical factors, which enable the development and maintenance of these structures.

The oral cavity is one of the regions of the body more densely innervated with nerve fibers and receptors and exquisitely sensitive to tactile stimulation. Oral surfaces are formed by the lips, palate, tongue, uvula and teeth and serve roles in taste and tactile sensations during oral processing (Figure 8) (Bourne, 2002). The lips, being highly sensitive, assess the surface roughness and temperature when in contact with food. The teeth are mainly involved in the food breakdown. The interaction between the tongue and food is important for sensory perception of taste and mouthfeel attributes. The capability of the tongue to sense surface and geometrical properties of food and perceiving small differences in size, shape, roughness, and firmness, allows to determining bolus readiness for swallowing (René A. De Wijk, Janssen, & Prinz, 2011). The oral cavity also acts as a protection system against the ingestion of toxic or potentially toxic substances, screened by the sensorial analysis, involving in gustatory, olfactory, tactile, thermal and painful perception (Tambeli, 2014).

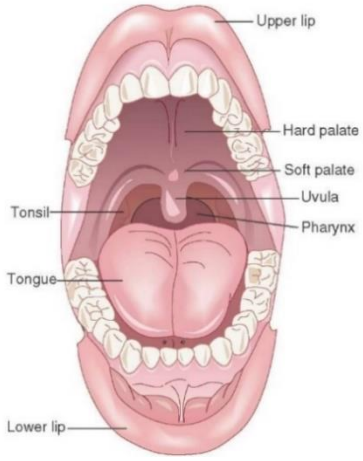


**Chapter II - Figure 8 -** Surfaces of the oral cavity.

**Source**: (Bourne, 2002)

Foster et al. (2011) described sensory perception during oral processing as a dynamic process. Oral physiology, is then the link between food structure (input) and texture perception (output). The oral manipulations range from simply placing the food on the tip of the tongue to a diversity and complexity of movements, and oral compounds, braking down the food and transporting it through the mouth while it is converted in a swallow bolus. Sensations of the food attributes are collected during each step of the mastication process. This process involves four different phases (Pascua et al., 2013): (1) Initial ingestion and oral preparation where the is formed by a series of masticatory cycles and mixture with saliva needed to comminute and soften the food; (2) Transport of the bolus; (3) Expulsion of the bolus from the oral cavity; (4) Impulsion of the bolus through the oesophagus to the stomach.

Through this process, various elements of the oral system work in a unique way so that everything flows smoothly. For example, oral system characteristics such as bite force, chewing performance and salivary flow rate will influence the chewing process. The tongue, as the muscular organ of the mouth, plays an important role in deciding whether food particles are appropriate and moisture to be swallowed, being the bolus constantly monitored for its readiness. Consequently, this developing bolus will influence, for example, the decision to swallow according to the reduction of food particle size, salivation and mixing of food particles.(Malone, Appelqvist, & Norton, 2003; van der Bilt, Engelen, Pereira, van der Glas, & Abbink, 2006).

Food structural elements can control the tribological properties (morphology, size and deformability of food particles) and determine the lubrication behaviour of the food and oral systems (K. Liu, 2016). Oral tribology research is important to address the unique natures of the

oral system to make an impact and improve the quality of food and life itself.

- **Friction**

The key parameter of tribology measurement in oral processing is the friction coefficient (μ), calculated as the ratio between the measured friction force and the normal load (Figure 9) (Berrien, 1999). That is why surface interactions, that generate friction, are of utmost importance and mainly originate from: friction generated between food particles and oral surfaces, friction between tongue and palate and the adherence of food particles and bolus to oral cavity. Friction at the interface of the food with the oral mucosa is also detected by mechanoreceptors in the oral mucosa (Rene A De Wijk & Prinz, 2006).

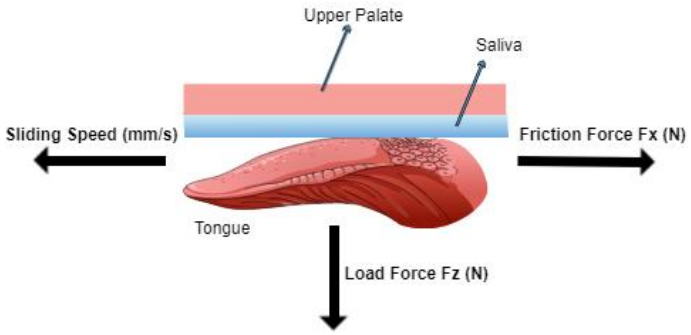


**Chapter II - Figure 9 -** Tribology set-up (forces and surfaces involved) in oral processing.

**Source:** Adapted from (Laguna & Sarkar, 2017)

Different speeds and pressures, due to surface interactions, are used to perceive different food properties. Moreover, friction forces depend on the speed of movement of the food bolus and the tongue, and on the pressure exerted by the tongue on the bolus. Speed and pressure will continuously change during the complex series of oral movements during food processing (Prinz et al., 2007).

Malone et al. (2003) determined friction coefficients at different speeds to assess the slipperiness and estimated that oral speeds during sensory valuations were probably between 10 and 100 mm/s. Malone et al. (2003) refer also that some unpublished results from their laboratory using sensors glued to the surface of the tongue while eating a range of semisolids put the range at 10–30 mm/s. Likewise, Mossaz et al. (2010) mentioned that when a yoghurt is eaten, during swallowing, the tongue contracts to eject the bolus from the oral cavity to the esophagus. This takes place in three steps: i) the product is squeezed between the tongue and the palate at a

constant speed, generally estimated (10 to 30 mm/s); ii) squeezing of the product at a constant force ranging from 0.25 N to 40 N, depending on the nature of the product being consumed, and in particular its viscosity; iii) relaxation phase (Terpstra et al., 2005).

Nevertheless, such measurements may not be, at the moment, where a simple friction coefficient can be used to predict a texture or mouthfeel attribute or to rationally design products. Sometimes, it can be challenging to use a large range of configurations (with different surfaces and geometries), just because they're not well-defined, which makes it difficult to determine underlying mechanisms for observed tribological responses. Moreover, the following important aspects should be noted (Stokes et al., 2013):

- Many sensory mouthfeel/textural attributes have many modalities (e.g., creaminess)
- The surfaces used in tribology do not have the same surface chemistry or topology as real oral surfaces;
- Differences in hydrodynamic conditions exist during tribological measurements and those occurring in mouth;
- Different mechanisms affect the friction in the boundary, mixed and hydrodynamic lubrication regimes;

To move towards tribology as a truly predictive tool, significant developments are required in each of these areas so that a universal approach is obtained.

## • Lubrification

The importance of lubrication in food oral processing and sensory perception has been recognized. In-mouth lubrication is a well-known process responsible for the perception of surface-related mouthfeel attributes such as roughness and astringency**.** Lubrication is a surface property, and its magnitude depends on the surface roughness and geometry of the interacting surfaces as well as the nature of the lubricant (Selway & Stokes, 2013).

The majority of the tribological studies focused on characterizing model food systems to understand the role of individual phases and components in lubrication processes. Lubrication in the mouth was proposed to be dependent on saliva coating the oral surfaces before eating. The salivary film is a viscoelastic gel that protects the oral mucosa from mechanical and chemical damages, such as exposure to microorganism, toxic materials, environmental agressions, dehydration of oral mucosal epithelium and lubrication (Laguna & Sarkar, 2017).

According with tribological principles, three different lubrication regimes may be

experienced depending on the salivary film thickness (separation of tribo-surfaces), which is affected by a combination of fluid and surface properties, load, entrainment speed, etc. (Figure 10). The three regimes, are characterised in a representation of a Stribeck curve, namely boundary, mixed and hydrodynamic regimes, corresponding to three very different friction scenarios.

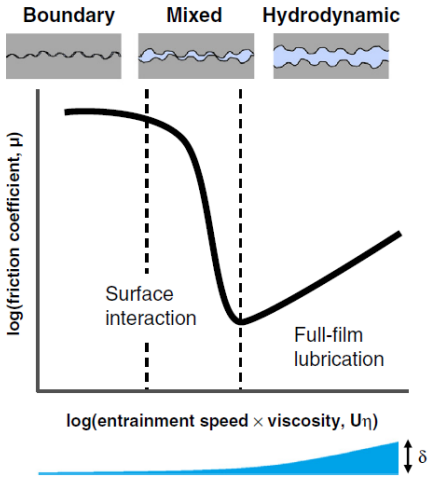


**Chapter II - Figure 10 -** Representation of the typical Stribeck curve and the film thickness in three regimes (boundary, mixed and hydrodynamic).

**Source:** (Selway & Stokes, 2013)

The first regime, occurring at low entrainment speeds, is the boundary regime. This phase is characterized by the presence of an immobile layer on tongue and palate surfaces that does not participate in the hydrodynamic flow of the bulk food (i.e. the point where the two interacting surfaces come into asperity contact and maybe the regime closely related to human perception of astringency, slipperiness). In this regime lubrication properties of the food depend on the ability of the food's constituents to form boundary films (Stokes et al., 2013; Svendsen & Lindh, 2009).

Nguyen et al. (2016) exposed some explanations for the origin of boundary lubrication, measuring lubricating properties of dairy products, such as pasteurized milks and cream cheeses. The first one is related to interactions between surfaces and the fluids involved. The authors explained that there is physio-absorption of polymers onto the surface, modifying the composition of the fluid in the contact zone due to Van der Waals forces, namely the London dispersion term. The second is related with the molecular ordering caused by the presence of solid surfaces that produce immobile, rigid layers and the last one, about the confinement effects which increase the concentration of polymers in the contact zone.

In the hydrodynamic regime, the oral process involved is characterized by the food that entered the contact zone between the two rubbing surfaces due to surface motion. The film thickness and friction generated also depends on velocity, load, lubricant viscosity and relation between pressure and viscosity. As explained by Cassin, Heinrich and Spikes (2001), the purpose of hydrodynamic lubrication is to introduce a thin, low-shear-strength food film between the tongue and palate separating the tongue and palate surfaces, and which is able to sustain the applied load.

Between the boundary and the hydrodynamic regime lies the mixed regime of lubrication. In this regime the food entrainment into the tongue–palate contact zone is sufficient to partly separate the two rubbing surfaces and the contact area is less compared to the boundary regime. However, the lubricant film thickness and the length of the asperities of the test surfaces are of similar sizes, so the contact load is caused by two phenomena: fluid pressure and asperity contact pressure. The coefficient of friction reaches a minimum in this regime, but if there is an increase in roughness contact or decrease in the thickness of the lubricant layer, the coefficient of friction will increase (Prakash et al., 2013).

Boehm et al. (2019) stated that the commonly measured parameter, lubrication, is mainly due to the contribution of rheology (viscosity) of the fluid confined between oral surfaces in relative motion, which depends on many factors. In the context of friction, they claim that to obtain a quantification of the lubrication parameter from tribological systems, the best reference state is the coefficient of friction for unstimulated, resting saliva expectorated and adsorbed, on soft substrates. To describe properly the influence of viscosity on lubrication and friction, the group explored both a low viscosity and high viscosity fluid. They highlight that the fluid can exhibit a low degree of lubrication (high friction), for both high and low viscosity. They point that a high viscosity may prevent surface contact but causes high resistance to motion, and that a low viscosity has little resistance to motion but is unable to prevent contact between surfaces.

Studies on food oral lubrication have been using a variety of elastomer substrates that are either commercially derived (usually with unknown surface chemistry) or house-made using polydimethylsiloxane (PDMS) with relatively well-defined surface properties. PDMS can be easily modified to be hydrophobic, hydrophilic, rough, smooth, etc. (Figure 11). This polymer can be micro-engineered to have specific topology to emulate the tongue surface and it's relatively easy to functionalise. PDMS readily adsorbs macromolecules such as salivary proteins including mucin and saliva itself, etc., making it possible to study adsorption and interactions with food components.

Using animal tongues is currently the only way to effectively study how the specific topology of the tongue surface influences lubrication, however, there is variability associated with the fact of being an animal harvested tissue (De Hoog, Prinz, Huntjens, Dresselhuis, & Aken, 2006).

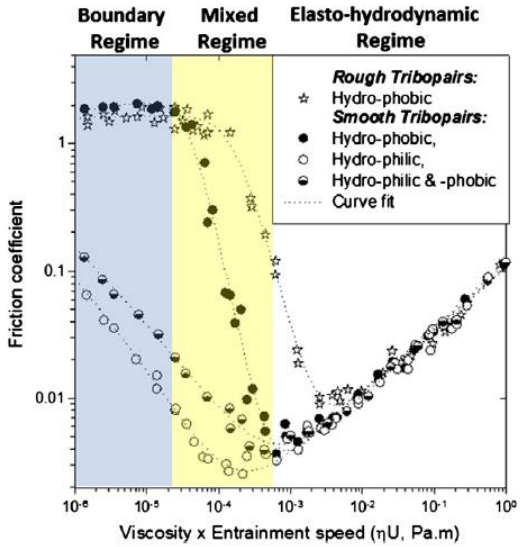


**Chapter II - Figure 11 -** Stribeck curves showing the influence of surface properties using PDMS ball-disk tribopairs using aqueous Newtonian fluids.

**Source:** (Stokes et al., 2013)

### 2.3.3 Simulation: Molecular Dynamics

The mechanism of astringency based on the interaction between tannins and some specific salivary proteins, namely, proline-rich salivary proteins, a type of conformational open proteins (random coils), constitute a valuable approach that could explain the synergistic effect observed and explain at the molecular level the mechanisms underlying that complex sensation (Ferrer-Gallego et al., 2017; Ramos-Pineda et al., 2017).

It is therefore important for the food branch to understand how the proteins behave during processing and how their structural modification leads to changes in their functional properties. Through the years many techniques have been widely used to understand protein structure and the relation to its functionality, such as nuclear magnetic resonance (NMR) and X-ray diffraction. But in order to fully understand the mechanism of the interactions between processing condition and proteins, it is necessary to investigate and understand the influence on properties at molecular or even atomistic level (A. Singh, Vanga, Orsat, & Raghavan, 2018).

The technique of molecular dynamics (MD) simulation studies the atomic and molecular

interactions. These interactions take place within a physical system, and they govern its microscopic and macroscopic behaviour. The technique has been widely used to develop novel drug systems in the field of pharmaceutical sciences (de Azevedo, 2011). However, its application in food process engineering has been rarely used. Molecular dynamics approaches that use food proteins that have been performed use lysozyme, soybean hydrophobic protein, soybean trypsin inhibitor (STI), peanut peptides and Arah6 (peanut protein allergen) ( A. Singh, Orsat, & Raghavan, 2013; A. Singh et al., 2018).

MD simulation is a computational method that usually uses atoms or molecules and serves as a complement to conventional experiments, since tribological experiments do not provide connections between macroscopic tribological properties and the material structure at the molecular level. (Ramos-Pineda et al., 2017). Computer simulations play an important role in understanding the tribological process. With this method it is possible to vary geometry, sliding conditions and interactions between atoms, which allows their effects on friction, lubrication and wear to be explored. It is important to remember that in atomic-level simulations, all information on each atom in a simulation, from exact coordinates in space to individual components of force, velocity, acceleration, etc., must be broken down in order to obtain a configuration similar to what it happens in tribology. Figure 12 is a schematic diagram of a typical configuration for a tribology simulation (Schall, Mikulski, Chateauneuf, Gao, & Harrison, 2007).

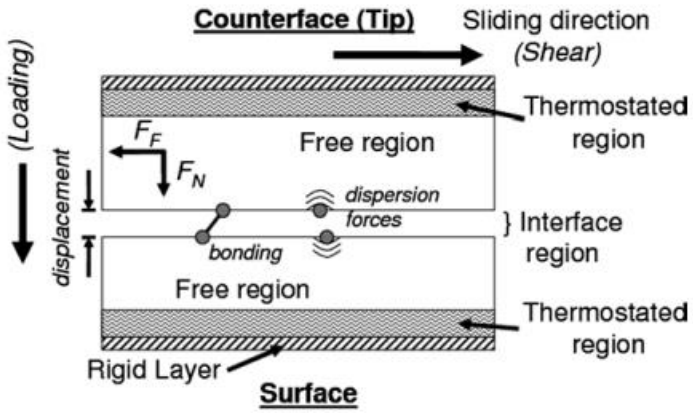


**Chapter II - Figure 12 -** Diagram of molecular dynamics setup for tribology simulation.

**Source**: (Schall et al., 2007)

Gerde and Marder (2001), used molecular dynamics (MD) simulations to investigate friction and its connection to the mechanism of self-healing cracks. Their simulations are based on a self-healing crack moving along the interface between the two surfaces, leading to slip between

the solids. They have thus obtained dynamic friction (steady-state) values from an atomic scale simulation.

Computer simulations act as a bridge (Figure 13) between microscopic length and time scales and the macroscopic world of the laboratory. We provide a guess at the interactions between molecules, and obtain 'exact' predictions of bulk properties. Simulations act as a bridge in another sense: between theory and experiment. We may test a theory by conducting a simulation using the same model. We may test the model by comparing with experimental results (Allen, 2004; Gerde & Marder, 2001).

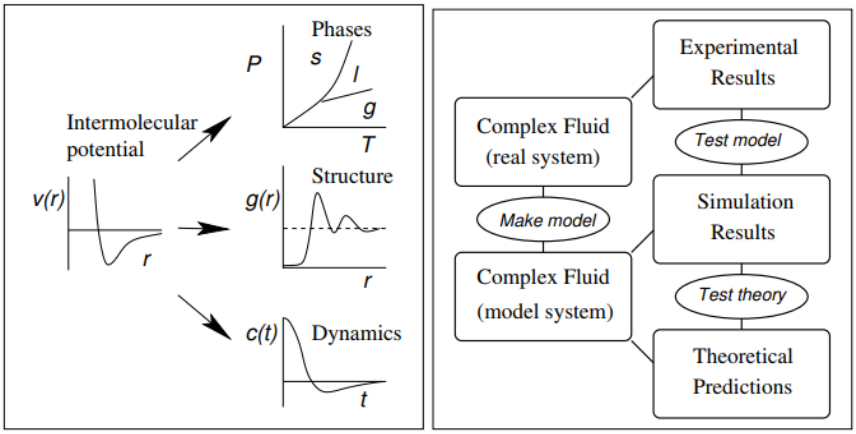


**Chapter II - Figure 13 -** Schematic picture of the relationship between theory and experimental data at both macroscopic and microscopic levels.

**Source:** (Allen, 2004)

More recently, new areas of tribology have emerged, including nanotribology, i.e. the study of friction, wear and lubrication at the nanoscale as applied, for example, to micro- and nano-electromechanical systems (MEMS/NEMS), magnetic storage and biotribology, which deals with human joint prosthetics, dental materials, skin, etc., and ecological aspects of friction, lubrication and wear (tribology of clean energy sources, green lubricants, biomimetic tribology). (Vakis et al., 2018).

Few studies have been quantifying astringency and are mostly related with the interactions between phenolic compounds and proteins as mechanisms that could explain the perception of the astringency in the wine. Ramos-Pineda et al. (2017) conducted a study by High-Performance Liquid Chromatography with Diode-Array Detection (HPLC-DAD), Isothermal Tritation calorimetry (ITC), and MD simulation the behaviour of ternary mixtures of salivary proteins/catechin/ in

comparison to the binary systems of salivary proteins/catechin and salivary proteins/epicatechin, maintaining constant the amount of flavanol. Their intention was to obtain evidence to support the synergisms of the astringency between flavanols that have been proposed in previous studies using sensory analysis. Indeed, Ferrer-Gallego et al. (2017) used nuclear magnetic resonance spectroscopy (STD-NMR) and molecular dynamics simulations methods that could explain the synergistic effect observed between phenolic compounds and salivary proteins and also postulated a tentative molecular mechanism to explain them.

- ## Background and Fundamentals of MD

Molecular dynamics (MD) is a simulation tool for modelling materials that predicts the motion of atoms under forces exerted by other atoms. This method was one of the first computer-based technique employed in the studies of the properties of materials. Pioneer studies using this technique remote to the 1950s, where Alder and Wainwright (1959) give an idea where this method is applicable to the solution of many systems: systems in equilibrium and nonequilibrium and systems related to the calculations of thermodynamic properties; both can be solved with the help of MD. They investigated mainly a solid-fluid transition in a system composed of hard spheres interacting by instantaneous collisions.

MD simulations are in many aspects very similar to real experiments. When performing a real experiment, we proceed as follows: a sample of the material to study is prepared. We connect this sample to a measuring instrument (e.g., a thermometer, manometer, or viscosimeter), and the property of interest is measured during a certain time interval (Shell, 2019). To measure an observable quantity in a MD simulation, we must first of all be able to express this observation as a function of the positions and moments of the particles in the system. The basis of MD lies in the core of the molecular mechanics method. The system being simulated is classical from the standpoint that the particles (e.g. atoms, molecules) are treated as obeying the laws of classical mechanics. (Zheng, 2014)

In the MD simulation the trajectory of a particle is derived from the previous position by using the interactions between the particles. For one particle $i$ in the system, another particle $j$ attracts or repels it, so the positions of both $\vec{r}_i$ and $\vec{r}_j$ will influence the interaction between them. All the interactions contribute to the total potential energy of the particle $i$. The potential energy of a system as a function of the position of the particles is given by $U(r_N)$. A force is implemented to particle $i$ under that potential, using:

$$\vec{F}_i = -\nabla \mathrm{U}(\vec{r}_i) \qquad (\mathbf{1})$$

Newton's second law states that the force on a particle equals its mass times its acceleration,

$$\vec{F}_i = m_i a_i = m_i \frac{d\vec{v}_i}{dt} = \qquad (\mathbf{2})$$

$$= m_i \frac{d^2\vec{r}_i}{dt^2}$$

Taking into account those equations, MD simulations calculate the velocity $\vec{v}_i$ of each particle at a given time, then lets every particle move with that velocity for a period of timestep. Then it re-evaluates the potential energy, force and consequently the new velocity.

The standard way for solving this equations on a computer is to break up the time t into discrete intervals and then solve the equations of motion over those intervals. The intervals are referred to as *timesteps* and denoted in this text by $\delta t$. One usually makes the further approximation that the properties of the system at $t + \delta t$ can be calculated from the properties at *t*. The approach will be to take steps forward in time, at each point solving for the position $\vec{r}_i$ and the velocity $\vec{v}_i$ at the next timestep. The Verlet algorithm is frequently used to calculate the trajectories of the particles in MD simulations. This method, which is used to integrate Newton's equations of motion, has many advantages, including its ease of programming and has a reasonable accuracy. On the other hand, this algorithm requires that at least two sets of positions has to be stored in memory, which is then an obstacle to his efficiency,

$$\vec{r}_i(t + \delta t) = 2\vec{r}_i(t) - \vec{r}_i(t - \delta t) + \frac{\vec{F}_i(t)}{m_i}\delta t^2 + \vec{v}_i\,(\delta t^4)$$

$$\vec{v}_i(t) = \frac{\vec{r}_i(t + \delta t) - \vec{r}_i(t - \delta t)}{2\delta t}$$

One alternative to the Verlet Algorithm, is the Velocity-Verlet algorithm that uses the velocity directly. This method is used to integrate the motion of each atom because it achieves a better accuracy and it is easy to implement, than the precious Verlet algorithm. Given the position $\vec{r}_i(t)$, velocity $\vec{v}_i(t)$, acceleration $\vec{a}_i(t)$ and the time $t + \delta t$ , with the Velocity-Verlet algorithm, it's possible to obtain the following equations 3 and 4:

$$\vec{r}_i(t + \delta t) = \vec{r}_i(t) + \vec{v}_i(t)\delta t + \frac{1}{2m}\vec{F}_i(t)\delta t^2 \qquad (\mathbf{3})$$

$$\vec{v}_i(t + \delta t) = \vec{v}_i(t) + \frac{1}{2}m\left(\vec{F}_i(t) + \vec{F}_i(t + \delta t)\right)\delta t \qquad (\mathbf{4})$$

The calculation is started with a known set of positions and velocities and the algorithm it is applied sequentially. The optimal size of the time step $\delta t$ is a balance between accuracy and

computer time. Each time step requires a force evaluation, which consumes the largest amount of computer time in the calculation. There is thus a balance between efficiency (large $\delta t$), with fewer force calculations, and accuracy (small $\delta t$), with more force calculations (LeSar, 2013; Shell, 2019; Zheng, 2014).

An additional consideration for the practical implementation of MD is how to introduce the concepts of temperature and pressure, which of course are important quantities for a real experiment. To relate the atomic trajectories of an MD simulation to such macroscopic properties, statistical mechanics is applied through the use of a thermodynamic ensemble. A thermo-dynamical ensemble represents all possible states of a system that have a set of common extrinsic properties, like: number of molecules or moles, mass, volume, internal energy, and entropy, among others (M. L. Jackson, 2017).

- ## Molecular Dynamics Force Fields

In terms of the interactions between the atoms, the force field development represents an important aspect of the molecules involved in the simulation. According to Vlachakis et al. (2014), the main roles of force field are to reasonably describe the general properties of molecules, like: molecular geometry, conformational and stereo-isometric energy, torsional barriers, torsional deformation, energy of intermolecular interactions, as well as to assess the geometry between interacting molecules, to evaluate the vibrational frequency and heat of formation.

In the context of molecular dynamics simulations of proteins, the term "force field" refers to the combination of a mathematical formula and associated parameters that are used to describe the energy of the protein as a function of its atomic coordinates. MD provides the actual movement of the molecules through these force fields (Monticelli & Tieleman, 2013).

Molecular interactions include the potential energy function which is written as the sum of contributions due to bond stretching, bond angle bending, dihedral angle torsion and non-bonded interactions. The terms representing bonded interactions seek to account for the stretching of bonds, the bending of valence angles, and the rotation of dihedrals. The terms representing nonbonded interactions aim to capture electrostatics, dispersion, and Pauli exclusion. The functional form of the force field in terms of the total potential energy is shown bellow (Guvench & MacKerell, 2008)

$$E_{Total} = E_{bonded} + E_{non-bonded} + E_{others} \quad (\mathbf{5})$$

Thus, energy terms common to these force fields are:

$$E_{bonded} = \sum_{bonds} K_b(b - b_0)^2 + \sum_{angles} K_\theta(\theta - \theta_0)^2 + \sum_{dihedrals} K_\chi[1 + \cos(n\chi - \sigma)] \quad (6)$$

$$E_{non-bonded} = \sum_{non-bonded\ pairs\ ij} \left( \varepsilon_{ij} \left[ \left( \frac{R_{min,ij}}{r_{ij}} \right)^{12} - 2 * \left( \frac{R_{min,ij}}{r_{ij}} \right)^{6} \right] + \frac{q_i q_j}{r_{ij}} \right) \quad (7)$$

The beginning of the first molecular mechanics calculations date back to the 1940's, but significant progress in the field had to wait until the end of the 1960's, when the first computers became available. With the development of technology and research, the focus on the MD of complex system lead to the development of more complex force fields. Examples are: AMBER, DREIDING, CHARMM, UFF, GROMOS, OPLS, and COMPASS force fields, which differ in numerous properties (Allen, 2004).

AMBER, CHARMM, GROMOS, and OPLS offer all a reasonably large range of atoms types, such that many organic small molecules can be represented by assigning atom types based on chemical similarity. The AMBER force field includes the general AMBER Force Field (GAFF) OPLS-AA, with its emphasis on condensed-phase simulations of small molecules and provides a diverse set of compounds. The GROMOS force field atom type palette, which derives from parameters for biopolymers, also provides a reasonable amount of diversity for the construction of force field models of small molecules (Vlachakis, Bencurova, Papangelopoulos, & Kossida, 2014).

- ## Codes for MD

Large-scale Atomic/Molecular Massively Parallel Simulator or LAMMPS, has been developed to deterministically solve Newton's equations of motions. The LAMMPS code capabilities consist of being able to model a system of atoms with varying boundary conditions, such as periodic or free surfaces, while applying varying forces in a two or three dimensional framework (Capps, 2013). This classical MD code was developed by Sandia National Laboratory with a focus on materials modelling. It was designed to run efficiently on parallel computers that supports the MPI message-passing library. This includes shared-memory boxes and distributed-memory clusters and supercomputers. LAMMPS is an open-source code, distributed freely under the terms of the GNU Public License (GPL), written in C++. This software models ensembles of particles in a liquid, solid or gaseous state. It can model atomic, polymeric, biological, solid-state (metals, ceramics, oxides), granular, coarse-grained, or macroscopic systems using a variety of interatomic potentials (force fields) and boundary conditions. It can model 2d or 3d systems with only a few particles up to

millions or billions. There are also other commercial softwares for MD, with some of the most popular named GROMACS, NAMD and AMBER (Guvench & MacKerell, 2008).

In our study, this code was used to study the oral process, and the interactions between the tongue/food/palate systems. The input scripts are text files that give instructions to LAMMPS about units, positions, velocities, types of atoms, etc.

LAMMPS is run in the command shell, by calling its executable and providing it a series of flags for the number of MPI processes and OMP to use, as well as the input script file name (Corporation., 2013; Cruz, 2018).

The existence of many combined mechanisms of astringency, the utilization of new methodologies as molecular dynamics simulations or tribology and the application of instrumental techniques to unravel the astringency mechanisms and/or to predict the astringency sensations elicited by different compounds, may provide an objective explanation for the astringency of different food and beverages.

## 2.4 Food personalization with 3D Food Printing

Consumer food product acceptance is made considering the taste, cost, experience, convenience and nutrition, healthy concepts and functional claims. As reported by Millen (2012), in recent years foods are becoming more customized and consumers require food that tastes great, looks great and is healthy. Actually, according with the 2015 American Pantry Study, 47% of consumers described themselves as “health conscious”, and 35% described themselves as “ingredient sensitive”. This motivates a growing market for personalized healthy food, which aims to tailor and fabricate specific diets based on an individual’s health condition (Deloitte, 2015).

To be able to create completely customized foods there are two options: using a material set that is large enough to satisfy all consumers’ wants or using a small material set that can be combined in varying ratios. Food printing is a method to produce food in a personalized manner, being therefore an alternative to satisfy this demand (Millen, 2012). 3D food printing is an integration between 3D printing and digital gastronomy techniques to customize food products and allows the customization of food design and personalized nutrition control. It is indeed considered a market opportunity that leads to the development of food printers as prototyping tools to conduct

small batch production with an effective cost, time efficient and security way. (Sun, Peng, Yan, Fuh, & Hong, 2015). In this sense, reasonable use of 3D printing technology can be applied with valuable effects regarding human health and diseases. It is a customized approach towards the health need of an individual which satisfies both taste and medicinal requirement. Besides existing nutritional preferences, the concept of personalized nutrition care according to a person's dietary needs, allergies, or taste preferences is on the research agenda of food industries. Under the traditional food supply chain, foods with personalized nutrition are produced with additional cost (Moskowitz, Saguy, & Straus, 2009).

Apart from the health benefits, 3D food printing may be helpful in creating interesting food designs, decorations and textures. Printed foods may resemble traditional foods, such as a pizza, or they may even have a unique appearance. A wide variety of shapes, textures, and decorations can be created with the help of 3D food models with intricate designs or decorations that are created more easily by a printer than by hand (P. Singh & Raghav, 2018). Food printing technologies target to replace such traditional operation by providing a platform to experiment food design on shapes, colours and flavours automatically.

According to King et al. (2017), global population is expected to reach at least 9 billion by the year 2050, requiring 70% more food and requiring fully-sustainable food production systems. Meeting those food security challenge needs to be part of tackling equally big strategic issues for food research. Due to such growing demand for food, alternative ingredients extracted from algae, fungi, seaweed, lupine, and food by-products can be utilized as printing materials in the future (J. Liu et al., 2019). This step may also ease the growing demand for food production in an environmentally friendly and efficient manner (Winger & Wall, 2006). On 3D food printing, King et al. (2017) raised a number of concerns, chiefly the fact everyone could make food without having any real control of their self-created food, which will necessarily bring food safety risks. Obviously, 3D food printing, at consumer or industrial level, would be a powerful technology, if we compensate the evident lack of lookback in order to eliminate all risks to health.

### 2.4.1 Background

In the last decades, printing technology has advanced from two-dimensional (2D) printing to an additive process in which successive layers of material are distributed to form 3D shapes. 3D printing was first described in 1980s and was considered as one of the important symbols of

the third potential industrial revolution at the time (Hull, 1986). 3D Printing consists in robotic machines that create objects through a process also known as additive manufacturing (AM) (ASTM, 2015). Now, this technique is an emerging technology that is subjected to daily debate, grabbing a wide interest from the whole world with its different fields of applications, which are constantly growing such as medicine, gastronomy, engineering, manufacturing, art and education.

The concept three-dimensional food printing combines additive manufacturing and digital gastronomy techniques to produce 3D custom-designed food objects without object-specific tooling, moulding or human intervention.

The overall perception of food design covers visual appearance, sense of touch (stickiness, roughness, hardness), first bite, chewing, swallowing (flow properties, roughness or smoothness), and residual effects on mouth. This enables users to do things such as building back the texture of an existing food product after changing some key ingredients to upgrade nutritional profile, refining the texture of an existing product to become more appropriate, and developing new food products with desired texture as part of the overall eating experience. 3D Printing is not only a novel approach to food fabrication, but also an economical and powerful technique for mass customization (Sun, Zhou, Huang, & Yan, 2018).

The very first developments in industrial 3D printing technologies, binder jetting and stereolithography took place at the Massachusetts Institute of Technology (MIT) and at 3D Systems, which in 1987 became the very first company to produce a commercially available 3D printer (Sher & Tutó, 2015). In the food sector, the first-generation food printer designs were introduced to the general public more than 10 years ago. Nanotek Instruments, Inc., patented a rapid prototyping and fabrication method for producing 3D food objects, such as a customer-designed birthday cake; however, no physical prototype was built (Yang, Wu Wei, & Liu, 2001). Since then, a few printing projects have been carried out by many researchers, like Lipton *et al.* (2009) with the Fab@home and 3D printed food system for long duration space missions produce by NASA (National Aeronautics and Space Administration), which gave them an award for Small Business Innovation Research (SBIR) (NASA, 2013).

While all the previously mentioned projects are ambitious and hold an incredible long term potential, 2015 is likely to be remembered as the year when a kickstarter project of food 3D printer was implemented. Equipments like The Foodini 3D printer, was perhaps the most revolutionary and promising of all the commercial 3D printers. The underlying idea of this printer was to be able to robotically prepare healthy home-cooked meals for those whose lives are so busy that they have

little time for cooking anything. Foodini was developed by Elisava Barcelona School of Design and Engineering (Sher & Tutó, 2015).

Depending on the fabrication principle, 3D printing techniques can be introduced in the food field and adapted to meet the demand of food design and materials processing. Particular attention is given to the techniques involving the essential constituents of food (Godoi, Prakash, & Bhandari, 2016).

The earliest application of 3D printing in food was related to with the paste extrusion of a mixture of starch, yeast, sugar, corn syrup and frozen cakes. At present, 3D printing technology in chocolate products has already developed some level of maturity, and has been applied in actual innovative projects such as proteins, starch, fiber-rich food materials, sugar products with or without additives and meat products (transglutaminase and bacon fat have been used as additive in printing turkey meat-puree and scallop) (Lipton et al., 2010).

For 3D printing of bio-based products or foods, the following techniques are well-suited: extrusion-based printing (the most popular method in food printing); inkjet printing and laser-assisted printing (Guvendiren, Molde, Soares, & Kohn, 2016;; Shirazi et al., 2015).

- ## Process and Parameters of Food Printing

3D printer machines contains platforms with XYZ three-axis, dispensing/sintering units, and a user interface. The multi-axis stages used in food printing include Cartesian, Delta, Polar and Scara configurations (Figure 14). Many first generation food printers use the cartesian coordinate configuration, since a machine with this configuration is simpler to design, easier to maintain and calibrate. Examples of this Cartesian configuration include Choc Creator, Foodini, BeeHex Robot pizza printer. The Cartesian configuration has X, Y, and Z axes for left to right, front to back and up and down motion, respectively (Sun et al., 2018).

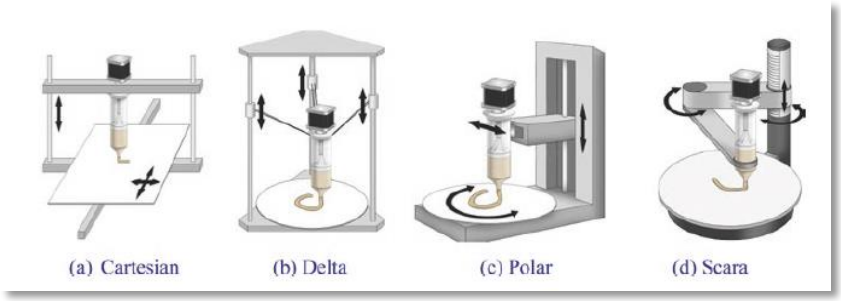


**Chapter II - Figure 14 -** Coordinate systems of a 3D Printer.

**Source:** (Sun et al., 2018)

The consumers user interface for food printing is quite direct, although the interface depends on the printer. For example, Foodini has a very simplistic graphical interface while others require more knowledge of slicing and printing parameters. Usually the straightforward way to use these interfaces starts with input files and relies on a Computer Aided Design (CAD) model to plan and construct food pieces. Since many consumers can't create designs using professional CAD software, support systems are created that maybe possible to follow and guide those users unfamiliar with 3D modeling, such as the Digital Cookbook software that helps encourage the use of 3Dsystems ChefJet Series (Quick, 2014).

The 3D printers platforms can manipulate food fabrication process in real-time, with computer-controlled, three-axis motorized stage and material feeding system. A food design model, after being translated into machine path planning language (G-code, M-code, etc.), can be easily defined in terms of printing speed, deposition speed, and a set of other parameters. Food composition can be deposited mainly path-by-path, layer-by-layer, according to computer design model and path planning. After the printing phase, the design printed can for instance be baked in an oven, cooked by immersing in boiling water or deep fried. In the pursuit of a cooking-resistant structures, an accurate selection of materials with appropriate physical-chemical, rheological and mechanical properties are essential (Godoi et al., 2016; Zoran & Coelho, 2011).

The applicability of AM technology is also ruled by the materials properties. There's some parameters to be controlled when it comes to the 3D printing process and 3D materials that are used. That said, they should be divided into two parts: first the parameters concerning the printer machine and second the parameters concerning the food itself (Figure 15) (Severini, Derossi, & Azzollini, 2016).

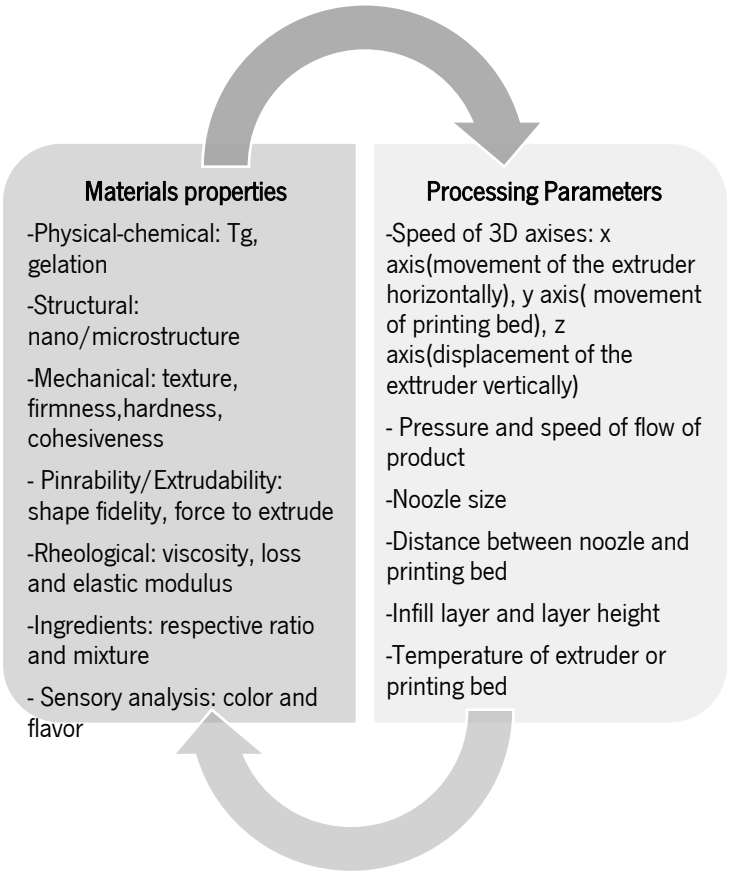


**Chapter II - Figure 15 -** Features and examples of parameters that must be controlled to obtain the best 3D product.

**Source:** (Adapted from (Severini et al., 2016))

Therefore, simplifying the process of manufacturing of a specific product into simple steps and combining them together to form a simulation model for manipulation is essential. Therefore, one of the critical challenges in the 3D food printing field has been to align food grade materials with printing processes. Three food materials property related critical factors are suggested here (Godoi et al., 2016):

1) Printability: This feature relies on how the properties of the material enable handling and deposition by a 3D printer and hold its structure post-deposition. 3D printing based on extrusion techniques can be affected by specific gelation mechanisms and thermal properties.
2) Applicability: AM technologies can be attractive by their capability of building complexes structures and textures. In addition, AM becomes more interesting when nutritional value is incorporated to the unique designed structures.
3) Post-processing: Ideally, the 3D construct of food should resist to post-processing, such as, baking in an oven, being cooked by immersing in boiling water or deep frying.

In the pursuit of a cooking-resistant structures, an accurate selection of materials with appropriate physical-chemical, rheological and mechanical properties are essential

Thus, reproducing by example the steps of Wang et al. (2018), that studied some effects of the printing parameters of printed surimi gels, the 3D printing technology should the always improved both on the material properties as on the process itself. Optimizing several parameters of the printing process (chain of processing, ingredients), the outcome can result in novel 3D printed shapes using different food substrates (Dankar, Haddarah, Omar, Sepulcre, & Pujolà, 2018; Wang, Zhang, Bhandari, & Yang, 2018).

### 2.4.2 3D Food Bio-printing

According to the Food and Agriculture Organization of the United Nations (FAO), the demand for meat will increase by over two-thirds in the next forty years and current production methods won't be sustainable. In the near future, meat and other staple foods are likely to become expensive luxury items thanks to the increased demand on crops for meat production. That is, unless we find a sustainable alternative (Sher & Tutó, 2015).

Marga (2012), states that the bio-printed meat would find acceptance by the vegetarian community which rejects meat for ethical reasons. Upon affordable price, in the future this technology would benefit the masses with religious restrictions on meat consumption and populations with restrict access to safe meat production. The bio-printing of meat, however, shows many drawbacks to overcome, most of them associated to the spatial resolution of the final construct and long maturation processes.

Lipton et al. (2015) address the topic of manufacturing whole muscle tissue for human food supply, where the idea would be to remove the need to farm livestock in order to produce meat muscle and fat cells, in which case the nutritional value of these products would supposedly be identical or near-identical to 'conventional' meat.

According to, Trends in Food Science & Technology one of the goals of American start-up Modern Meadow, is to 3D printing stem cells, which should be able to render a meat-like matrix. However, even if right now these approaches are still in their early days, we can already see the kind of difficulties to come in the future: the economics, nutritional and organoleptic properties, industrial scale-up, nutrient inputs needed for cell culture, food safety, ethics issues, and the list goes on. There are two different technology pathways to re-value-stream meat, especially beef

which is currently either processed as ground beef patties or undervalued as its initial tenderness is mediocre at best: 1) work on mechanical tenderization of chunked meat, by optimizing the tumbling processes ; 2) design innovative foods by AM. In both cases, the goal is to fashion meat products presenting a fully process-controlled texture. (Daudin et al., 2015)

A successful fabrication of tissue constructs requires understanding the dynamic interaction between different disciplines. Bioprinting is a multi-disciplinary area that allows precise deposition of cells and biomaterial components in pre-defines designs (Seol, Kang, Lee, Atala, & Yoo, 2014).

AM today, though, aggregates both types of processing (3D Food Bio-printing), which is precisely why 3D food printing research needs to press ahead, to attempt to minimize the use of additive inputs trying to keep food more clean and natural as possible, since today's consumers tend to prefer clean label products containing as few additives as possible. As Lupton and Turner (2017) state, 3D food printing technologies will only expand if they manage to keep the food 'natural'.

## 2.5 References


Akyıldız, A., Aksay, S., Benli, H., Kıroğlu, F., & Fenercioğlu, H. (2004). Determination of changes in some characteristics of persimmon during dehydration at different temperatures. *Journal of food engineering*, 65(1), 95-99

Alder, B. J., & Wainwright, T. E. (1959). Studies in molecular dynamics. I. General method. The *Journal of Chemical Physics*, 31(2), 459-466.

Allen, M. P. (2004). Introduction to molecular dynamics simulation. Computational soft matter: from synthetic polymers to proteins, 23, 1-28.

ASTM (2004). Standard definitions of terms relating to sensory evaluation of materials and products. *Annual book of ASTM standards. Philadelphia: American Society for Testing and Materials*

ASTM. (2015). Standard Terminology for Additive Manufacturing Technologies. Retrieved from https://www.astm.org/Standards/F2792.htm

Bajec, M. R. (2010). Astringency and other oral sensations: biological sources of individual variation and association with food and beverage behaviour.

Bajec, M. R., & Pickering, G. J. (2008). Astringency: mechanisms and perception. *Critical reviews*

*in food science and nutrition*, 48(9), 858-875.

Bate-Smith, E. C. (1954). Astringency in foods. Food, 23(124).

BEN‐ARIE, R. U. T. H., & SONEGO, L. (1993). Temperature affects astringency removal and recurrence in persimmon. *Journal of food science*, 58(6), 1397-1400.

Berrien, L. S. J. (1999). Biotribology: studies of the effects of biochemical environments on the wear and damage of articular cartilage (Doctoral dissertation, Virginia Tech).

Bhuiyan, F. R., & Rahim, A. T. M. (2015). Consumer's sensory perception of food attributes: A survey on flavor. *Journal of Food and Nutrition Sciences*, 3(1-2), 157-160

Bhushan, B. (1999). Principles and applications of tribology. John Wiley & Sons.

Biegler, M., Delius, J., Käsdorf, B. T., Hofmann, T., & Lieleg, O. (2016). Cationic astringents alter the tribological and rheological properties of human saliva and salivary mucin solutions. *Biotribology*, 6, 12-20.

Boehm, M. W., Yakubov, G. E., Stokes, J. R., & Baier, S. K. (2019). The role of saliva in oral processing: reconsidering the Breakdown Path paradigm. *Journal of texture studies*

Brossard, N., Cai, H., Osorio, F., Bordeu, E., & Chen, J. (2016). "Oral" tribological study on the astringency sensation of red wines. *Journal of Texture Studies*, 47(5), 392-402.

Brostow, W., Hinze, J. A., & Simões, R. (2004). Tribological behavior of polymers simulated by molecular dynamics. *Journal of materials research*, 19(3), 851-856.

Canon, F., Neiers, F., & Guichard, E. (2018). Saliva and flavor perception: perspectives. *Journal of agricultural and food chemistry*, 66(30), 7873-7879.

Capps, N. A. (2013). Molecular dynamics simulations of cascade evolution near pre-existing defects

Cassin, G., Heinrich, E., & Spikes, H. A. (2001). The influence of surface roughness on the lubrication properties of adsorbing and non-adsorbing biopolymers. *Tribology Letters*, 11(2), 95-102.

Çelebioğlu, H. Y., Gudjónsdóttir, M., Chronakis, I. S., & Lee, S. (2016). Investigation of the interaction between mucins and β-lactoglobulin under tribological stress. Food Hydrocolloids, 54.

Charlton, A. J., Baxter, N. J., Khan, M. L., Moir, A. J., Haslam, E., Davies, A. P., & Williamson, M. P. (2002). Polyphenol/peptide binding and precipitation. *Journal of agricultural and food chemistry*, 50(6), 1593-1601

Chen, J. (2009). Food oral processing—A review. *Food Hydrocolloids*, 23(1), 1-25.

Chen, J., & Rosenthal, A. (2015). Food texture and structure. In *Modifying Food Texture* (pp. 3-24).

Woodhead Publishing.

Chen, J., & Stokes, J. R. (2012). Rheology and tribology: Two distinctive regimes of food texture sensation. *Trends in Food Science & Technology*, 25(1), 4-12.

Corporation, S. (2013). LAMMPS Documentation. Retrieved from https://lammps.sandia.gov/doc/Manual.html

Courregelongue, S., Schlich, P., & Noble, A. C. (1999). Using repeated ingestion to determine the effect of sweetness, viscosity and oiliness on temporal perception of soymilk astringency. *Food Quality and Preference*, 10(4-5), 273-279

Cruz, S. E. (2018). ATOMISTIC SIMULATION OF RADIATION DAMAGE IN *MATERIALS FOR NUCLEAR FUSION REACTORS*. Instituto Superior de Engenharia do Porto.

Dankar, I., Haddarah, A., Omar, F. E., Sepulcre, F., & Pujolà, M. (2018). 3D printing technology: The new era for food customization and elaboration. Trends in *food science & technology*.

de Almeida, P. D. V., Gregio, A. M., Machado, M. A., De Lima, A. A., & Azevedo, L. R. (2008). Saliva composition and functions: a comprehensive review. J Contemp Dent Pract, 9(3), 72-80.

de Azevedo Brandão, E. J. F. (2018). INOVAD-Development of new formulations based on polysaccharides to reduce the astringency of beverages.

de Freitas, V., & Mateus, N. (2012). Protein/polyphenol interactions: past and present contributions. Mechanisms of astringency perception. *Current Organic Chemistry*, 16(6), 724-746

De Hoog, E. H., Prinz, J. F., Huntjens, L., Dresselhuis, D. M., & Van Aken, G. A. (2006). Lubrication of oral surfaces by food emulsions: the importance of surface characteristics. *Journal of food science*, 71(7), E337-E341.

De Wijk, R. A., & Prinz, J. F. (2006). Mechanisms underlying the role of friction in oral texture. *Journal of Texture Studies*, 37(4), 413-427.

De Wijk, R. A., Janssen, A. M., & Prinz, J. F. (2011). Oral movements and the perception of semi-solid foods. *Physiology & behavior*, 104(3), 423-428.

Delarue, J., & Sieffermann, J. M. (2004). Sensory mapping using Flash profile. Comparison with a conventional descriptive method for the evaluation of the flavour of fruit dairy products. *Food quality and preference*, 15(4), 383-392.

Deloitte (2015) The 2015 American pantry study: The call to re-connect with consumers. Viewed 28 February 2018,

http://www2.deloitte.com/content/dam/Deloitte/us/Documents/consumer-business/us-cb-2015-american-pantry-study.pdf

Drake, M. A. (2007). Invited review: Sensory analysis of dairy foods. *Journal of dairy science*, 90(11), 4925-4937.

Engelen, L., & Van Der Bilt, A. (2008). Oral physiology and texture perception of semisolids. *Journal of Texture Studies*, 39(1), 83-113

F de Azevedo, W. (2011). Molecular dynamics simulations of protein targets identified in Mycobacterium tuberculosis. *Current medicinal chemistry*, 18(9), 1353-1366.

Ferrer-Gallego, R., Hernández-Hierro, J. M., Brás, N. F., Vale, N., Gomes, P., Mateus, N., & Escribano-Bailón, M. T. (2017). Interaction between wine phenolic acids and salivary proteins by saturation-transfer difference nuclear magnetic resonance spectroscopy (STD-NMR) and molecular dynamics simulations. *Journal of agricultural and food chemistry*, 65(31), 6434-6441.

Fleming, E. E., Ziegler, G. R., & Hayes, J. E. (2016). Salivary protein levels as a predictor of perceived astringency in model systems and solid foods. Physiology & *behavior*, 163, 56-63.

García-Estévez, I., Ramos-Pineda, A. M., & Escribano-Bailón, M. T. (2018). Interactions between wine phenolic compounds and human saliva in astringency perception. *Food & function,* 9(3), 1294-1309.

Gerde, E., & Marder, M. (2001). Friction and fracture. *Nature*, 413(6853), 285.

Gibbins, H. L., & Carpenter, G. H. (2013). Alternative mechanisms of astringency–what is the role of saliva? *Journal of texture studies*, 44(5), 364-375.

Godoi, F. C., Prakash, S., & Bhandari, B. R. (2016). 3d printing technologies applied for food design: Status and prospects*. Journal of Food Engineering*, 179, 44-54.

Goh, S. M., Versluis, P., Appelqvist, I. A. M., & Bialek, L. (2010). Tribological measurements of foods using a rheometer. *Food research international*, 43(1), 183-186.

Graca, M., Bongaerts, J. H., Stokes, J. R., & Granick, S. (2007). Friction and adsorption of aqueous polyoxyethylene (Tween) surfactants at hydrophobic surfaces. *Journal of Colloid and Interface Science*, 315(2), 662-670.

Green, B. G. (1993). Oral astringency: a tactile component of flavor. *Acta psychologica*, 84(1), 119-125.

Guinard, J. X., & Mazzucchelli, R. (1996). The sensory perception of texture and mouthfeel. Trends

in *Food Science & Technology*, 7(7), 213-219.

Guvench, O., & MacKerell, A. D. (2008). Comparison of protein force fields for molecular dynamics simulations. In *Molecular modeling of proteins* (pp. 63-88). Humana Press.

Guvendiren, M., Molde, J., Soares, R. M., & Kohn, J. (2016). Designing biomaterials for 3D printing. *ACS biomaterials science & engineering*, 2(10), 1679-1693.

He, M., Tian, H., Luo, X., Qi, X., & Chen, X. (2015). Molecular progress in research on fruit astringency. *Molecules*, 20(1), 1434-1451.

Hull, C. W. (1986). U.S. Patent No. 4,575,330. Washington, DC: U.S. Patent and Trademark Office.

ISO, Geneva (Switzerland), ISO 11036-1994: Sensory analysis – Texture profile. (1994)

Jackson, M. L. (2017). Atomistic simulations of materials for nuclear fusion

Jackson, R. S. (2008). Wine science: principles and applications. Academic press.

Jellinek, G. (1964). Introduction to and Critical Review Od Modern Methods of Sensory Analysis (odour, Taste and Flavour Evaluation): With Special Emphasis on Descriptive Sensory Analysis (flavour Profile Meth). Print and Publishing House.

Jiang, Y., Gong, N. N., & Matsunami, H. (2014). Astringency: A more stringent definition. *Chemical senses*, 39(6), 467.

Jöbstl, E., O'Connell, J., Fairclough, J. P. A., & Williamson, M. P. (2004). Molecular model for astringency produced by polyphenol/protein interactions. *Biomacromolecules*, 5(3), 942-949.

Joslyn, M. A., & Goldstein, J. L. (1964). Astringency of fruits and fruit products in relation to phenolic content. In *Advances in food research* (Vol. 13, pp. 179-217). Academic Press.

Jost, H. P. (1990). Tribology — Origin and future. Wear, 136.

Kallithraka, S., Bakker, J., & Clifford, M. N. (1997). Effect of pH on astringency in model solutions and wines. *Journal of Agricultural and Food Chemistry*, 45(6), 2211-2216

-Kallithraka, S., Bakker, J., Clifford, M. N., & Vallis, L. (2001). Correlations between saliva protein composition and some T–I parameters of astringency. *Food Quality and Preference*, 12(2), 145-152

KATO, K. (1987). Astringency removal and ripening as related to temperature during the de-astringency by ethanol in persimmon fruits. *Journal of the Japanese Society for Horticultural Science*, 55(4), 498-509

Kelly, M., Vardhanabhuti, B., Luck, P., Drake, M. A., Osborne, J., & Foegeding, E. A. (2010). Role of protein concentration and protein–saliva interactions in the astringency of whey

proteins at low pH. *Journal of dairy science*, 93(5)

Kershaw, J. C., & Running, C. A. (2019). Dose–response functions and methodological insights for sensory tests with astringent stimuli. *Journal of sensory studies*, 34(1), e12480.

King, T., Cole, M., Farber, J. M., Eisenbrand, G., Zabaras, D., Fox, E. M., et al. (2017). Food safety for food security: Relationship between global megatrends and developments in food safety. Trends in *Food Science & Technology*, 68, 160–175

Kouzani, A. Z., Adams, S., Whyte, D. J., Oliver, R., Hemsley, B., Palmer, S., & Balandin, S. (2017). 3D printing of food for people with swallowing difficulties. KnE Engineering, 2(2), 23-29.

Kupirovič, U. P., Elmadfa, I., Juillerat, M. A., & Raspor, P. (2017). Effect of saliva on physical food properties in fat texture perception. Critical reviews in *food science and nutrition*, 57(6), 1061-1077

Laaksonen, O. (2011). Astringent food compounds and their interactions with taste properties.

Lamy, E., Rodrigues, L., Louro, T., & Capela e Silva, F. (2017). The role of saliva in food sensory perception: relevant knowledge to design healthy foods

Lawless, H. T., Horne, J., & Giasi, P. (1996). Astringency of organic acids is related to pH. *Chemical Senses*, 21(4), 397-403

Lee, C. A., & Vickers, Z. M. (2008). The astringency of whey protein beverages is caused by their acidity. *International Dairy Journal*, 18(12), 1153-1156

Lee, C. A., Ismail, B., & Vickers, Z. M. (2012). The role of salivary proteins in the mechanism of astringency. *Journal of food science*, 77(4), C381-C387.

Lee, C. B., & Lawless, H. T. (1991). Time-course of astringent sensations. *Chemical senses*, 16(3), 225-238.

LeSar, R. (2013). Introduction to computational materials science: fundamentals to applications. Cambridge University Press.

Lesschaeve, I., & Noble, A. C. (2005). Polyphenols: factors influencing their sensory properties and their effects on food and beverage preferences. *The American journal of clinical nutrition,* 81(1), 330S-335S

Lipton, J. I., Cohen, D., Heinz, M., Lobovsky, M., Parad, W., Bernstien, G. & Masanoff, R. (2009, August). Fab@ home model 2: Towards ubiquitous personal fabrication devices. In *Solid Freeform Fabrciation Symposium*.

Lipton, J., Arnold, D., Nigl, F., Lopez, N., Cohen, D. L., Norén, N., & Lipson, H. (2010, August). Multi-material food printing with complex internal structure suitable for conventional post-

processing. In *Solid freeform fabrication symposium* (pp. 809-815).

Liu, J., Sun, L., Xu, W., Wang, Q., Yu, S., & Sun, J. (2018). Current advances and future perspectives of 3D printing natural-derived biopolymers. *Carbohydrate polymers*.

Liu, K. (2016). Lubrication and perception of foods: tribological, rheological and sensory properties of particle-filled food system (Doctoral dissertation, Wageningen University).

Luck, G., Liao, H., Murray, N. J., Grimmer, H. R., Warminski, E. E., Williamson, M. P.& Haslam, E. (1994). Polyphenols, astringency and proline-rich proteins. *Phytochemistry*, 37(2), 357-371

Malone, M. E., Appelqvist, I. A. M., & Norton, I. T. (2003). Oral behaviour of food hydrocolloids and emulsions. Part 1. Lubrication and deposition considerations. *Food hydrocolloids*, 17(6), 763-773.

Marga, F. S. (2012). Engineered Comestible Meat. National Institute of Food and Agriculture

Matz, S. A. (1962). Food texture. Food *texture*.

McRae, J. M., & Kennedy, J. A. (2011). Wine and grape tannin interactions with salivary proteins and their impact on astringency: a review of current research. *Molecules,* 16(3), 2348-2364.

Millen, C. I. (2012). The development of colour 3D food printing system: a thesis presented in partial fulfilment of the requirements for the degree of Master of Engineering in Mechatronics at Massey University, Palmerston North, New Zealand (Doctoral dissertation, Massey University).

Monticelli, L., & Tieleman, D. P. (2013). Force fields for classical molecular dynamics. In *Biomolecular simulations* (pp. 197-213). Humana Press, Totowa, NJ.

Moskowitz, H. R., Straus, T., & Saguy, S. (2009). An integrated approach to new food product development. CRC Press.

Mossaz, S., Jay, P., Magnin, A., Panouillé, M., Saint-Eve, A., Déléris, I. & Souchon, I. (2010). Measuring and predicting the spreading of dairy products in the mouth: sensory, instrumental and modelling approaches. *Food hydrocolloids*, 24(8), 681-688.

Murray, J. M., Delahunty, C. M., & Baxter, I. A. (2001). Descriptive sensory analysis: past, present and future. *Food research international*, 34(6), 461-471.

NASA (2013). 3D Printing: Food in Space, viewed 26 February 2018, http://www.nasa.gov/directorates/spacetech/home/feature_3d_food.html#.VWfTnc-qpBc

Nguyen, P. T., Bhandari, B., & Prakash, S. (2016). Tribological method to measure lubricating properties of dairy products. *Journal of food engineering*, 168, 27-34.

Olivares Vergara, C. A. (2014). Efecto de las mezclas de vinos syrah–viognier y cabernet sauvignon-syrah sobre la fracción de polisacáridos y la percepción de astringencia

Oxford. (n.d.). Lexico Dictionairy. Retrieved from https://www.lexico.com/en/definition/perception

-Ozawa, T., Lilley, T. H., & Haslam, E. (1987). Polyphenol interactions: astringency and the loss of astringency in ripening fruit. *Phytochemistry*, 26(11), 2937-2942.

Ozdal, T., Capanoglu, E., & Altay, F. (2013). A review on protein–phenolic interactions and associated changes. *Food Research International*, 51(2), 954-970.

Pascua, Y., Koç, H., & Foegeding, E. A. (2013). Food structure: Roles of mechanical properties and oral processing in determining sensory texture of soft materials. Current opinion in *colloid & interface science*, 18(4), 324-333

Peleg, H., Bodine, K. K., & Noble, A. C. (1998). The influence of acid on astringency of alum and phenolic compounds*. Chemical senses*, 23(3), 371-378.

Peryam, D. R., & Pilgrim, F. J. (1957). Hedonic scale method of measuring food preferences*. Food technology*.

Piggott, J. R., Canaway, P. R. (1981). Finding the word for it: methods and uses of descriptive sensory analysis. In *Flavour '81* (pp. 202– 243). Berlin: Walter de Gruyter & Co, Berlin

Portanguen, S., Tournayre, P., Sicard, J., Astruc, T., & Mirade, P. S. (2019). Toward the design of functional foods and biobased products by 3D printing: A review. Trends in *Food Science & Technology*.

Prakash, S., Tan, D. D. Y., & Chen, J. (2013). Applications of tribology in studying food oral processing and texture perception. *Food Research International,* 54(2), 1627-1635.

Prinz, J. F., De Wijk, R. A., & Huntjens, L. (2007). Load dependency of the coefficient of friction of oral mucosa. *Food Hydrocolloids*, 21(3), 402-408.

Quick, D. (2014). 3D Systems cooks up ChefJet 3D printers to print sugary treats. Retrieved from https://newatlas.com/3d-systems-chefjet-sugar-candy-printer/30407/

Ramos-Pineda, A. M., García-Estévez, I., Brás, N. F., Martín del Valle, E. M., Dueñas, M., & Escribano Bailon, M. T. (2017). Molecular Approach to the Synergistic Effect on Astringency Elicited by Mixtures of Flavanols. *Journal of agricultural and food chemistry*, 65(31), 6425-6433.

Rawel, H. M., Meidtner, K., & Kroll, J. (2005). Binding of selected phenolic compounds to

proteins. *Journal of Agricultural and Food Chemistry*, 53(10), 4228-4235

Robichaud, J. L., & Noble, A. C. (1990). Astringency and bitterness of selected phenolics in wine. *Journal of the Science of Food and Agriculture*, 53(3), 343-353.

Ross, C. F., & Weller, K. (2008). Effect of serving temperature on the sensory attributes of red and white wines. *Journal of sensory studies*, 23(3), 398-416

Rossetti, D., Bongaerts, J. H. H., Wantling, E., Stokes, J. R., & Williamson, A. M. (2009). Astringency of tea catechins: More than an oral lubrication tactile percept. *Food Hydrocolloids*, 23(7), 1984-1992.

Rossetti, D., Yakubov, G. E., Stokes, J. R., Williamson, A. M., & Fuller, G. G. (2008). Interaction of human whole saliva and astringent dietary compounds investigated by interfacial shear rheology. *Food Hydrocolloids*, 22(6), 1068-1078.

Sano, H., Egashira, T., Kinekawa, Y., & Kitabatake, N. (2005). Astringency of bovine milk whey protein. *Journal of dairy science*, 88(7), 2312-2317.

Schall, J. D., Mikulski, P. T., Chateauneuf, G. M., Gao, G., & Harrison, J. A. (2007). Molecular dynamics simulations of tribology. In *Superlubricity* (pp. 79-102). Elsevier Science BV.

Scherge, M., Gorb, S. N., & Gorb, S. (2001). Biological micro-and nanotribology. *Springer Science & Business Media*

Schöbel, N., Radtke, D., Kyereme, J., Wollmann, N., Cichy, A., Obst, K., ... & Wetzel, C. H. (2014). Astringency is a trigeminal sensation that involves the activation of G protein–coupled signaling by phenolic compounds. *Chemical senses*, 39(6), 471-487.

Selway, N., & Stokes, J. R. (2013). Insights into the dynamics of oral lubrication and mouthfeel using soft tribology: Differentiating semi-fluid foods with similar rheology. *Food research international*, 54(1), 423-431.

Seol, Y. J., Kang, H. W., Lee, S. J., Atala, A., & Yoo, J. J. (2014). Bioprinting technology and its applications. *European Journal of Cardio-Thoracic Surgery*, 46(3), 342-348

Severini, C., Derossi, A., & Azzollini, D. (2016). Variables affecting the printability of foods: Preliminary tests on cereal-based products. *Innovative food science & emerging technologies*, 38, 281-291.

Sher, D., & Tutó, X. (2015). Review of 3D food printing. Temes de disseny, (31), 104-117.

Shirazi, S. F. S., Gharehkhani, S., Mehrali, M., Yarmand, H., Metselaar, H. S. C., Kadri, N. A., & Osman, N. A. A. (2015). A review on powder-based additive manufacturing for tissue engineering: selective laser sintering and inkjet 3D printing. *Science and Technology of*

*Advanced Materials*, 16(3), 033502.

Singh, A., Orsat, V., & Raghavan, V. (2013). Soybean hydrophobic protein response to external electric field: a molecular modeling approach. *Biomolecules*, 3(1), 168-179.

Singh, A., Vanga, S. K., Orsat, V., & Raghavan, V. (2017). Application of molecular dynamic simulation to study food proteins: A review. Critical reviews in *food science and nutrition*, 1-11.

Singh, P., Raghav, A. (2018). 3D Food Printing: A Revolution in Food Technology. *Acta Scientific Nutritional Health* 2.2 11-12

Sjostrom, L. B. (1954). The Descriptive Analysis of Flavor. *In Food Acceptance Testing Methodology: A Symposium Sponsored by the Quartermaster Food and Container Institute for the Armed Forces*, *Quartermaster Research and Development Command*, US Army Quartermaster Corps [at The] Palmer House, Chicago, 8-9 October 1953 (Vol. 1, p. 25). National Academies.

Smith, A. K., June, H., & Noble, A. C. (1996). Effects of viscosity on the bitterness and astringency of grape seed tannin. *Food quality and preference*, 7(3-4), 161-166

Stokes, J. R., Boehm, M. W., & Baier, S. K. (2013). Oral processing, texture and mouthfeel: From rheology to tribology and beyond. Current Opinion in *Colloid & Interface Science*, 18(4), 349-359.

Sun, J., Peng, Z., Yan, L., Fuh, J. Y., & Hong, G. S. (2015). 3D food printing—An innovative way of mass customization in food fabrication. *International Journal of Bioprinting*, 1(1), 27-38.

Sun, J., Zhou, W., Huang, D., & Yan, L. (2018). 3D Food Printing: Perspectives. *In Polymers for Food Applications* (pp. 725-755). Springer, Cham.

Svendsen, I. E., & Lindh, L. (2009). The composition of enamel salivary films is different from the ones formed on dental materials. *Biofouling*, 25(3), 255-261

Szczesniak, A. S. (1963). Classification of Textural Characteristics a. *Journal of food science*, 28(4), 385-389.

Szczesniak, A. S. (2002). Texture is a sensory property. *Food quality and preference*, 13(4), 215-225.

Tambeli, C. H. (2014). Fisiologia Oral: Série Abeno. Bookman Editora

Terpstra, M. E., Janssen, A. M., Prinz, J. F., De Wijk, R. A., Weenen, H., & Van Der Linden, E. (2005). Modeling of thickness for semisolid foods. *Journal of texture studies*, 36(2), 213-233.

Troszyńska, A., Narolewska, O., Robredo, S., Estrella, I., Hernández, T., Lamparski, G., & Amarowicz, R. (2010). The effect of polysaccharides on the astringency induced by phenolic compounds. *Food Quality and Preference*, 21(5), 463-469.

Turner, B., & Lupton, D. (2017). 'Both fascinating and disturbing': Consumer responses to 3D food printing and implications for food activism. In *Digital Food Activism* (pp. 169-185). Routledge.

Upadhyay, R., Brossard, N., & Chen, J. (2016). Mechanisms underlying astringency: introduction to an oral tribology approach. *Journal of Physics* D: Applied Physics, 49(10), 104003.

Valentova, H., & Panovska, Z. (2003). SENSORY EVALUATION| Taste. In *Encyclopedia of Food Sciences and Nutrition*.

Van der Bilt, A., Engelen, L., Pereira, L. J., Van der Glas, H. W., & Abbink, J. H. (2006). Oral physiology and mastication. *Physiology & behavior*, 89(1), 22-27.

Vidal, S., Courcoux, P., Francis, L., Kwiatkowski, M., Gawel, R., Williams, P., ... & Cheynier, V. (2004). Use of an experimental design approach for evaluation of key wine components on mouth-feel perception. *Food Quality and Preference*, 15(3), 209-217.

Vlachakis, D., Bencurova, E., Papangelopoulos, N., & Kossida, S. (2014). Current state-of-the-art molecular dynamics methods and applications. In *Advances in protein chemistry and structural biology* (Vol. 94, pp. 269-313). Academic Press.

Wakabayashi, K. (2000). Changes in cell wall polysaccharides during fruit ripening. *Journal of Plant Research*, 113(3), 231-237.

Wang, L., Zhang, M., Bhandari, B., & Yang, C. (2018). Investigation on fish surimi gel as promising food material for 3D printing. *Journal of Food Engineering*, 220, 101-108

Winger, R., & Wall, G. (2006). *Food product innovation*.

Yakubov, G. E., McColl, J., Bongaerts, J. H., & Ramsden, J. J. (2009). Viscous boundary lubrication of hydrophobic surfaces by mucin. Langmuir, 25(4), 2313-2321.

Yamamoto, T., Yuyama, N.., Kato, T., & Kawamura, Y. (1984). Gustatory responses of cortical neurons in rats. I. Response characteristics. *Journal of neurophysiology*, 51(4), 616-635.

Yang, J., Wu, L. W., & Liu, J. (2001). U.S. Patent No. 6,280,785. Washington, DC: U.S. Patent and Trademark Office

Zheng, X. (2014). Molecular dynamics simulation of boundary lubricated contacts.

Zhou, Z. R., & Jin, Z. M. (2015). Biotribology: recent progresses and future perspectives. *Biosurface and biotribology*, 1(1), 3-24.

Zoran, A., & Coelho, M. (2011). Cornucopia: the concept of digital gastronomy. *Leonardo*, 44(5), 425-431.

# CHAPTER III: Materials and Methods

## 3.1 Materials and Equipments

Throughout the work developed the reagents and equipments used during this study are indicated in table I, with the proper manufacturers.

**Chapter III - Table I** - Description and manufacturers of the compounds and equiments used in the study.

| Reagents/Equiments | |
|---|---|
| **Designation** | **Company** |
| Chitosan | Sigma-Aldrich |
| Iron(III) chloride hexahydrate | Sigma Aldrich |
| Carboxymethyl Cellulose –High Viscosity | Sigma-Aldrich |
| Gellan Gum | Guzman |
| Sodium Chloride (NaCl) | Sigma-Aldrich |
| Potassium Chloride (KCl) | Sigma-Aldrich |
| Sodium Bicarbonate (NaCHO3) | Sigma-Aldrich |
| Whey Protein | Bulk Powders |
| Bovine Submaxillary Mucin | Sigma-Aldrich |
| PLA + HA Shining Silver | ColorFabb |
| RhodamineB | Sigma Aldrich |
| Glass | Marienfeld |
| Polydimethylsiloxane (PDMS) | Sylgard |
| Trichloro(1H,1H,2H,2H-perfluorooctyl)silane | Sigma-Aldrich |
| Plasma Cleaner | Harrick Plasma |
| 3D Printer | byFlow Focus |
| Tribometer (UMT) | CETR |
| CLSM 780 | Zeiss |
| Atomic Force Microscopy | Bruker Icon |
| Scanning Electron Microscopy | Quanta FEG 650 |
| Drop Shape Analyser | KRÜSS Scientific Instruments |

## 3.2 Food Formulations (DOE)

The compounds are initially weighed, in a microbalance. Both Whey (WPI) and Gellan Gum (GG) after weighing are dissolved in distilled water during magnetic stirring until homogenous dissolution.

During this procedure, it is necessary to keep in mind that sometimes it is necessary to mix the samples manually, so that there is a homogenous mixture (since the WPI is a little hydrophobic and the GG is very viscous). The compounds are allowed to stir for at least 1h to form the mixture.

When the compounds are finally well homogenized, they are joined together with a standard pipette (1ml) and a viscous pipette (suitable for solutions such as GG).

Following the standard runs of the experimental design, the samples are joined one by one with the two compounds and added with water as needed. The compounds are placed in the following order: 1:Water, 2:GG, 3:WPI.

The mixtures are then vortexed for 1 min and placed in a hot bath until they reach 81°C (temperature control is done with the aid of a thermometer). Reaching the desired temperature the mixtures are placed in a ice bath, to be cooled until they are ready for the tribological tests.

The preparation of the mucin solutions is a relatively simple procedure. They should constitute 3.2 ml of the final solutions for tribology. Therefore, for better control, they are placed in 5 ml syringes and sealed with parafilm. The mucin is dissolved in artificial saliva and shaken manually to favor its mixing.

## 3.3 Preparation of controls solutions

In order to study the influence of astringent and noon-astringent compounds on the lubrication and friction behaviours of artificial saliva, several control solutions were prepared. The astringents: Chitosan medium molecular weight (Chitosan), Iron chloride hexahydrate (Iron), Whey (WPI) and Bovine Submaxillary Mucin (BSM), and the non-astringents: Carboxymethyl Cellulose (CMC), Gellan Gum Texture (GG) (Biegler et al., 2016).

The solutions for the controls of the experiment were of similar preparation. The controls were initially weighed at the same concentration of 1.5% (w/v), requiring a total volume of 14.4 ml per compound for the various tests. However about 30 ml were prepared, so that there is sufficient quantity, preventing losses from affecting the required volume. Chitosan, Iron, CMC and Gellan

Gum were prepared for this concentration. To prepare the Chitosan, it was necessary to dilute it in HCl (0.1M). The rest of the compounds were diluted in distilled water.

The mucin solutions used as controls correspond to the high and low concentrations used in the DOE (0,1% and 0,25% (w/v)). They're meticulously measured and diluted in salivary fluid.

As for the WPI, a concentration of 10% (w/v) was used. This compound is also diluted in distilled water, but after achieving a minimally homogeneous mixture, this solution is placed in a falcon, which is placed in the thermoblock, shaken at 300 rpm and a temperature of 81 °C for 15 min.

## 3.4 Artificial Saliva Preparation

The preparation of artificial saliva is a relatively rapid process. After the quantities of each required reagent were selected and sized, a 1 L beaker was filled with distilled water. The reagents with the corresponding concentrations shown in Table II were placed in no specific order in the beaker subjected to magnetic stirring. The saliva was then allowed to stir for 30 min.

After agitation, it was necessary to confirm that the pH of the solution was neutral. The pH was measured with the aid of a pH meter and corrected with a solution of HCl (0.1M). The ready-to-use solution is then placed in the refrigerator, to avoid degradation.

**Chapter III - Table II** - Estimated values for the respective constituents of artificial saliva adapted for this study.

**Source:** (PYTKO-POLONCZYK1, JAKUBIK1, PRZEKLASA-BIEROWIEC1, & MUSZYNSKA2, 2017)

| Reagents | Quantities (mg/L) |
|---|---|
| NaCl | 1500 |
| KCl | 1000 |
| NaHCO3 | 750 |

## 3.5 Tribological Experiments

### 3.5.1 Tribological Set-up

In this dissertation it was necessary to produce a sample holder prototype able to confine the liquid sample during the tribological experiments.

The carriage of the tribometer drive, in this case, rotary, to fix the sample holder of the tests to be carried out in this work, has a diameter of 96.50 mm. The purpose was to place a glass slide (20x26x0,4 $mm^3$) on a cylinder-shaped object that held the sample (WPI+GG+Mucin+Saliva). A cover has also been developed in order to avoid sample projection. In order to hold PDMS hemispheres, a pin holder was also developed (Figure 1).


**Chapter III - Figure 1-** Tribological experimental set-up.

The sketches were translated to AutoCad for later printing using the 3D Printer.

- ## Suport Base

To develop this piece (Figure 2), a cylinder with a diameter corresponding to that of the rotary base of the drive, 96.5 mm, and a height of 10 mm was built. After 2D sketches were drawn with two squares with the following dimensions: 45.3 x 45.3 $mm^2$ and 40.3 x 40.3 $mm^2$, two small 2-pin inserts were also designed, to anchor the sample holder during the rotational movement. These two entrances have a dimension of 4.15 x 4.15 $mm^2$ and a depth of 1mm. The 2D drawings are finally extruded with heights of respectively 8 mm and 3 mm.

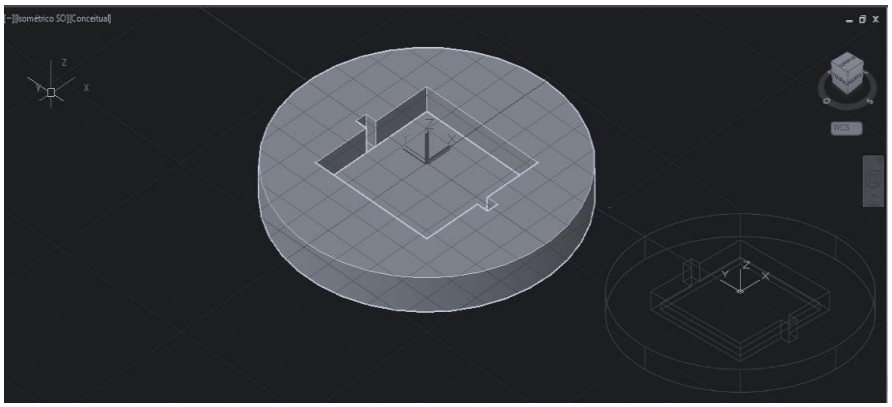

**Chapter III - Figure 2 -** AutoCAD design of Custom Visual Styles of the Support (Conceptual and 2D Wire structure).

- ## Sample holder

The sample holder piece (Figure 3) was designed following the same methodology as the base support. In this case, two well joined pieces were created: one that will be the perfect fit with the support piece and another where the sample is poured.

In the insert, using the 3D Tools, two boxes are drawn, with respectively 44.5 mm and 40.5 mm sides. These boxes are extruded with heights suitable for fitting in the support piece; the largest with 8 mm and the other with 5 mm, and then united by the command "Union". Two small pins (dimensions 3x3x8 $mm^3$) were also drawn, which are attached to the frame, which will interlock the sample holder.

Still in this component, a depression is built where a glass coverslip will be placed using the 2D tools, a Polyline constructed that includes the dimensions of the blade (26x20 $mm^2$), taking into account the clearance, calculated for 3D printing of 0.15 mm. The 2D sketch should be then extruded, using the command "Extrusion" to a height of 0.4 mm. The component was then subtract to the main piece creating the depression.

As for the part where the sample is deposited, 2 cylinders were designed, with respectively 40.5 mm and 38 mm diameter, 20 mm high, which are subsequently subtracted with the Subtract command. This piece is joined to another, giving rise to a glass format where it is possible to place the glass sheet and the sample, which will be submitted to the tribological tests.

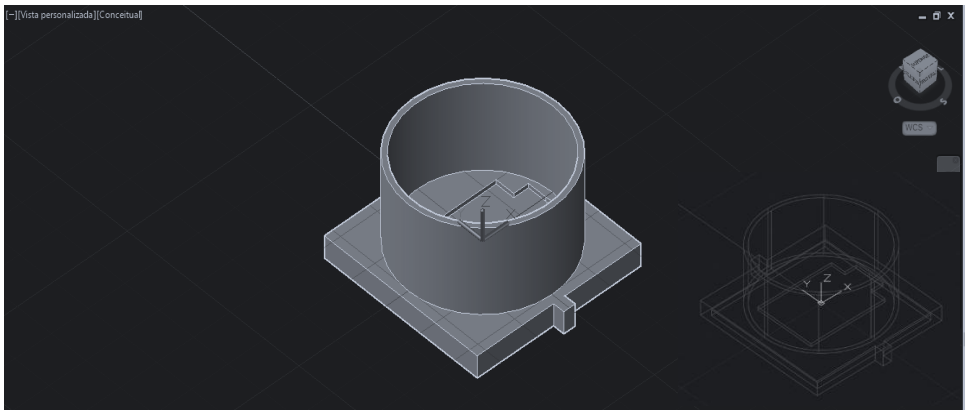

**Chapter III - Figure 3 -** AutoCAD design of Custom Visual Styles of the Sample Holder (Conceptual and 2D Wire structure).

- ## Cover piece

In order to construct the cover, it was necessary to resort to drawing 3D structures once more (Figure 4). Two cylinders were extruded: the outer cylinder has a diameter of 46 mm and a height of 30 mm and an inner cylinder with a diameter of 40 mm and height smaller 1 mm in relation to the outer cylinder. Afterwards, "Subtract" command was used to create a hollow structure inside.

A 30 mm hole was made in this opening and using the press pull command, the desired hole was generated.

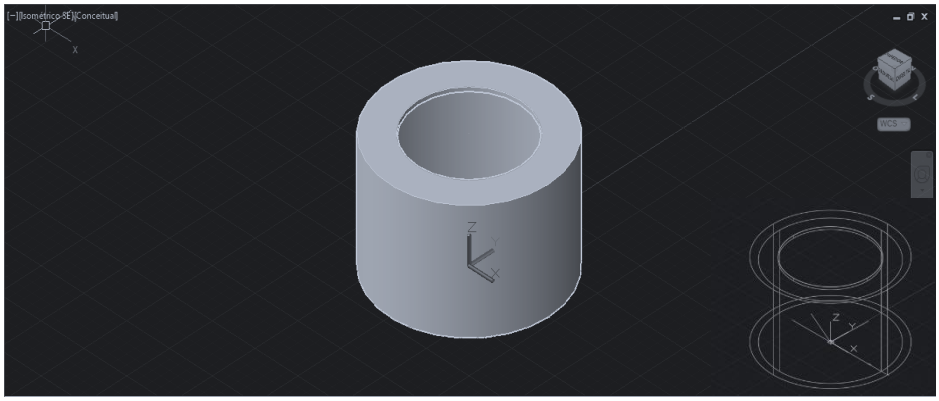

**Chapter III - Figure 4 -** AutoCAD design of Custom Visual Styles of the Cover (Conceptual and 2D Wire structure).

- ## Upper specimen holder

This structure was assembled in order to keep the PDMS beads, thus preventing the hemispheres from moving during the tribotests.

For this purpose, two pieces were constructed (Figure 5): An inner cilindrical pin where the

hemisphere is positioned and an outer ring that will lock securely the PDMS samples.

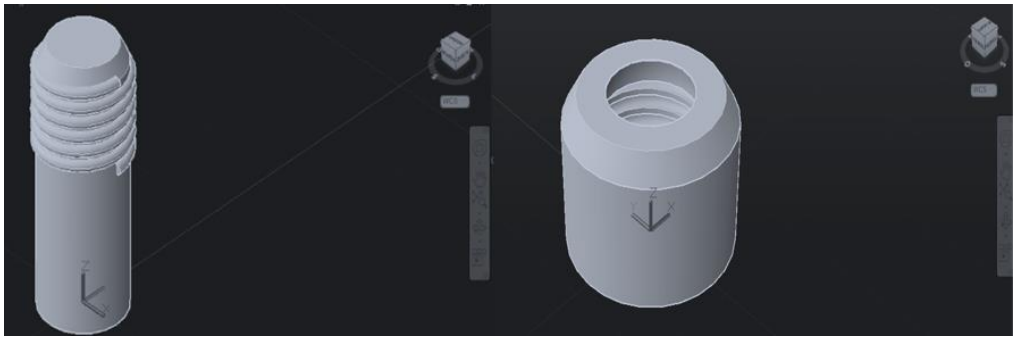

**Chapter III - Figure 5 -** AutoCAD design of Custom Visual Styles of the upper specimen: inner and outer piece (Conceptual structure).

For the outer piece, two cylinders are drawn: 11.3 mm and 16.5 mm in diameter and a height of 10 mm, which are subsequently subtracted with the "Subtract" command. To produce a thread in the cylindrical pin the command Helix was used, adjusting as diameter and height, identical values to the ones of the inner wall, resulting in a helix with 6 turns. An auxiliary circle was designed with the use of 2D tools (diameter 0.6mm). By selecting the circle, it is necessary to place it in the solid mode and using the Sweep Command select the circle and the helix, to become a 3D structure. The propeller is then subtracted from the part.

In order to be able to secure the sphere, a cone-shaped 3D structure with a height of 4 mm was drawn. To obtain a cone it was necessary to make an opening and this is done resorting to the 3D tools, drawing a sphere with a diameter of 9.5 mm, which was then subtracted from the cone.

For the inner part, a cylinder was built, with 28 mm of height and a diameter of 10.5 mm. To create the thread, the same commands used in the outer piece were applied, but in this case the purpose was not no subtract the helix instead it was to unite it with the cylinder. To hold the hemisphere against the outer piece, a cone-shaped 3D structure was produced with a height of 2mm.

The designs were printed on the byFlow Focus 3D printer, using PLA + HA Shining Silver, as the printable material. This material was printed at 215°C, in a heated bed at 50°C.

### 3.5.2 PDMS Hemispheres Preparation

PDMS hemi-spheres and corresponding mold, were prepared using the Sylgard 184 Silicone Elastomer Kit. There is two main steps of preparation: the development of the mold (in a 15:1 proportion between PDMS and cross linker), where the PDMS hemi-spheres would be framed on, using a master (composed by 20 stainless steel balls of 10 mm diameter); and the other is the elaboration of the hemi spheres (10:1) (development and cleaning). The preparation of the mold is started with a stock solution of 15:1, prepared from the PDMS kit. 50g of solution are then weighed, with 45g PDMS and 3g of cross linker. After weighing, they're mix together very well and then placed in a falcon to be centrifuged (removing the air bubbles).

PDMS cross linker mixture is added to a petri dish in order to cover the bottom and then subsequently the air bubbles were removed in vacuum. The petri dish was cure for an hour at 65°C. It was then necessary to create a second layer of PDMS where the master would be put on, adding more PDMS (≈30 ml) and repeating the vacuum step and finally adding the master. The sealing is further enhanced by heating the layers again in the oven for 1 h at 65 °C.

- **PDMS surface modification: Plasma Oxygen Modification, Silanization and Plasma Cleaner**

The thin layer which is still on the mold and the bored thick layer were put in a plasma cleaner unit (Harrick Plasma, Ossining, USA) with exposure to a plasma of oxygen during 60 s at a stable pressure in the chamber of 0.8 Torr. To generate the plasma, the power source was adjust for medium level Radio Frequencies (RF). The mold is leaved there for 15minutes.

After the mold is completed and prior to use, the mold was subjected to silanization, with Trichloro (1H,1H,2H,2H-perfluorooctyl) silane (with a very small droplet) in order to facilitate peeling of the PDMS device from its mold. The mold was then closed and vacuum seal and put in the oven for 1h at 65 °C. For new hemi-spheres the modification with silanes, is the same as previously described, however the time in the oven is reduced to 30 min.

The finished hemi-spheres should be cleaned using the same plasma unit refered earlier. In this step, the chamber is evacuated down to 300 mTorr with posterior injection of $O_2$. After introducing the hemispheres, the oxygen will elevate the pressure to about 1000 mTorr and stabilizes at 800mTorr.

After the pressure stabilized, RF power was turned on to low configuration, being possible

to see, with visual inspection that the plasma (white) was ignited. The hemispheres were exposed to the $O_2$ rich atmosphere for 15 min.

### 3.5.3 Tribological Experiments

The friction tests were conducted on a Universal Tribometer (UMT-2) with a rotatory sliding system, supplied by Bruiker (USA). The geometry of contact chosen was the ball-on-disc geometry, where the PDMS hemisphere is attached to a cylindrical pin, subjected to a normal force of 1N, in contact with a spinning disc.

In relation to the tribopair, PDMS was chosen as the tribopair for the pin and smooth glass was chosen for the disc. Their properties (see Table III) allowed to obtain, through a hertzian calculator, the maximum contact pressure that had to be applied to the system. For each experiment, the tribopair PDMS/GLASS was used once and discarded to avoid cross contamination between measurements.

**Chapter III - Table III -** Mechanical and surface parameters of the materials used for tribological measurements in this study.

| | Young Modulus (MPa) | Poison ratio | Maximum Hertezian Contact Pressure (MPa) |
|---|---|---|---|
| **PDMS** | 2 | 0.5 | 0.4 |
| **GLASS** | 70000 | 0.35 | |

- **Procedure Script used in the Tribometer**

The procedure script was defined with preliminary tests. Based on Biegler et al. (2016), two methods of evaluating both the coefficient of friction and the lubrication regimes were established.

The samples were subjected to a initial mixing in order to promote homogenization between the paste/compound and the artificial saliva with BSM. The mixing was done using a velocity of 0.1 mm/s for 30 min (this velocity allows the mixing phase to be made, without overlapping the lubrication regimes that will be studied).

The next phase was called 2nd Stage: Speed Ramp. In this step it was necessary to create an acceleration ramp that allowed to cover all the regimens of lubrication. Since the Stribeck curve covers velocities from 0.1mm/s to 300mm/s, and considering the limitations of the test, which did not allow the velocity to be reached without compromising the amount of sample inside the sample holder, it was considered a ramp that would evolve from 0.1mm/s to 314.159mm/s (≈500rpm). This ramp allows to cover all the regimes having a duration of 60 seconds. After this ramp the Tribometer receives another information that indicates that it slows down for 20s and then rises.

### 3.5.4 Data Analysis software's

- **Excel**

The files taken from the machine are a priori transformed into text files.

To import the contents of the ".txt" files into Excel, follow these steps: Data→ From the text→ Select the file→ Configure (tabulate, delimit and format) the data→ Add to the spreadsheet.

Thus, from the tables provided, it is necessary to obtain the linear velocity, to obtain the Stribeck curves as a function of velocity. Considering to be in the presence of a uniformly accelerated circular motion, represented by Equation 1, where the omegas represent the angular velocity at any instant and initial, and the alpha the angular acceleration; And that the Tribometer provides a constant angular acceleration until it reaches the $w_f$ adjusted in the script and in the indicated time, it is enough then to convert to linear velocity using the expression, being then:

$$w_f(t) = w_0 + \alpha * t \tag{1}$$

$$\frac{v(t)}{r} = \frac{v_0}{r} + \alpha * t$$

$$v_{linear}(t) = v_0 + \alpha * t * r$$

Being that,

$$v_0 \rightarrow 0.1mm/s$$

$$w_0 \rightarrow 0.16\,rpm$$

$$\alpha = \frac{w_f - w_0}{\Delta t}$$

$$\Delta t = 60\,s$$

$$w_f(\frac{rad}{s}) = \frac{500\ rpm * 2\pi}{60\ seg}$$

$$w_0 = \frac{0.16\ rpm * 2\pi}{60\ seg}$$

$$\alpha = (500 - 0{,}16)\frac{2\pi}{60 * 60}$$

, assuming a constant acceleration and circular radius of motion = 6mm, linear velocity is given by Equation 2:

$$v_{linear}(t) = v_0 + \alpha * t * r \quad \textbf{(2)}$$

$$v_{linear}(t) = 0{,}1 + (500 - 0.16)\frac{2\pi}{60 * 60} * t * 6$$

Since t is the sequence of time points given by the equipment.

- **Qtiplot**

The qtiplot software allows the organization and visualization of the graphs of the various samples, being possible to observe the results by block or in a graph all together, as for example in the controls.

In this research we have used QtiPlot platform to represent all the graphs, namely the COF vs.sliding speeds.

1) Export a text files data
2) Organize the columns (names and units)
3) Do the smoothing by SG or Adjacent Average models (using a range of 500-1500 points) to achieve a well-smoothed graph (Adjacent Averaging method does wide smoothing).
4) Select the columns and plot the graphs using the commands. Change the scale to see more clearly the data.
5) Create a graph template that it can be used to all graphs and save all the projects.

## 3.6 Confocal Microscopy

### 3.6.1 Microstructure

The mixed solutions were prepared as described before. Proteins were stained with Rhodamine B (83689-1G). The samples were staining in the flow hood at room temperature. Firstly, the samples were fixed by slowing adding fixative solution (Formaldehyde 37% (v/v)) during 15

minutes. Then, it's necessary to remove the fixative and wash x3 with PBS. The next step is adding Rhodamine B enough to cover the sample (choose the smallest space to reduce solution waste), leaving it for 15minutes or longer and protect it from light (covering with aluminum foil). To remove Rhodamine B the samples have to be extensively wash with PBS until it is clear.

The solutions were placed on a slide with the corresponding coverslip sealed to prevent losses and was stored in the fridge to cool to 20ªC and stored in the absence of light. The microstructure of the samples was analysed 5 days after. The samples were observed with a 63x objective under a confocal laser scanning microscope (Confocal Laser Scanning Microscope LSM780 from Zeiss) in the fluorescence mode, excited at 561 nm with a laser Rhodamine B and and the emission fluorescence was recorded between 567 nm and 658 nm. Images were analysed and optimized with the software ImageJ and Zen Blue.

### 3.6.2 Roughness of PDMS

Laser scanning confocal microscope Zeiss LSM 700 used in this study belongs into the group of point scanning confocal microscopes. The study will provide data on objective selection, in this case x40 and x63oil objectives where used. To perform z-stack at several positions of the hemisphere were followed some steps as : choosing the center vs First/Last; manually focus the center of sample; set the same range and step size for each position o X-Y-Z coordinate and then the Software sets an offset to relate to center of the first position.

- **Image J**

Imaging analysis of the z-sactk file, was done to the 32 bit image and consisted on using some plugins. The plugins responsible for visualizing the stack, obtaining height-map + roughness data are, respectively, EPFL (Extended Depth of Field of EPFL) and SurfCharJ_1q. I performed a "Level surface", given the expected curvature of the sample, a "Local roughness analysis" and it was used a "Median Filter", on the latter applied to the entire stack. Running this plugins, it was obtained a serial of data (20) to which an average was applied, to obtain the RMS value.

## 3.7 Atomic Force Microscopy (AFM)

- **Roughness of Glass**

Atomic Force Microscopy (AFM) imaging was completed with the Bruker Icon Atomic Force Microscope, which incorporates the latest evolution on nanoscale imaging with characterization technologies on a large sample tip-scanning AFM platform. The cantilevers had resonant frequency of 251.76 kHz and a nominal force constant that range 10-130 N/m. Root mean square (Rms) roughness values were obtain using the Gwyddion software.

## 3.8 Scanning Electron Microscopy (SEM)

The morphologic characterization of the WPI and GG solutions was performed by Scanning electron microscopy (SEM) using a Quanta FEG 650 (FEI, USA). Dry samples were affixed on aluminium stubs covered by carbon ribbon, and then the samples were coated with gold and observed using an accelerating voltage of 5 kV under vacuum conditions.

## 3.9 Water Contact Angle: Goniometer Technique

The static water contact angle (WCA) of the modified and unmodified PDMS surfaces and glass was measured at room temperature using a Drop Shape Analyser 100 (DSA 100, KRÜSS Scientific Instruments, Germany). The used liquid was ultra-pure water and the droplet volume was 2 μL. The angles were obtained using the sessile drop method to extract the angle between the baseline and the tangent line at the solid-liquid interface. At least five measurements were carried out for every sample

## 3.10 DOE: Statistic Analysis

To deal with many parameters, statistical Design of Experiments (DOE) may be a particular useful tool. DOE provides experimental schemes where the parameters (factors) under study are combined at different levels to determine the influence of a particular factor on the response.

To plan the experiment and quantify the impact the variables studied and the impact of interactions between those variables in friction behaviour, was used design of experiments (DOE). The influence of the independent variables% GG,% WPI, %Mucin and sliding speed(mm/s) on

dynamic and static friction coefficient was analysed employing a central composite design with 3 factors, 3 central points and 3 blocks.(Table IV) (Wrobel et al., 2003).

**Chapter III - Table IV** - DOE of the study for WPI, GG and Mucins.

| Standard Run | Block | % WPI | % GG | % Mucin |
|---|---|---|---|---|
| **1** | 1 | 5.500 | 1.000 | 0.100 |
| **2** | 1 | 5.500 | 1.500 | 0.250 |
| **3** | 1 | 10.000 | 1.000 | 0.250 |
| **4** | 1 | 10.000 | 1.500 | 0.100 |
| **5 (C)** | 2 | 7.750 | 1.250 | 0.175 |
| **6** | 2 | 5.500 | 1.000 | 0.250 |
| **7** | 2 | 5.500 | 1.500 | 0.100 |
| **8** | 2 | 10.000 | 1.000 | 0.100 |
| **9** | 2 | 10.000 | 1.500 | 0.250 |
| **10 (C)** | 2 | 7.750 | 1.250 | 0.175 |
| **11** | 3 | 3.985 | 1.250 | 0.175 |
| **12** | 3 | 11.514 | 1.250 | 0.175 |
| **13** | 3 | 7.750 | 0.831 | 0.175 |
| **14** | 3 | 7.750 | 1.668 | 0.175 |
| **15** | 3 | 7.750 | 1.250 | 0.049 |
| **16** | 3 | 7.750 | 1.250 | 0.300 |
| **17 (C)** | 3 | 7.750 | 1.250 | 0.175 |

| | |
|---|---|
| **Mucin(%)** | 1 |
| **Whey(%)** | 40 |
| **GG(%)** | 2.5 |

The Central Composite Design (CCD) is an effective design that is ideal for sequential experimentation and allows a reasonable amount of information for testing the lack of fit while not involving an unusually large number of design points. CCD model experiments can be represented in the form of the following equation:

$$Y = b_o + \sum_{i=1}^{n} b_i x_i + \sum_{i=1}^{n} b_{ii} {x_i}^2 + \sum_{i=1}^{n-1} \sum_{j=i+1}^{n} b_{ii} x_i x_j \qquad (3)$$

where Y is the predicted response; n is the number of factors; $x_i$ and $x_j$ are the coded variables; bo is the offset term; $b_i$, $b_{ii}$, and $b_{ij}$ are the first-order, quadratic, and interaction effects, respectively; i and j are the index numbers for factor (Demirel & Kayan, 2012).

The quality of the polynomial model was expressed by the coefficient of determination, namely, $R^2$ and Adj-$R^2$. The statistical significance was verified with adequate precision ratio and by the F test. The main effect estimates and factors interactions, model fitting, ANOVA and surface curves were made using Statistica (Tibco).

A set of center points, experimental runs whose values of each factor are the medians of the values used in the factorial portion are often replicated in order to improve the precision of the experiment. For each of the studied variables, high (coded value: +1.67) and low (coded value: -1.67) set points were selected as shown in Table V.

**Chapter III - Table V** - DOE central point.

| Variable Name | -1.67 (LOW) | -1 | 0 | | +1 | +1.67 (HIGH) |
|---|---|---|---|---|---|---|
| %WPI | 3.98 | 5.5 | **7.75** | **CenterPt** | 10 | 11.51 |
| %GG | 0.831 | 1 | **1.25** | **CenterPt** | 1.5 | 1.668 |
| %MUCIN | 0.049 | 0.1 | **0.175** | **CenterPt** | 0.25 | 0.300 |
| FOOD-INK %(V/V) | — | 50 | **60** | **CenterPt** | 70 | — |

## 3.11 Molecular Dynamics Simulation

The MD simulation in this thesis was carried out with the Large-scale Atomic/Molecular massively parallel simulator (LAMMPS) MD code.

### 3.11.1 Simulation methodology and stages

MD is routinely applied for the investigation of dynamical properties and processes in the field of structural biochemistry, molecular biology, pharmaceutical science, and biotechnology. This tool helps researchers to generate a trajectory of macromolecules such as protein, which generates a progress of simulated structure with respect to time.

Typically, in an MD simulation, it is important to guide through a methodology to accurately replicate the experimental conditions. In this case, the objective was to obtain a similar replicate

of what happens in the tribological experiments, trying to reproduce similar conditions, molecules and methodology used. To obtain the starting structure coordinates of the proteins of interest, it was necessary to search in 3D Data Banks. With the structures conceived, it is necessary to generate topology files, which contain all the information including bonded and non-bonded interactions required to define the molecule within the simulation.

Using tools like the Avogadro molecular editor software, it is possible to optimize the geometries of the molecules. Meanwhile, it is necessary to draft the script of the simulations by introducing some generic coefficients for the Force fields and test the geometry. The structures are put into the simulation box and usually immersed in water. When the simulator runs without errors, it was possible to accurately determine the box dimensions and confirm the atomic structures presented in the simulation. In this study various molecules were selected that correspond to the ones used in the tribological system and that were included in the simulation box: Beta-lactoglobulin, Gellan gum, PDMS, Water (TIP4P model) and Mucins (5B and 7). It was important to note that in nature, most proteins are at least partially within an aqueous environment. Once the required structures are optimize the force-fields are selected and the protein structure is put into a simulation box and immersed in water.

After minimization, the system undergoes NVE (fixed number of atoms, N, fixed volume, V, and fixed energy, E) integration to update position and velocity for atoms each time step, at a temperature of 300K. At this point, the system is called as an ensemble, which is defined as a collection of all possible systems that have varied microscopic state, but have a single thermodynamic state (A. Singh et al., 2018).

The MD simulation only reproduces one formulation of the DOE, as a result of limited time available and since this system is representative:

**7.75% WPI + 1.25% GG + 0.175% Mucin (5B and 7)**

### 3.11.2 Databases

The structures used in MD simulation were obtain in multiple databases. The atomic coordinates and other information describing the proteins were avaible in the Protein Data bank (PDB) file format. The molecules, Beta-Lactoglobulin (PDB ID:2Q2M), Gellan Gum (PolySac3DB ID: Gellan Native) and Mucins 7 and 5B (Modbase ID: Q9HC84.2 and Q8TAX7) were obtain from

RCSB PDBs, CERMAV Database of Polysacharides 3D Structures (PolySac3DB) and Salilab Database of Comparative Protein Structure Models (ModBase).

### 3.11.3 Avogadro

After downloading the PDB files from the respective databases, it is necessary to import the ".pdb" files into Avogadro, in order to optimize the geometry of the molecules (ForceField Optimization). This Optimizer tool continuously optimizes molecular geometry through molecular mechanics, allowing to manipulate a molecule while molecular geometry is being optimized (energy minimization of the atomic configuration).

When optimizing, an adequate the force field must be use. This parameter is chosen based on the literature and may be different for the different types of molecules. Since Avogadro provides 5 force fields (UFF, GAFF, Ghemical, MMFF94 and MMFF94s), with the optimizations being carried out using force field like the Universal Force Field (UFF) and Merck Molecular Force Field (MMFF94). The GROMACS package, with GOMOS9643a1 force field was chosen to help to assess some of the parametrizations of the force fields to use in the processing stage of the simulations. Once the optimization is done the file is exported as a LAMMPS file (.lmpdat).

In the following are presented some of the parameters used to minimize the energy of the molecules in Avogadro (Table II):

**Chapter III - Table VI** - Optimization parameters used in Avogadro.

| | Force field | Optimization algorithm | Energy tolerance | Steps |
|---|---|---|---|---|
| **Mucins 5B and 7** | MMFF94 | Conjugate Gradients | $10^{-6}$ | 500 |
| **Gellan Gum and β-Lactoglobulin** | UFF | Conjugate Gradients | $10^{-6}$ | 500 |

### 3.11.4 Parameters to the simulation

- **Number of molecules in simulation box**

In order to calculate number of molecules and the size of the simulation box (Table IV), it is necessary to calculate the number of molecules present in 100 ml of solution, considering the concentration (%) of the molecule in the final solution: The molecules molar mass (Table II) was obtained from the Avogadro software, by means of the molecule properties tool.

**Chapter III - Table VII** - Molar mass of molecules involved in MD simulation.

| Molecules | Molecular Weight (Da) |
|---|---|
| **WPI (Beta-lactoglobulin)** | 19497 |
| **GG** | 500 |
| **Mucin 5B** | 7226.186 |
| **Mucin 7** | 6783.309 |

The following Equations were used to obtain the number of each type of biomolecules in the prepared solutions and simulation domain, respectively.

$$N_{solution} = \frac{m_{molecule(\%)}}{M} \times N_A \quad (\mathbf{4})$$

$$N = \frac{Volume_{simulation\ box} \times N_{solution}}{Volume_{solution}} \quad (\mathbf{5})$$

**Chapter III - Table VIII -** Box dimensions and number of molecules used in MD simulation.

| BOX DIMENSIONS (A) | (M^3) |
|---|---|
| 1758120 | 1.75E-24 |
| **MOLECULES** | **NUMBER OF MOLECULES IN THE SIMULATION** |
| WPI | 17 |
| GG | 106 |
| Mucin 5B | 1 |
| Mucin 7 | 1 |

Since the MD simulations were performed using the units "real" of the LAMMPS code, the following expression were used to convert from macroscopic units used in the tribological system. In order to calculate the force to be used on the top PDMS layer, it was used the following equation:

$$P_{máx} = \frac{F}{A} \quad (\mathbf{6})$$

$$F\left(\frac{kcal}{mol.\text{Å}}\right) = 6.94 \times 10^{-11}(N)$$

, where, A, represents the area of the upper specimen in the simulation $1\text{Å} = 10^{-10}m$ and $P_{máx}$ , represents the maximum contact pressure applied $P_{máx} = 0.4MPa$.

For the sliding speeds values the following conversion factors was used:

$$V\left(\frac{\text{Å}}{fs}\right) = 10^5(\frac{m}{s})$$

The values adjust for the atomistic simulations are indicated in Table IX and their respective equivalents in macroscopic units.

**Chapter III - Table IX -** Velocity's used in MD simulation.

| Velocity | m/s | A/fs |
|---|---|---|
| **Min** | 0.0001 | $1x10^{-9}$ |
| **Max** | 0.3141578 | 3.14158E-06 |

## 3.11.5 MD simulation script

In this section the most important LAMMPS commands used in our input script file are explained in more detail. The entire script can be found in Appendix.

Initially, two variables are declared to easily change the timestep values and damping factor for thermostating. As such, the timestep, Langevin thermostat damping factor and applied normal force values used are shown in snippet of LAMMPS code, as follows:

```
variable dt equal 0.001 # timestep (fs)
variable Tdamp equal ${dt}*100 # damping factor in Langevin thermostat
variable load equal -37.93 # units: kcal/mole-Angstrom (6.9477E-2 nN)
```

The next step consist in the definition of the units. This command sets the style of units used for a simulation. It determines the units of all quantities specified in the input script and data files, as well as quantities to output to the screen, log file, and dump files:

```
units real
dimension 3
boundary p p p
atom_style full
```

Subsequently, the size of the simulation box (computational domain) is defined according to the previously declared region dimensions (in Å units): This command defines a geometric region of space. Commands to define 3D simulation, periodic boundaries conditions in all axis are also defined. This box was constructed, using the command “create_box”, like shown:

```
region box block -21 371 -136 169 -38 190 units box
create_box 70 box bond/types 12 angle/types 17 dihedral/types 19 extra/bond/per/atom 4
extra/angle/per/atom 6 extra/dihedral/per/atom 36
```

Then the molecules (WPI, GG, MUC5B,MUC7, water and PDMS) were inserted into the simulation, using the "read_data" command (only one example is herein shown for reference).

```
read_data m7_mol_ID.data add append offset 34 2 1 0 0 shift 180 0 111 group muc7
```

One of the most important parts in an MD simulation is the section which implements, the force fields and correspponding parametrization. Hybrid models where specified pairs of atom types interact via different pair potentials can be setup using the "hybrid pair_style" command. The hydrid style chosen, one pair style is assigned to each pair of atom types. The water model used was the four-point TIP4P/2005 rigid water model.

In the next section of the script, were listed the styles and coefficients formulas that are consistent for built-in LAMMPs and CHARMM force fields for all type of interactions , namely non-bonded, bonded and long-range interactions and between the atoms involved. The keywords englobe "pair", "bond", "angle" and "kspace" styles that are adequate for each type of intermolecular and intramolecular interactions. The coefficients associated with each style were set for every pair of atom types, and are specified by a set of commands, as follow:

```
pair_style hybrid lj/cut/tip4p/long 1 2 1 1 0.1546 13.0 8.5 lj/cut/coul/long 13.0 8.5
lj/class2/coul/long 13.0 8.5 lj/long/coul/long cut long 13.0 8.5 lj/cut 3.0
                                        (…)
bond_style hybrid harmonic class2 # PDMS/Water
                                        (…)
angle_style hybrid harmonic charmm # for H2O + biomolecules
                                        (…)
kspace_style pppm/disp/tip4p 1.0e-5 # long range solver
```

Parameters values for water molecules and mixed interactions are described in the following lines of LAMMPS code. Values for the bond parameters for the various biomolecules are also indicated.

```
# TIP4P/2005 water model LJ coefficients (epsilon, sigma)
pair_coeff 1 1 lj/cut/tip4p/long 0.1852 3.1589 # O-O
pair_coeff 2 2 lj/cut/tip4p/long 0.0 0.0 # H-H
pair_coeff 1 2 lj/cut/tip4p/long 0.0 0.0 # O-H
bond_coeff 1 harmonic 0.0 0.9572 # H-O # bond
angle_coeff 1 harmonic 0.0 104.52 # H-O-H
                                        (…)
# INTERMOLECULAR INTERACTIONS
# mixed interactions H2O/biomolecules
pair_coeff 1*2 3*65 lj/cut 0.3 4.0
# parameters mixed interactions H2O/PDMS
pair_coeff 1*2 66 lj/cut 0.394360 4.39 # H2O-C interactions
                                        (…)
```

```
# BIOMOLECULES AND PDMS FF COEFFS
# biomolecules intramolecular interactions
pair_coeff 3*65 3*65 lj/long/coul/long 3.0 6.0
#PDMS-PDMS interactions
pair_coeff 66*67 66*67 lj/cut/coul/long 0.1944 3.73 # C-C, H-H, C-H interactions
                                        (…)
# dihedral coeffs for BLG and GG molecules
dihedral_coeff *18 harmonic 8.0 1 2
# for PDMS, if using COMPASS class2 dihedral style.
dihedral_coeff 19 class2 100 75 100 70 80 60
                                        (…)
bond_coeff 2*10 harmonic 0.0 0.9572 # values for biomolecules
bond_coeff 11*12 class2 1.0 100.0 80.0 80.0 # values for PDMS
angle_coeff 2*17 harmonic 1.0 80.0 # angle coeffs for PDMS and biomolecules
```

After defining the force field parameterization, it is necessary to treat the molecules as independent rigid bodies and for this the "fix rigid" command was used, which allows each body to move and rotate as a single entity when the coordinates, velocities, and orientations of the atoms are updated:

```
fix rgd rigidmol rigid/nve molecule langevin 300 300 ${Tdamp} 428984
```

In this case, the "fix_rigid/nve" style was used, constrained to a Langevin thermostat set at 300K.

The dynamic section of the script includes multiples runs and "fix" commands. From this section a tribological was simulated at the nanoscale. In it commands are applied so that sets of molecules such as water H2O, become indivisible molecules throughout the simulation (fix_shake command). Other commands were declared that describe the syntax for recording the forces applied in the PDMS, as well as to perform the relative movement of the PDMS.

All of these simulation dynamics end with the creation of dump.file outputs that contain parameters trajectory of all simulation atoms or other properties of the simulations. These outputs were used in OVITO visualization.

```
fix shakeh2o water shake 0.0001 200 5000 b 1 a 1
                    (…)# Apply normal force on upper glass specimen
fix load1 Si_hi addforce 0.0 0.0 $(v_load) # apply external force to fixed Si atoms
fix load2 O_hi addforce 0.0 0.0 $(v_load*16.00/28.0855) # apply external force to fixed
Oxyg atoms
                      (…)# move upper specimen w/ constant speed
fix 4 hi-fixed move linear 1E-1 NULL NULL units box
```

In addition to dump.files, LAMMPS script still provides the data with the forces ($Fx$,$Fy$,$Fz$) that that are used to achieve the effective COF. That data is obtained using a “fix_file” command where the output is a file that contains the vectors with the intended forces. The file has a filename where it is specified the place output generated by this fix will be written.

```
fix f_av_time_lo lo-fixed ave/time 10 10 100 f_1a[*] file f_glass-lo.W${load}.txt
fix f_av_time_hi hi-fixed ave/time 10 10 100 f_1b[*] file f_glass-hi.W${load}.txt
```

# CHAPTER IV

*To be submitted in an international journal*

## Study of friction and astringency of phase-separated 3D food-inks by oral tribology and molecular dynamics

**M.A.Pires,C.S.Abreu[b], S.M.Oliveira[a]**

[a]INL(International Iberian Nanotechnology Laboratory), Av. Mestre José Veiga, Braga 4715-330, Portugal

[b]Center for Microelectromechanical Systems (CMEMS-UMinho), University of Minho, Guimarães, Portugal

### 4.1 Abstract

The friction assessment is increasingly becoming an innovative technique to study the oral processing of food-inks. Mouthfeel and textural characteristics such as astringency have been linked to friction on the tongue and palate. Astringency is characterized by an unpleasant oral mouthfeel (dry mouth) affecting the consumer perception of food quality. In the present study, through tribological characterization and molecular dynamics modelling, phase-separated food-inks were optimized towards the reduction of astringency perception. Design of experiments approach employed demonstrated the main effects of the food-inks and their correlation on friction assessment. Molecular dynamics simulation technique allowed to model the tribological system and obtain friction magnitudes observing prevailing friction mechanism at the nanoscale.

### 4.2 Introduction

In the earlier years, numerous studies associated milk and dairy consumption with favourable effects on body weight and metabolic control (Anderson, Luhovyy, Akhavan, & Panahi, 2011). Milk and dairy products have numerous advantages over competitors when used as ingredients: they are colourless, have a bland taste, are rather stable to process and are essentially free of toxins. As ingredients, dairy products are used mainly because of their unique physicochemical properties.

Milk proteins and whey proteins, in particular, exhibit high nutritional values, contributing to many functional properties to food formulations. These proteins are widely used as ingredients in formulated foods, being recognized as safe (GRAS) for the Food and Drug Administration (FDA), for its intended use (Rodrigues et al., 2015).

Throughout the time, a flavour related to a high level of astringency in food and beverages containing whey proteins, appear to be concerning. The astringency perception is considered in the context of taste and sensations as it is an oral mouthfeel typically caused by food. According to Peleg (1998) it is a complex phenomenon that elicits a range of sensations, but the majority of the publications relate it with dryness, roughing, and puckering feelings of the oral epithelium (ASTM, 2004; Dinu et al., 2018; R. Jackson, 2016; Jiang et al., 2014; Peña-Neira, 2019; Valentova & Panovska, 2003a).

Whey proteins include β-Lactoglobilun (β-LG), α-Lactalbumin (α-LA), Bovine serum albumin (BSA), Lactoferrin and Immunoglobulins. β-LG is the major whey protein in bovine milk, constituting >50% of the total whey proteins. β-LG is characterized by their high pH-dependent structure and properties, containing many charged groups (Kontopidis, Holt, & Sawyer, 2004). This strong pH dependency suggests that electrostatic interactions could play a significant role in the interactions of β-LG with other molecules. The amino acid sequence and its three dimensional structure, makes this protein apart of the lipocalin family, meaning it can bind to small hydrophobic ligands (Vardhanabhuti, B.; Foegeding, 2009).

Understanding the interaction characteristics between β-LG and mucins is related to a current discussion on the basis of astringency phenomenon. Mucins are a family of large, extracellular glycoproteins and are known to be responsible for the slipperiness of saliva (Çelebioğlu et al., 2016). One of the most known models is that astringents interact with saliva to form aggregates to deplete the lubricant (saliva) from the tribological interactions inside the mouth (Vardhanabhuti, Cox, Norton, & Foegeding, 2011).

Food products are complex multi-component mixtures that hinder comprehension of the role of each ingredient in their interactions and thus their influence on the properties of the final product. Relevant food structures can be obtained by the combination of native or denatured proteins with polysaccharides (Picone & da Cunha, 2010). Polysaccharides and proteins are biopolymers that are often found together in foods. Their interactions in solution and with the solvent (water in this case), rule the solubility and co-solubility, the viscoelastic properties of the final mixture and their behaviour when facing different interfaces. The mixing of these biopolymers

under repulsive conditions often results in the phase separation phenomenon. Phase separation in protein-polysaccharide systems is a kinetic process, regulated by the complexity of the gel microstructures and multiple factors that influence their compatibility (molecular weight, pH, ionic strength, ratio, total concentration, heat treatment, pressure, shearing, etc) (Benichou, Aserin, & Garti, 2002; Turgeon, Beaulieu, Schmitt, & Sanchez, 2003).

Gelling polysaccharides such as carrageenans, gellan gum and agar show helix (ordered)–coil (disordered) transition with increasing temperature, corresponding to a gel–sol transition. Gellan gum is a linear and anionic hetero-polysaccharide produced by *Sphingomonas elodea* (Miyoshi & Nishinari, 1999). The conformational state of the polysaccharide may also determine interactions with other biopolymers, such as proteins. Proteins usually interact with the polysaccharide junction zones in the helix state if the pH value is low (Burova et al., 2007).

In order to quantify the Astringency phenomenon multiples systems (direct, indirect and by simulation) are discussed. In the study of Vidal et al. (2004), they commented that experiments are required to link assembly processes with sensory perception. They expressed succinctly that *"constructing mouthfeel perception can be a highly complex process, this process depends on the presence of each component by itself but also depends on interactions between components and on the structure of the resulting molecular assemblies".* Meaning that the study of the behavior, not only of the components individually but with each other, must converge with the use and help of several techniques of different fields (Scollary, Pásti, Kállay, Blackman, & Clark, 2012).

Recently, tribology has raised as an innovative instrumental approach to study the oral processing of food emulsions in a simulated oral environment (Chen & Stokes, 2012). Tribometers are also able to quantify in-mouth sensory features, such as astringency. Some authors have explored sensory astringency using tribology tools, taking into account two critical factors in the design of a Tribometer, to mimic oral processing, involving (1) the control of the sliding and or rotating between the two surfaces and (2) the surface properties of the substrate materials(Prakash et al., 2013; Upadhyay et al., 2016).

More recently, new areas of tribology have appeared, including nanotribology, i.e. the investigation of friction, wear and lubrication at the nanoscale as applied, for example, to micro- and nano-electromechanical systems (MEMS/NEMS), magnetic storage and biotribology (Vakis et al., 2018). The main tools used in tribological modelling start from analytical models to continuous models, discrete, mechanical and multiphysical approaches, appropriate for simulations characterized by diverse times and length-scales.

Authors like Ramos-Pineda et al. (2017), and Ferrer-Gallego et al. (2017), recently dedicated their time to add to the knowledge of the interactions between phenolic compounds and salivary proteins, using several techniques combined with molecular dynamics (MD) simulation and MD simulation methods that could explain the synergisms of the astringency observed between that compounds and also postulate a molecular mechanism.

In this paper, we intend to highlight the mechanisms responsible for the oral astringency phenomenon, leading atomistic computational simulations (Molecular Dynamics) and subsequent experimental validation by Tribological tests, to characterize the friction behaviour and the interactions of 3 systems: proteins (whey protein), polysaccharides (gellan gum) and mucins.

The food-inks were produced by phase separated gellan gum (GG) and whey protein (WPI) and tested in lubricated conditions using mucins and artificial saliva. In order to assess the potential of those food-inks, resorted to the Design of Experiments (DOE) approach to analyse the impact of WPI, GG and mucins on the static and dynamic COF, on different velocities. Correlating those, with the microstructure of the food-inks and molecular dynamics simulation could result in relevant information that may contribute to the sensation of astringency perceived in the oral cavity.

In addition, the tribo-pairs used in tribological assessment were designed and characterized by Confocal and Atomic Force microscopy for roughness analysis, Scanning Eletron microscopy for topography and Water contact angle to gauge about the wettability.

## 4.3 Materials and Methods

### 4.3.1 Materials

Materials used in this research are mentioned here and were provided by the following companys: Chitosan (Sigma-Aldrich), Iron(III) chloride hexahydrate (Sigma Aldrich), Carboxymethyl Cellulose –High Viscosity (Sigma-Aldrich), Gellan Gum (Guzman), Sodium Chloride (Sigma-Aldrich), Potassium Chloride (Sigma-Aldrich), Sodium Bicarbonate (Sigma-Aldrich), Whey Protein (Bulk Powders), Bovine Submaxillary Mucin (Sigma-Aldrich), PLA + HA Shining Silver (ColorFabb, Netherlands), RhodamineB (Sigma Aldrich), Glass (Marienfeld), Polydimethylsiloxane (Sylgard), Trichloro(1H,1H,2H,2H-perfluorooctyl)silane (Sigma-Aldrich).

## 4.3.2 DOE: Design of Experiments

To plan the samples to be tested, to quantify the influence of the studied variables and their correlation on friction and lubrication behaviour, a statistical design tool (DOE) was used. The influence of the independent variables % GG, % WPI, % mucin and sliding speed (mm/s) on dynamic and static friction coefficient was analysed employing a central composite design with 3 factors, 3 central points and 3 blocks (Table I). The CCD is an effective design, ideal for sequential experimentation and permits an amount of information for testing the lack of fit while not involving an unusually large number of design points. CCD model responses can be represented in the form of the following equation:

$$Y = b_o + \sum_{i=1}^{n} b_i x_i + \sum_{i=1}^{n} b_{ii} {x_i}^2 + \sum_{i=1}^{n-1} \sum_{j=i+1}^{n} b_{ii} x_i x_j \qquad (\mathbf{1})$$

where Y is the predicted response; n is the number of factors; $x_i$ and $x_j$ are the coded variables; bo is the offset term; $b_i$, $b_{ii}$, and $b_{ij}$ are the first-order, quadratic, and interaction effects, respectively; i and j are the index numbers for factor (Demirel & Kayan, 2012; Gorji & Bahram, 2010).

**Chapter IV - Table I -** DOE for the study of WPI, GG and Mucins variables

| Standard Run | Block | % WPI | % GG | % Mucin |
|---|---|---|---|---|
| **1** | 1 | 5.500 | 1.000 | 0.100 |
| **2** | 1 | 5.500 | 1.500 | 0.250 |
| **3** | 1 | 10.000 | 1.000 | 0.250 |
| **4** | 1 | 10.000 | 1.500 | 0.100 |
| **5 (C)** | **1** | **7.750** | **1.250** | **0.175** |
| **6** | 2 | 5.500 | 1.000 | 0.250 |
| **7** | 2 | 5.500 | 1.500 | 0.100 |
| **8** | 2 | 10.000 | 1.000 | 0.100 |
| **9** | 2 | 10.000 | 1.500 | 0.250 |
| **10 (C)** | **2** | **7.750** | **1.250** | **0.175** |
| **11** | 3 | 3.985 | 1.250 | 0.175 |
| **12** | 3 | 11.514 | 1.250 | 0.175 |
| **13** | 3 | 7.750 | 0.831 | 0.175 |
| **14** | 3 | 7.750 | 1.668 | 0.175 |
| **15** | 3 | 7.750 | 1.250 | 0.049 |
| **16** | 3 | 7.750 | 1.250 | 0.300 |
| **17 (C)** | **3** | **7.750** | **1.250** | **0.175** |

The main effect estimates and factors interactions, model fitting, ANOVA and surface curves were made using Statistica (Tibco).

- **Food-ink Formulation**

Concentrated solutions of 40% whey protein and 2% gellan gum were dissolved in distilled water during magnetic stirring. The biopolymers were allowed to stir for at least 1h. Following the standard runs of the experimental design, the mixtures are prepared one by one, order as: (1) Water, (2) GG, (3) WPI.

Phase separation is promoted when the mixtures were vortexed for 1min and placed in the hot bath until they reach 81°C. Reaching the desired temperature, they're placed in the ice bath.

Mucin solutions were dissolved in artificial saliva and shaken manually to favor its mixing. For better volume accuracy, they were placed in 5 ml syringes, sealed and put in the fridge.

Salts and quantities used in the preparation of the artificial saliva are based on Pytko-Polonczyk et al. (2017), it was used: 1500 mg/L of NaCl, 1000 mg/L of KCl and 750 mg/L of NaHCO3. After mixing the salts in distilled water, it was necessary to guarantee that the pH of the solution was neutral, which was done with HCl (0.1M). Saliva was then kept in the refrigerator.

- **Preparation of controls solutions**

Astringents and non-astringents compounds were prepared to serve as control solutions in the tribo-experiments: Chitosan medium molecular weight (Chitosan), Iron chloride hexahydrate (Iron), Carboxymethyl Cellulose (CMC), GG, Saliva and Bovine Submaxillary Mucin (BSM). They were weighing and then dissolved during magnetic stirring.

### 4.3.3 Tribology

- **Tribology Experiment: Ball-on-disk tribometry**

The friction tests were conducted on a Universal Tribometer (UMT-2) with a rotatory sliding system, supplied by Bruiker (USA), using a ball-on disc contact geometry.

Polydimethylsiloxane (PDMS) hemispheres attached to a customized sample holder were slide against glass cover slides under a constant load of 1N. As shown in Table II, the maximum contact pressure corresponding to the applied load was calculated from Hertzian calculator. For each measurement, the tribopair of PDMS-glass was used only once and discarded to avoid cross contamination between experiments.

**Chapter IV - Table II** - Mechanical and surface parameters of the materials used for tribological measurements in this study (Çelebioğlu et al., 2016).

| | Young Modulus (MPa) | Poison ratio | Maximum Hertzian Contact Pressure (MPa) |
|---|---|---|---|
| **PDMS** | 2 | 0.5 | 0.4 |
| **glass** | 70000 | 0.35 | |

The tribology procedure was based on Biegler et al. (2016) approach, in which two methods of evaluating both the coefficient of friction and the lubrication regimes were analysed. The procedure was divided in two steps:

- 1st Stage (Mixing): This step consisted of a uniform circular motion at a constant velocity of 0.1 mm/s, during 30 minutes.
- 2nd Stage (Speed Ramp): In this step, it an acceleration ramp was implemented, in order to cover all the lubrication regimens. A ramp that would vary from 0.1 mm/s to 314.159 mm/s (≈500 rpm) in 60 s was set.

## • Geometry Design

To carry out the tribological experiments a prototype design of the sample holders had to be developed with the help of AutoCAD 2017 (Autodesk). The tribometer consisted of a lower drive, where the lower specimen sample holder was fixed and possesses a rotational motion. A glass cover slide with dimensions of 20 x 26 x 0.4 $mm^3$ (Marienfield) was securely placed in an intended base, surrounded by a cylinder (20 mm of height) to contain the viscous sample. A cover cylinder has also been developed in order to avoid sample leakage during rotation. To secure the PDMS hemispheres, a ball holder was also developed as illustrated in Figure 1.

(a)

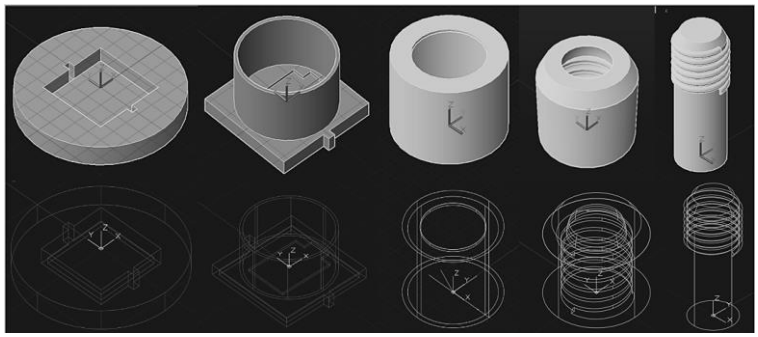

(b)

**Chapter IV - Figure 1** - AutoCAD designs of Custom Visual Styles: a) Conceptual structures and 2D Wire Structure and b) expanded 3D printed structures and final set-up.

The designs were printed on the byFlow Focus, which is a multi-material 3D printer, using PLA + HA Shining Silver, as the printable material.

- **PDMS Hemispheres Preparation**

PDMS hemispheres and mold were prepared using the Sylgard 184 Silicone Elastomer Kit. There were three main steps of preparation: (1) development of the mold (15:1), where the PDMS hemi-spheres would be framed on, using a master (composed by 20 stainless steel balls of 10mm diameter); (2) silanization; and (3) elaboration of the hemi-spheres (10:1) (development and cleaning).

The surface of the mold was put in a plasma cleaner unit (Harrick Plasma, Ossining, USA) with exposure to plasma oxygen during 60 s at a stable pressure of 0.8 Torr. After the mold was completed and prior to use, the surface of the mold was modified with silanization, using Trichloro(1H,1H,2H,2H-perfluorooctyl)silane, in order to facilitate peeling of the PDMS device from the mold. The mold was closed and vacuum seal, and put in the oven for 1 h at 65 °C. The mold was reused after short modification with silanes (30 min). The hemispheres produced in the mold, were cleaned using the same Plasma Unit and used after 2 days.

### 4.3.4 Confocal Microscopy (CLSM)

- **Roughness analysis**

Confocal laser scanning microscopy (Confocal Laser Scanning Microscope LSM780 from Zeiss) was utilized to determine the profile and surface roughness of PDMS hemispheres. The z-stacking (a.k.a. image processing method) was used to obtain RMS (Rq) roughness data from the PDMS specimens. Stack images with ".lsm" extension were analyzed and processed in the Image j software, by means of Extended Depth of Field and SurfCharJ1q plugins, using a workflow described in (Centre, 2012).

- **Microstructural analysis**

The WPI and Gellan gum inks were stained with Rhodamine B (83689-1G) dye. The samples were observed with a 63x magnification objective, in a Confocal Laser Scanning Microscope (LSM780) from Zeiss, adjusted to fluorescence mode by excitation of Rodhamine B fluorescent dye with a 561nm laser light. The emission fluorescence was recorded between 567 nm and 658 nm wave lengths. Finally images were analysed and optimized resorting to the: ImageJ, Zen Black and Zen Blue softwares.

### 4.3.5 Atomic Force Microscopy (AFM)

Atomic Force Microscopy (AFM) scaning of the glass samples, were carried out with the Bruker Icon Atomic Force Microscope, which that incorporates nanoscale imaging with characterization technologies on a large sample tip-scanning AFM platform. The cantilevers were adjusted to a resonant frequency of 251.76 kHz and a nominal force constant between 10 - 130 N/m. RMS roughness values were assessed from the analysis of the AFM images in Gwyddion software (Klapetek, Necas, & Anderson, 2019).

### 4.3.6 Scanning Electron Microscope (SEM)

The morphological characterization of the PDMS and glass was performed by Scanning electron microscopy (SEM), using a Quanta FEG 650 (FEI, USA). Dry samples were fixed on aluminium stubs covered, by carbon ribbon, subsequently coated with gold and observed using an

accelerating voltage of 5 kV under vacuum conditions.

### 4.3.7 Water Contact Angle (WCA)

The static WCA of modified and unmodified PDMS surfaces and glass specimens was measured at room temperature using a Drop Shape Analyser 100 equipment (DSA 100, KRÜSS Scientific Instruments, Germany). The liquid used was ultra-pure water and the droplet volume was 2 μL. The angles were measured using the sessile drop method to extract the angle between the baseline and tangent line at the solid-liquid interface. At least five measurements were carried out for every sample.

### 4.3.8 Molecular Dynamics Simulation

- **Methodology and Databases**

MD simulation was used to model the tribological systems studied, in order to assess friction magnitudes and observe prevailing friction mechanism at the nano scale, under conditions equivalent to macroscopic assays. By running LAMMPS classical MD parallel code in a Beowulf cluster with 48 Xeon 26xx E-series cores.

The structures of the biomolecules β-Lactoglobulin (PDB ID:2Q2M), Gellan Gum (PolySac3DB ID: Gellan Native) and Mucins 7 and 5B (Modbase ID: Q9HC84.2 and Q8TAX7) were obtain from RCSB Protein Data Bank (PDB), CERMAV Database of Polysacharides 3D Structures (PolySac3DB) and Salilab Database of Comparative Protein Structure Models (ModBase). Files that contain the topology, namely information, regarding bonded and nonbonded interactions needed to adequately define each molecules within the simulation, were converted from the aforementioned database native formats. Subsequently, the geometries of the molecules were optimized and immersed in water molecules (PDB ID: TI4P model) in the simulation domain. When the cluster ran without errors, it was possible to obtain the box dimensions and, consequently, calculate the atoms present in the simulation. The MD simulation only reproduces one formulation of the DOE, as a result of limited time available and since this system is representative: **7.75% WPI + 1.25% GG + 0.175% mucin (5B and 7)**.

After minimization, the system undergoes NVE integration to update position and velocity for atoms each time step, at a temperature of 300K. At this point, the system is called as an ensemble, which is defined as a collection of all possible systems that have varied microscopic

state, but have a single thermodynamic state (A. Singh et al., 2018). The cut-offs used in the simulation, depended on the type of interaction throughout the simulation: **Cut-off of TIP4P**: 6.0 Å; **Cut-off $H_2O$ and Biomolecules interactions**: 4.0 Å; **Cut-off $H_2O$ and PDMS interactions**: ($H_2O$ -C) 4.39 Å; ($H_2O$ -H) 4.39 Å; ($H_2O$ -Si) 4,67 Å; **Cut-off Biomolecules and PDMS interactions**: 4.5 Å; **Cut-off Glass**: ($SiO_2$-$SiO_2$) 2.0 Å; ($SiO_2$-Biomelcules) 3.5 Å; ($SiO_2$-Glass) 4.5 Å.

Visualization of the atoms trajectories and analysis of the generated MD data was performed in the Ovito visualization tool.

- **Geometry Optimization**

Using tools like Avogadro software, it was possible to optimize the geometries of the molecules. The MD simulations were carried out using force field like the Universal Force Field (UFF) and Merck Molecular Force Field (MMFF94) for a number of optimization steps of 500, using the Conjugate Gradients algorithm, and a convergence between $10^{-6}$ and $10^{-8}$. The GROMACS package, with GOMOS9643a1 force field was chosen to help discover C6 and C12 parameters for molecules of the simulation, important parameters in modelling with the Lennard-Jones potential LJ(12,6). General parameters of potential strength ($\varepsilon$) and zero-crossing distance ($\sigma$) of the LJ(12,6) potential, for interactions between the different structures were used.

## 4.4 Results

### 4.4.1 Tribogeometry validation

Initially, we conduct tribological experiments to verify the tribological system worked and had the capacity to distinguish between compounds reported as astringents and non-astringents (Figure 2).

Friction coefficient (COF) was measured at increasing speeds from 0 to 314.15 mm/s, with the intent of detecting the behaviour in all the lubrication regimes. Table III shows the COF values obtained at different sliding speeds (1,10 and 300 mm/s). All the controls presented the initial peak, corresponding to the Static COF in the boundary regime, then the value decreases substantially in the mixed regime, however when reaches the highest speed, no typical up-turn of

the COF for the hydrodynamic regime was seen.

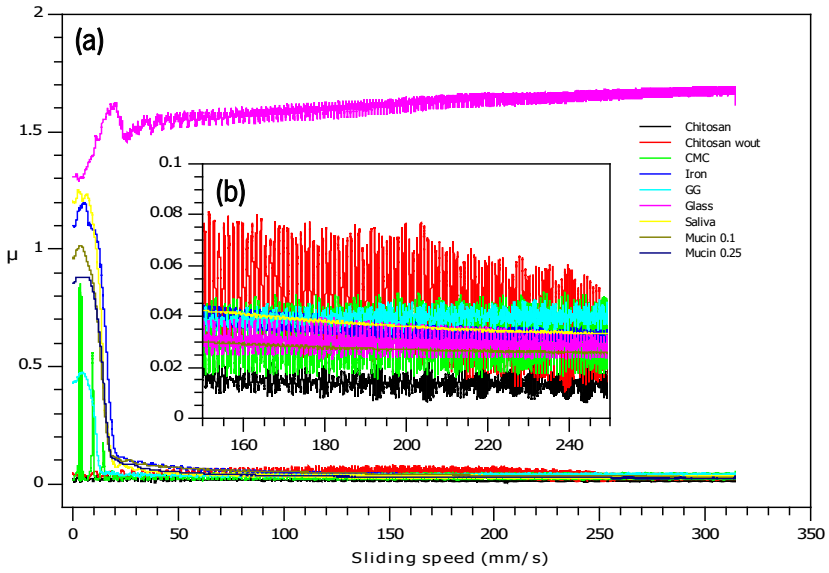


**Chapter IV - Figure 2 -** Representative curve of the control samples: a) at increasing speeds from 0 to 314 mm/s; b) in more detail between speeds of 150 mm/s and 250 mm/s.

Besides the glass, that presents the highest COF, iron trichloride revealed a high COF values (both in the static regime, as in the mixed regime, where the sensory perception occurs), constituting itself as the most astringent. Chitosan and CMC both exhibit similar behaviour, maintaining the COF at low values (μ between 0.01-0.1), throughout the regimes.

**Chapter IV - Table III** - Friction coefficients at the end of the controls experiments. The parenthesis values denote the standard deviation

| CONTROLS | COF (μ) | | |
|---|---|---|---|
| | BOUNDARY REGIME | MIXED REGIME | HIDRODYNAMIC REGIME |
| Sliding speed | 1 mm/s | 10 mm/s | 300 mm/s |
| CHITOSAN | 0.01 (0.01) | 0.02 (0.01) | 0.01 (0.01) |
| CHITOSAN W/OUT SALIVA | 0.04 (0.01) | 0.05 (0.02) | 0.02 (0.02) |
| CMC | 0.03 (0.01) | 0.11 (0.12) | 0.03 (0.01) |
| GG | 0.44 (0.56) | 0.29 (0.39) | 0.04 (0.01) |
| IRON | 1.11 (0.07) | 1.08 (0.03) | 0.03 (0.01) |
| GLASS | 1.31 (0.12) | 1.41 (0.07) | 1.68 (0.14) |
| SALIVA | 1.20 (0.19) | 1.07 (0.20) | 0.03 (0.01) |
| MUCIN 0.1% | 0.97 | 0.84 | 0.03 |
| MUCIN 0.25% | 0.86 | 0.80 | 0.03 |

The mucins (with artificial saliva), showed high COF values (μ ≈ 0.8-0.9) in the boundary and mixed regimes. However when the sliding speed evolve to higher values, their COF values decrease substantially. Artificial saliva had as well high initial friction values, yet when mucins were added to the saliva those COF values decreased.

All the controls revealed a steady-state when entering the hydrodynamic velocities, maybe due to low shear strength fluids.

### 4.4.2 DOE

The surface curves showing the effect of the variables in the different COFs at different speeds that had an acceptable fitting are shown in Figure 3.

By establishing the comparison between the responses and the tables with the effects of the parameters, it was possible to obtain more concrete information about the behaviours of each variable and its interaction. After the fitting of the model, it was determine how well the model fits the data. These resulted in: three equations that model the effect of the variable responses. These equations had a R-squared ($R^2$) statistically significant.

The Static COF (Figure 3a and 3b), was influenced by WPI and Mucin and not GG. WPI revealed a linear effect, reducing the COF. On the other hand, mucin exhibited a quadratic behaviour, which increased the COF. On the other hand, when both interact, they showed a synergism (combination of factors that tend to improve COF), towards reducing the COF. In combination with the regression models the impact of Mucin and WPI on the static COF, corresponds to the following equation:

$$\mu_s = 0{,}156 + 0.144 - 0.099(WPI) + 0.091(Mucin)^2 - 0.089(WPI * Mucin) \qquad (\mathbf{2})$$

The behaviour of the COF at 10 mm/s was slightly different from the Static COF (Figure 3c and 3d). The effect of the biopolymers was not linear and tend to decrease the COF value. The estimated effects of the parameters still showed the impact of the interaction between WPI and Mucin point out to the smallest COF, at the 11.515% WPI and 0.175% Mucin, respectively. In addition the dynamic COF was also influenced by the content of the polysaccharide. It could be modelled by the following equation:

$$\mu_d^{(10)} = 0.218 + 0.081 - 0.087(WPI) - 0.066(GG)^2 - 0.078(WPI * Mucin) \qquad (\mathbf{3})$$

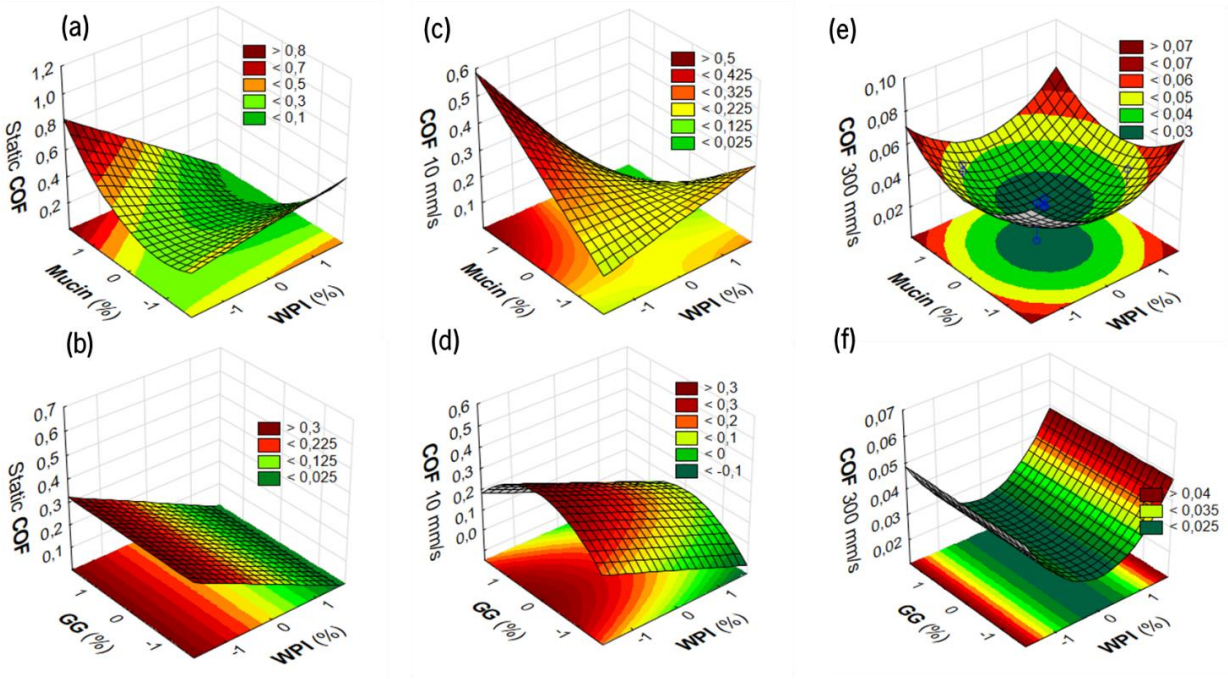


**Chapter IV - Figure 3 -** 3D Fitted Surfaces of the interaction of the variables on the Static COF: a) WPIxMucin, b) WPIxGG; Dynamic COF at 10mm/s: c) WPIxMucin, d) WPIxGG; and Hydrodynamic COF at 300mm/s: e) WPIxMucin, f) WPIxGG. The variables not mentioned are at level 0.

The hydrodynamic COF at 300mm/s could also be modelled. It showed that the impact of each variable on the COF was different from the other cases, Figure 3(e) and 3(f). Both WPI and Mucin presented a quadratic behaviour that increased the COF. Yet when combining the linear behaviour of Mucin and Gellan Gum, there was a synergism that tended to decrease the COF and consequently the lowest COFs were obtained at the central points. In the last two regimes, it was possible to observe that GG benefits the reduction of dynamic COF, but its contribution to the reduction of COF, analysed in the hydrodynamic regime, is smaller, because the mucin decreases the effect of GG (reduction of 1 order of magnitude). The equation representing those interactions is:

$$\mu_d^{(300)} = 0.023 + 0.008(WPI)^2 + 0.007(Mucin)^2 - 0.005(GG * Mucin) \qquad (4)$$

## 4.4.3 Microstructure (CLSM)

Figure 4 showed the microstructure of WPI and GG solutions (with different ratios), some without the influence of mucins (Figure 4a, 4c and 4e) and others with mucins and saliva (Figure 4b, 4d and 4f). The red areas in the image correspond to the protein phase and the dark areas correspond to the gellan gum.

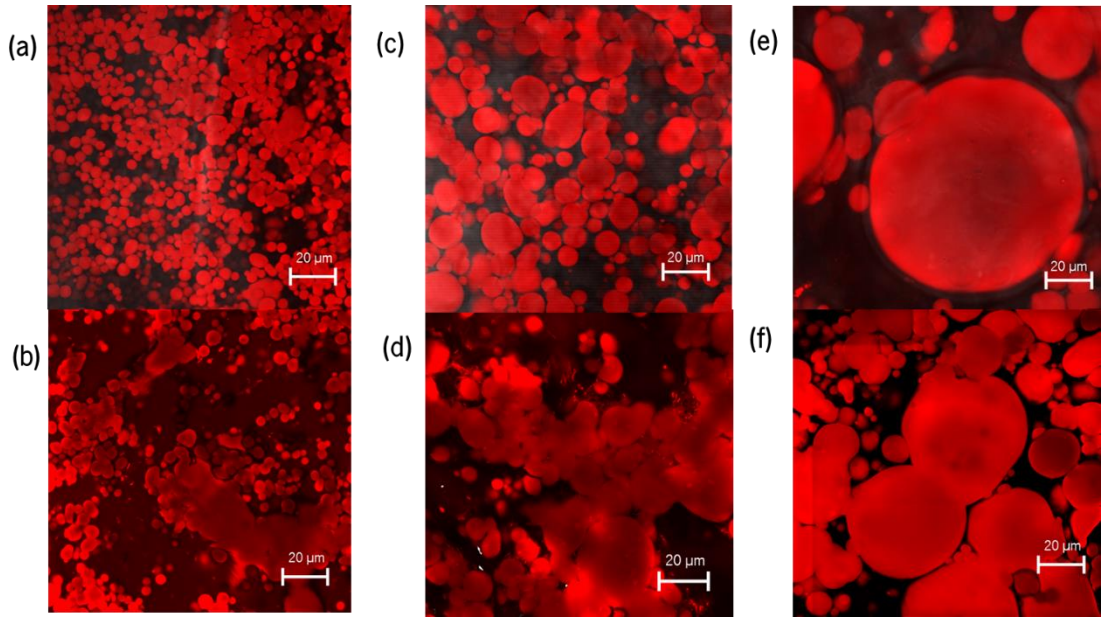


**Chapter IV - Figure 4 -** Confocal images of the micro-structure of the food-inks before and after tribology tests: a)5,5%WPI+1,5%GG; b) 5,5%WPI+1,5%GG+0,25%Mucin; c) 7,75%WPI+1,25%GG; d)7,75%WPI+1,25%GG+0,175%Mucin; e) 10%WPI+1%GG; f) 10%WPI+1%GG+0,25%Mucin.

Microstructure and morphology of WPI structures was characterized by spherical protein particles, evenly distributed in a matrix composed by Gellan gum (Figures 4a, 4c and 4e). The images indicated that the density of particles networks was inversely proportional to the protein concentration, i.e, as the WPI content increases the density of particles is reduced, as a result of size growth. Interstitial separation grows accordingly.

After tribological assessment, WPI particles do not show signs of disintegration, appearing only to have sustained plastic deformation. Figures 4(b), showed that the protein-rich beads (incorporating mucins) were more dispersed in the polysaccharide matrix after tribological interaction. Images of figures 4(d) and 4(f) revealed a clustering effect as well, but with larger aggregates. However, it is noteworthy that the presence of mucin is usually linked to an increase in volume of the particles, although such effect is not directly observed in these images.

Considering the diameter of the individual aggregates, a study was done concerning the

effect of the biopolymers on the morphometric features (diameter, %particles and WPI and GG content) of WPI structures, using the confocal images analysed by image-based analysis. Figure 5 displays how the features varied with the composition of the ink. Figure 5(a) shows that almost none of the particles in food-inks have sizes below 1µm and after tribological assessment no occurrence of these sizes were found.

Generally speaking, the balance between the percentage of medium size particles (≤ 5 µm and ≤ 10 µm) present positive increase after tribological assessment (Figure 5b and 5c). For minor WPI contents there was a decrease in the percentage of particles after tribological tests: for 3.98 %WPI +1.25%GG, to particles sizes of ≤ 5 µm and ≤ 10 µm, a 77% and 45% decrease was obtained, respectively. Moreover, the food-inks that present the larger sizes ≥ 25 µm correspond to those with 10% of WPI.

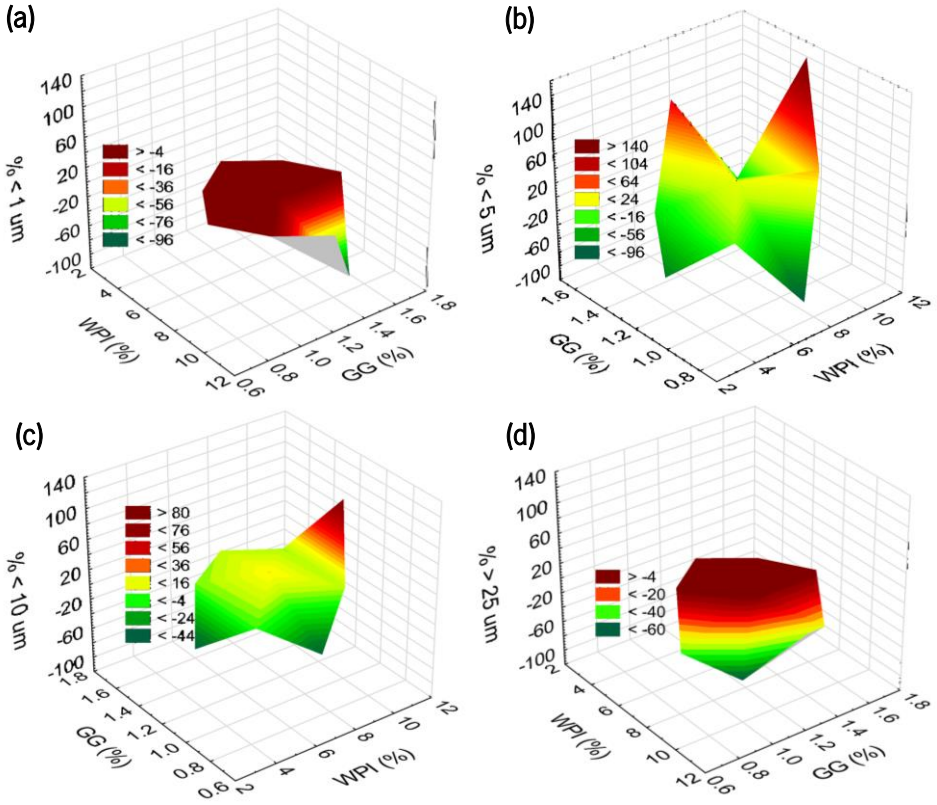


**Chapter IV - Figure 5 -** 3D Surfaces of the effect of %GG, %WPI and the balance of the percentages before and after tribological assessment with diameters : (a) ≤ 1 µm, (b) ≤ 5 µm, (c) ≤ 10 µm and ≥ 25 µm.

## 4.4.4 Contact Angles Measurements

We investigated the wettability of 2 types of PDMS elastomer (one with the silanes on the surface and the other without) and Glass by contact angle measurements through the time, by

Figure 6(a). This method was used to accurately measure the hydrophilic characteristic of a surface for a polymer like PDMS, whose surface properties change speedily with post exposure time.

PDMS was hydrophobic by nature, but after plasma treatment, the structure changed and resembled due to rough or nano-structured surface, increasing the hydrophilicity. PDMS sample was measured throughout the 72 hours of aging and it was possible to see that in both cases of PDMS (with silanization or not), hydrophobicity was reversed. After the 72 hours of the preparation/modification, The PDMS was slightly hydrophilic (76°), while the glass was more hydrophilic (35°).

### 4.4.5 Morphology and Roughness of the Tribopairs

For PDMS, surface roughness was a critical parameter and it was only achieved with CLSM techniques to determine 3D surface roughness characteristic. Imaging assessment was done performing the z-stack showed in Figure 6(b). For PDMS, the results of roughness obtain from Image J, were namely 3.7 μm for roughness average (Ra) and 5 μm for mean square roughness (RMS).

The roughness and micro-asperity contacts were important in determining the adhesion behaviour, and those can be confirmed by topographic images of the glass, showed in Figure 6(c). The absolute value, however, might be affected by tip-sample interactions. Such interactions had to be taken into account as long as the physical/chemical properties of the glass pattern were not known. Given that information, from AFM and consequently analysis in Gwyddion, was detect a RMS, for the glass, of 6.12 nm.

Figure 6(d) showed SEM images of oxygen plasma treated PDMS sample at a magnification of 1000x and of the glass sample at a magnification of 5000x. It was possible to see that the surface of PDMS presented a rough topography, unlike the glass that presented a smooth surface, with minimal defects.

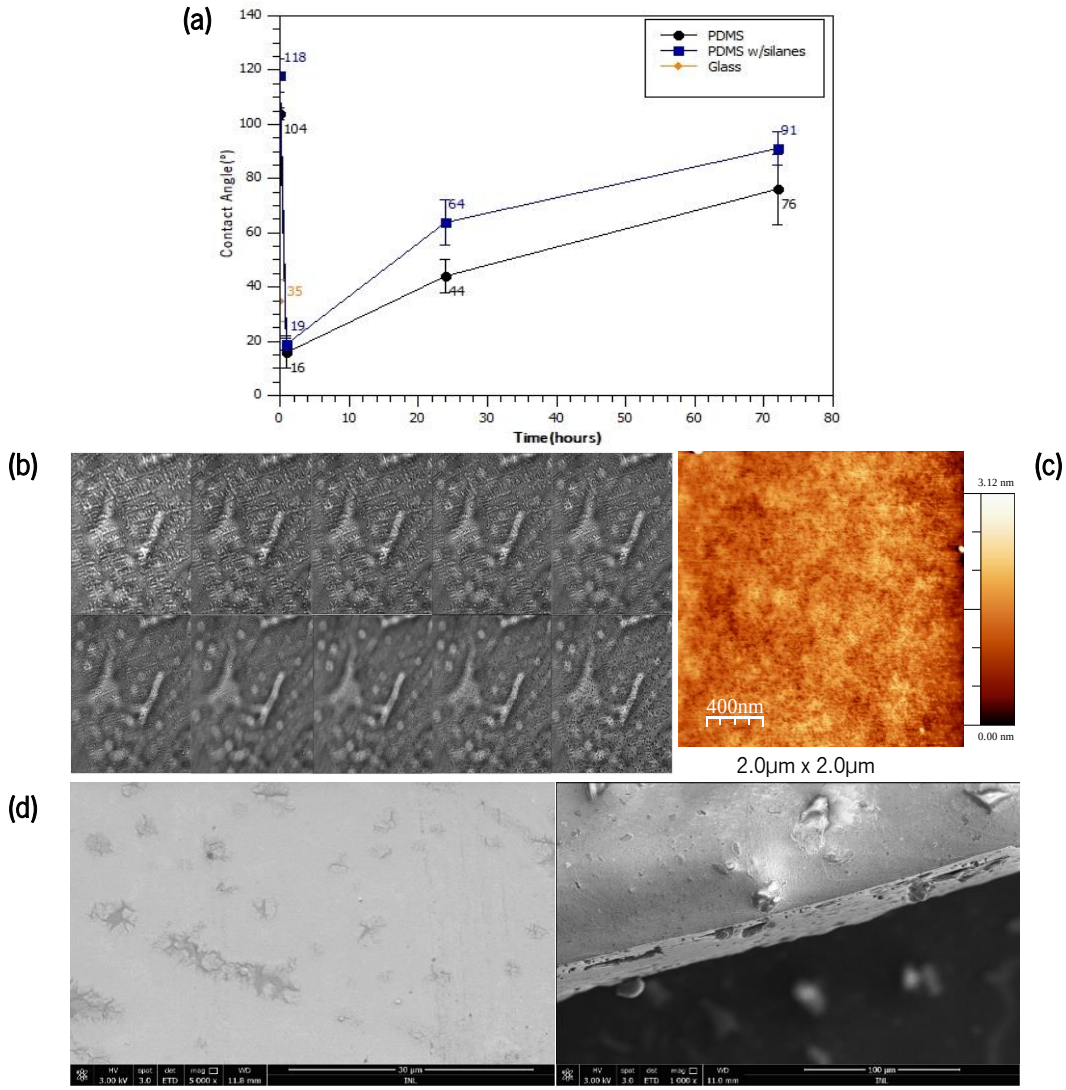


**Chapter IV - Figure 6 -** Surface characterization of the tribo-pair (PDMS-Glass): a) Contact angles throughout the time (immediately, 1h, 24h and 72h after; b) Stack images (10) from CLSM; c) AFM of glass sample; d) SEM of glass and PDMS hemisphere treated with oxygen plasma.

## 4.4.6 MD Simulation

Attempting to model the tribological system at nanoscale, the structures were submitted to a range of 0.8-2.5 nanoseconds in explicit solvent and with external forces being applied on a surface of PDMS. The surface moved at two different velocities: low (0.1 mm/s) and high speed (300 mm/s). From script developed on LAMMPS it was possible to obtain the box simulation, as shown in Figure 7, which illustrates the organised structures that were involved in the MD simulations.

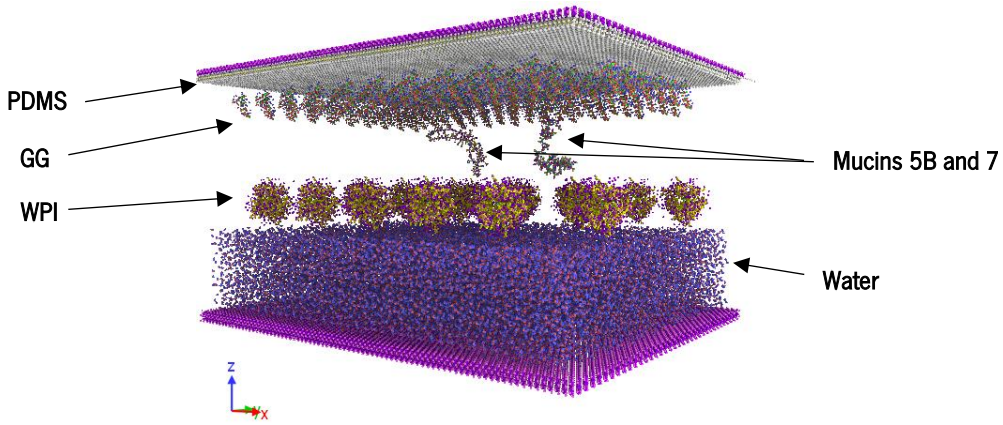


**Chapter IV - Figure 7** - Snapshot of the simulation box previous to biomolecules (PDMS, GG, WPI and Mucins 5B and 7) mixing into the water layer.

To start the simulation, PDMS layer approaches the water layer that already has the biomolecules mixed together (Figure 8a). Once the simulation begins, a vertical downward force is applied to the system and it is possible to observe that the biomolecules are interacting with each other and that the PDMS layer is deforming, also coming in contact with the biomolecules (Figure 8b).

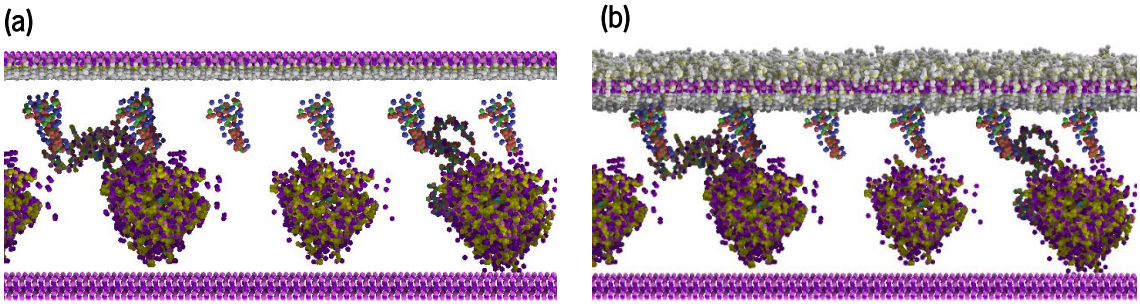


**Chapter IV - Figure 8** - Snapshots of the simulation box: (a) after PDMS and biomolecules approximation; (b) during the simulation. The water molecules were not consider.

The contribution of those forces result in a COF (μ) value, that can be compared with the COF values from the tribology experiments. The LAMMPS script provides the data with the forces ($F_x, F_y, F_z$), that are calculated using the following equation to obtain the effective COF:

$$COF_{eff} = \sqrt{\frac{{F_x}^2 + {F_y}^2}{F_z}} \quad (5)$$

Analysing the graphic representation (Figure 9) of the friction behaviour of the atomic species at 0.1 mm/s and 300 mm/s, a similar linear zone was chosen, between 1.3-1.5 ns, to obtain a mean COFeff value for those speeds. For the simulation at 0.1mm/s (the lower speed),

the mean COFeff had a value of 0.013, with a standard deviation of 0.011. For the high speed, the mean COFeff value is 0.012 with a standard deviation of 0.005. Both curves have similar behaviour, with high COFeff values at the beginning and decreases as the time passes by. Along the curves, the occurrence of some events was highlighted, with a zoom representation of these areas, which substantially change the COF (Figure 9b). For higher speeds these events happen earlier.

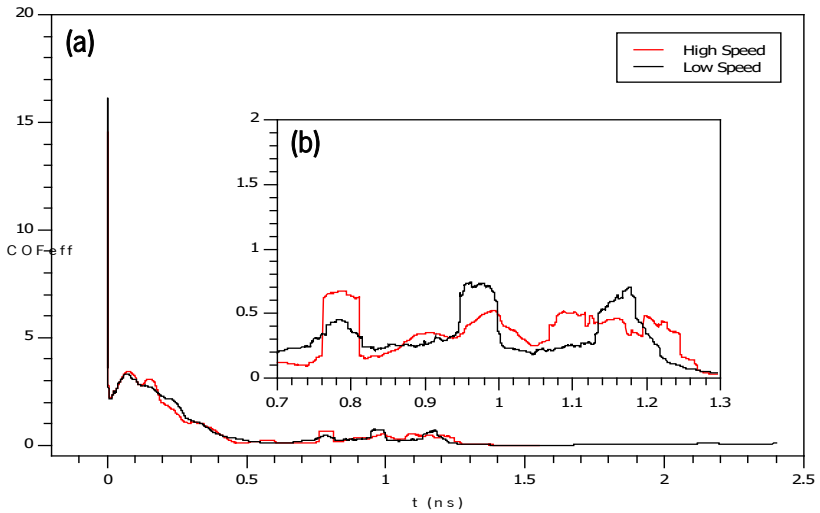


**Chapter IV - Figure 9 -** Friction coefficient over time of the smoothed curve during MD simulation: (a) at low speed (0.1 mm/s) and high speed (300 mm/s); (b) highlighting some events occurring during the simulation.

## 4.5 Discussion

Throughout the previous work we investigated few properties capable of influencing the perception of the food, as well as all methods to work with them, aiming to optimize the 3D phase separated food-inks towards the reduction of astringency sensation. First, we produced the samples to be studied composed by: WPI, GG and mucins. Second, we used design of experiments to select the interactions of the independent variables that were important to analyse. We also considered the composition and microstructure of the food-inks. The food-inks were then submitted to tribological assessment, in a lubricated system (incorporating mucins and artificial saliva), tested earlier for astringent detection with control solutions. The tribopairs for those studies were smooth glass and PDMS surfaces. These components were also characterised by SEM, AFM, CLSM and WCA to investigate the influence of surface hydrophobicity, as well as surface roughness. Recently, it has been documented, that the molecular approach has been used to study, in more detail, the

interactions occurring during the tribological assessment. That was achieved with molecular simulation, using the LAMMPS code.

To approximate surfaces to the soft tongue tissue and upper palate properties, it was taken into account the pressure values of the tribopairs, used in oral mimicking conditions. In the present work, the combined properties of PDMS and smooth glass surface range MPa, which is 3x larger (usually in kPa) the oral/ palate pressure, possibly causing deviations on the lubrication degree during the normal oral processing (Sarkar, Andablo-reyes, Bryant, Dowson, & Neville, 2019).

The composition of the PDMS was 10:1 between the polymer and the curing agent. According to Lamberti et al. (2012) this proportion correspond to a polymeric network with a minimum amount of defects and unreacted species. However it is important to mention that PDMS hemi-spheres used were not polish and that the Glass is commercial, and the procedure of how it was processed is unknown.

Trough Figure 6, it is possible to see that the tribopairs surfaces were influenced by the treatments that they were submitted, previously reported as affecting lubrication, especially for PDMS (Dresselhuis, Klok, Stuart, & Vries, 2007). The PDMS altered after surface modification by recovering its hydrophobic properties over time, mainly the PDMS with silanes on their surface. The glass preserves through all the experiments is hydrophilic behaviour.

Surface roughness parameters, for PDMS were done by CLSM, which was the technique that presented the adequate resolution for this material. The roughness values taken from Figures 6(b) and 6(c), allows to say that glass is a much smoother surface than PDMS. PDMS topology reveals several patterns in the polymer and some irregularities on its surface. These statements are supported by SEM images, which showed the typical micro and nanoroughness of the two surfaces and also reveal that PDMS roughness values can be due to small particles that present in the surface. Since the particles sizes of the WPI structures, in general, are around 5 μm, and the PDMS roughness is also around 5 μm, entrapment couldn't be the answer, so the particles may have adhere to the PDMS surface (Cortese et al., 2008).

To identify astringents substances, by their influence on the COF, varying speed in the tribotests were carried out by submitting the controls substances to speed ramps, in order to span the different lubrication regimes (Figure 2). Nonetheless, such tribotests were not sufficient to indisputably assess astringency, since number of factors such as artificial saliva composition, surface properties of the tribopairs, electrostatic interactions and properties of the materials must be taken into account, because they also regulate the perception of astringency (Beecher et al.,

2008). Glass and the PDMS interactions in the control tests were done in a dry environment and had high friction coefficients ($\mu$= 1.5) and increasing throughout the test. Since PDMS was activated by $O_2$ plasma modification the interaction between this material and glass yields from the Si–O–Si bonds after loss of a water molecule, that promotes the adhesion of PDMS to glass and not even increasing speed can break this adhesion (Xiong, Chen, & Zhou, 2014). Given that, adsorption and interfacial interactions (i.e., adhesion) then become more predominant, increasing the COF.

Iron trichloride is an iron coordination entity and according to PubChem it has a role as Lewis acid and as an astringent. As a control of this study it revealed a high COF, confirming this characteristic. The tribological system could not detect the astringent behaviour expected Chitosan although it had an acidic pH. That can be due to the fact that chitosan is a polyelectrolyte and in the presence of salts such as saliva, hydrate the tribological system. The astringency of chitosans decreases with increasing content of the positively charged amino-groups; suggesting an electrostatic-based interaction (P. Luck, Vårumb, & Allen Foegeding, 2015). Chitosan was composed only by neutral and positively charged entities, which offered the possibility to be used in further studies of the mechanism of astringency.

Gellan Gum, although viscous, negatively charged and hydrophilic compound, it was able to adhere to PDMS, and therefore has relatively high COF values. CMC is also a negatively charged polysaccharide, with high viscosity, which contributes for the lubrication behaviour. Saliva and mucins exhibited high initial COF values (up to 1.2), thus apparently behaving like astringent substances. However, the addition of mucins to the artificial saliva showed a reduction in friction.

According to data found in the literature, the observed COF values of mucins in artificial saliva ($\mu \approx 0.9$) are in agreement with published results ($\mu \approx 0.8$ for lubrication experiments), meaning that the mucins are, in fact, lubricating the tribosystem and, therefore, non-astringent (Rene A. de Wijk & Prinz, 2005). Mucins are reported to contribute favourably to the boundary lubrication with their hydrated characteristic, adsorption in a broad range of surfaces and ability to form sterically repulsive, extended surface layers (Coles et al., 2010).

Tribological assessment when applied to study the formulations given by the DOE, was similar but more complex, because englobed a three systems and more interactions to be studied. Considering that, it was important to analyse the morphology and characteristics of the gels. The process to develop edible gels, included multiple steps that could influence the lubrication, when submitted to experimental tests. According to Stading and Hermansson (1990), the pH to which

the protein gel formed was subjected to, depends on the pH and cation levels, and according to them, whey protein gels could range from fine-stranded (transparent) to particulate (opaque). These specific food-inks were phase-separated, which introduced a crucial control of gels characteristics, and therefore an important process in future 3D printing.

The microstructure and morphological features of the food-inks were characterized by Figure 4. Accordingly to Turgeon et al. (2003), protein-polysaccharides interactions result from strong repulsive interaction and phase separation is promoted. They say that the biphasic morphology allows to control the microstructure of protein–polysaccharide phase-separated mixtures. Phase separation of WPI and GG form of spherical protein rich domains with diameters sizes of microns. Overall gels showed different size and spatial distribution, but a similar internal morphology after phase separation and gelation. From Berg et al. (2009) it was possible to gauge that being the GG used as the polysaccharide, it will interact with the protein aggregates and their spatial distribution within the protein phase was related to the polysaccharide charge density. Microstructural observation, with respect to the microstructure of the gels when mixed with mucin and artificial saliva, revealed that these compounds do not abruptly influenced the gels. However the addition of this components, should affect the protein volume after tribological experiments.

Furthermore, from confocal images, WPI structures were quantified, in particles sizes. The specific effects of particles on the perception of astringency, could be related to their dimensions.

According to Figures 5, the vast majority of particles presented diameters between 5 and 10 μm, for the different WPI and GG contents. However, for WPI concentrations of 10% a significant percentage of particles exhibited larger diameters (≥ 25 μm). After tribological assessment, particles with sizes ≤ 1μm were not observed, which could imply that the particles got entrapped in the PDMS surface topography, which has higher length scale roughness (Rq = 5 μm). This phenomenon can be compared to similar processes reported in the mouth, where it is hypothesized that particles entrapment in the tongue could contribute to astringency perception. Another explanation for the disappearance of these particles could be related to their aggregation as a result of the tribological stresses, which once more could induce the astringency perception, given that those aggregates can disrupt the salivar film initially formed (Upadhyay et al., 2016).

The interactions between the variables and the COFs were analysed and the three-dimensional (3D) plots and equations (Figure 3; Equations 2, 3, 4) modelling the responses will be further discussed. The DOE results allowed to analyse the main effects of the influencing parameters as well as the interactions between the factors (WPI, GG and Mucins content), but

those effects are not immediate.

From the effects and synergies of the variables, it was possible to observe that the parameters statistically significant, showed the largest impacts on the COF. For main effects observed (independent or combined effect of the variables), there were some interesting interactions, which the interpretation was a bit more difficult. Nevertheless, modelling using the Design of Experiments proved to be a promising approach. This approach was a useful tool which allows to had a considerable number of variations and concentrations and complete interpretations of the data without having to go through n of configurations (Mason, Gunst, & Hess, 2003).

Looking at the results of the DOE, in more detail, the study was found to be significant at three COFs: Static COF (for initial speeds), Dynamic COF (for 10 mm/s sliding speed) and Hydrodynamic COF (for 300 mm/s sliding speed). Remembering that estimated oral velocities during sensory valuations were probably between 10 and 100 mm/s, it was possible to verify that the evaluated sliding speeds correspond to those where the sensory perception is performed (Malone et al., 2003).

The interaction of the protein with mucin result in a positive synergism in the two first regimes. In the presence of Mucins, under oral processing conditions, that synergism could be attributed to mucin adsorbed PDMS surfaces, reducing roughness contacts and consequently reducing COF values. Wijk & Prinz (2005) did not find results that verify the effect of artificial saliva on the friction of custard when compared the friction of natural saline containing mucins and amylase with artificial saliva containing mucins adding that to starch custard. The present study, on the contrary revealed an influence of the artificial saliva with mucins in the friction of the food-inks used.

Nonetheless, interactions between mucins and GG were noteworthy for the hydrodynamic COF, because it is believed that lubrication properties of GG change when they interact to some extent with artificial saliva containing mucins. Such interaction decreased the impact of GG in the COF, which at a speed of 10 mm/s independently reduced the COF. The GG lubrication mechanism is supposed to be viscous by default, but when interacted with mucins this mechanism altered. According to a study by Torres et al. (2019), comparing the viscosity and oral lubrication properties of GG, the increase in friction under simulated oral conditions was partly attributed to the reduction in viscosity due to dilution and partly to the mucin that might have interacted with GG, causing the depletion of lubricious mucins to the hydrophobic PDMS by electrostatic interaction. Interestingly, they also reported that GG has benefits in terms of increased lubrication

at lower concentrations, which enhances friction reduction.

The DOE points out that the lowest COF values corresponds to highest WPI concentrations (10% and 11.51%). From the results showed by Figure 5, for 10% WPI content, some structures presented particles with diameters ≥ 25μm. However, these larger diameters should be avoided, as this may impair the possible printability of food-inks (resulting in hard gels with a poor resolution to print, lacking surface homogeneity). Thus, in choosing the quantities to model by MD, one should go back a little for those with WPI quantities similar to those of the central point. Moreover the DOE results reveal that this point constitutes critical/inflection zones in the COF values, being the most reliable. So by balancing the properties of the gels with the DOE results and the printability requirements, we decided that the best food-ink to model in MD would be the central point: 7.75% WPI + 1.25% GG + 0.175% mucin (5B and 7).

In order to assess a possible correlation between the macroscale experiments and results at the nanoscale simulated by MD, in the following a quantitative comparison between friction coefficient values at the different time and length scales will be analysed. Moreover, the choice of interatomic potential (LJ 12-6) and respective parametrization to model the interactions between the distinct molecules will be correlated with the time evolution of the COFeff, in order to establish a relationship with the potential strength (ε) and zero-crossing distance (σ). Nonetheless, according to Gao et al. (2004), when it comes to molecular-level mechanisms of frictional processes, MD results indicated that spatial and temporal fluctuations allowed by the simulations could be different of those observed for macroscopic-like particles that were moving past each other.

In the macroscale system, the friction behaviour was clearly affected by the sliding speed, however when comparing the COF for high and low speeds at the nanoscale those differences were not evident, given that the curves follow the same trend and friction levels. However, a slight decrease in the average COFeff was obtained for the high velocities. For speeds of 0.1 mm/s and 300 mm/s, at a constant load of 1 N, the COF for the tribological experiments presented average values of 0.051 and 0.023, respectively. These results indicate an almost 5 fold and 2 fold increase in comparison with the nanoscale information, respectively. The differences observed could be attributed to the changes in the friction mechanisms resulting from the distinct time and length scales involved in the tribocontact between antagonistic structures (molecules versus asperities). Additionally, the correct choice of parameters for the intermolecular potential, as well as the molecules' models used to simulate the intrinsically chemically complex real samples will play an important role in the direct comparison between friction levels at the different domains. Thus, a

possible route to match the friction levels obtained from simulation in the steady-state regime with those from the tribotests will pass in the optimization of ε and σ parameters of the LJ(12,6) potential.

Analysing the COFeff evolution (Figure 9), it is noteworthy to indicate that the modelling of the interactions between atomic species in a tribological system followed a behaviour justified by the stability of an arrangement of atoms resulting from the adjusted repulsive distance and strength of the LJ 12-6 force field. This potential can describe the cohesive motion and behaviour accurately, but it cannot provide an accurate quantification of the frictional energy (Jiang, & Park, 2015). Representatively, in Figure 9(a), in the early stage of the simulation, when the PDMS molecules began to approach the WPI, GG and Mucin molecules, the nature of the intermolecular forces are mainly attractive due to prevailing London and van der Waals forces, which causes the COFeff to reach very high values (up to 16). With decreasing interatomic distances, which happens when the system is at a later stage of motion, the repulsive term of LJ 12-6 potential dominates, meaning that the COFeff decreases significantly thereof and reaches a quasi-steady state regime characterized by very low friction (0.012).

Furthermore, from Figure 9(b), some instabilities in the COFeff evolution curves can be seen for simulation times in the range 0.7-1.3 ns, which could be related to the interpenetration of glass atoms into the PDMS layer. Since the PDMS atoms are Newtonian and, therefore, constitutes a deformable structure, the rigid non-Newtonian atoms of the glass layer will eventually penetrate the former structure when imposing an applied vertical down force.

Additionally, lower amplitude fluctuations are present in the friction curves. Such behaviour could be explained by a phenomenon similar to the corrugation existing between solid surfaces in relative motion at the nanoscale, i.e. resulting from the atomic scale topography. On the other hand, given the existence of a velocity gradient between fluid layers (aqueous sample), the various biomolecules will be subjected to different velocities and approximations. Therefore, because the intermolecular interactions are modelled by the LJ(12,6) potential, the forces between the molecules could be predominantly attractive or repulsive at distinct time steps, resulting in slight increase or decrease of the COFeff.

## 4.6 Conclusions

- Food-inks based on whey protein and gellan gum were successfully produced and tribologically tested against PDMS and commercial glass, using a ball-on-disk contact geometry;
- The surface modification (silanization and modification with $O_2$ plasma) of PDMS surfaces influenced its wettability, although the hydrophobic behaviour remained. The glass, on the other hand, was characterized by a hydrophilic behaviour;
- Overall, astringents substances influenced the COF when varying speed in the tribotests. The astringency was regulated by multiple mechanisms such as friction, surface chemistry and properties of all the parts involved in the system;
- Phase separation of whey protein and gellan gum was successfully promoted by the formation of spherical protein rich domains with diameters sizes of the order of micrometers in a polysaccharide matrix. Protein particles with sizes ≤ 1μm were not observed after tribological assessment, probably resulting from the particles entrapment in the PDMS surface roughness or could be related to their aggregation and subsequent disruption of the salivar film, thus contributing to the astringency perception;
- DOE allow to observe the impact of interactions between the variables in friction behaviour. DOE showed that the interaction of WPI with mucin resulted in a positive synergism in the Static regime (for initial speeds), Dynamic regime (10 mm/s) and Hydrodynamic regime (300 mm/s). On the other hand, the interaction of GG with mucin resulted in a positive synergism in the Hydrodynamic regime (300 mm/s). The DOE also points out that the lowest COF values corresponds to highest WPI concentrations;
- Balancing the properties of the gels (e.g. particles sizes) with friction and the printability requirements, the best food-ink to model in MD was the central point: 7.75% of whey protein, 1.25% of gellan gum and 0.175% of mucins. However, although this food-ink was chosen to be modelled, the one with the lowest COF and with less variation in absorbed particles is 11.51% of whey protein, 1.25% of gellan gum and 0.175% of mucins.

- Classical MD simulation have showed that the nanoscale friction behaviour of modelled tribosystems containing 7.75% of whey protein, 1.25% of gellan gum and 0.175% of mucins is not considerably affected by changes in the sliding speed either for 0.1 mm/s as for 300 mm/s. On the other hand, macroscale tribotests indicate a reduction in the average dynamic COF from 0.051 to 0.023 with increasing speeds. This discrepancy could be attributed to one or more of the following reasons: prevalence of distinct friction mechanisms at the different time and length scales considered; approximations assumed in the modelled tribosystem for the MD simulations (rheology, viscosity variation with speed,...); adequate choice and parametrization for the force fields used to model intermolecular interactions.
- MD results showed that upon approximation of the PDMS layer and sample model, nanoscale friction is initially dominated by adhesion as a result of the attractive component of the Lennard-Jones potential employed. With decreasing interatomic distances, the repulsive term of the Lennard-Jones potential takes dominance, which will reflect in a substantial decrease of the dynamic effective COF, and subsequent setting of steady-state low friction regimes (COFeff = 0.012).

## 4.7 Future Work

The hemi-spheres that might have residual silanes, ideally should been through X-ray photoelectron spectroscopy to confirm the presence of this component.

Quantification of the protein volume of the samples before and after tribology can only be supported with quantification of total protein techniques, to complement with microstructure information to see the amount of protein absorbed on the surfaces.

Use complementary surface analysis techniques to acquire spacing roughness parameters, in addition to conventional amplitude indicators, to further validate protein particle entrapment in PDMS surfaces.

In MD simulations, investigate the influence of parameter values for the Lennard-Jones potential and/or the use of specific force fields and subsequent optimization to converge to a more comprehensive agreement between macroscopic tribological data and nanoscale frictional response of the simulated tribosystems.

3D printing the food-inks to study the printability and correlate the properties (e.g microstructure, viscosity) with sensory analysis tests and optimize the reduction in the astringency

sensation;

## 4.8 References


Anderson, G. H., Luhovyy, B., & Akhavan, T. (2011). General Aspects of Milk : Milk in Adult Nutrition Milk Proteins in the Regulation of Body Weight , Satiety , Food Intake and Glycemia, *67*, 147–159.

ASTM. (2004). Standard definitions of terms relating to sensory evaluation of materials and products.

Beecher, J. W., Drake, M. A., Luck, P. J., & Foegeding, E. A. (2008). Factors regulating astringency of whey protein beverages. *Journal of Dairy Science*, *91*(7), 2553–2560. https://doi.org/10.3168/jds.2008-1083

Benichou, A., Aserin, A., Garti, N., Benichou, A., Aserin, A., & Garti, N. (2010). Protein-Polysaccharide Interactions for Stabilization of Food Emulsions Protein-Polysaccharide Interactions for Stabilization of Food Emulsions, *2691*. https://doi.org/10.1080/01932690208984192

Berg, L. Van Den, Rosenberg, Y., Boekel, M. A. J. S. Van, Rosenberg, M., & Velde, F. Van De. (2009). Food Hydrocolloids Microstructural features of composite whey protein / polysaccharide gels characterized at different length scales. *Food Hydrocolloids*, *23*(5), 1288–1298. https://doi.org/10.1016/j.foodhyd.2008.10.013

Biegler, M., Delius, J., Käsdorf, B. T., Hofmann, T., & Lieleg, O. (2016). Cationic astringents alter the tribological and rheological properties of human saliva and salivary mucin solutions. *Biotribology*, 6, 12–20. https://doi.org/10.1016/j.biotri.2016.03.002

Burova, T. V., Grinberg, N. V., Grinberg, V. Y., Usov, A. I., Tolstoguzov, V. B., & de Kruif, C. G. (2007). Conformational changes in ι- and κ-carrageenans induced by complex formation with bovine β-casein. *Biomacromolecules*, *8*(2), 368–375. https://doi.org/10.1021/bm060761f

Çelebioglu, H. Y., Gudjonsdottir, M., Chronakis, I. S., & Lee, S. (2016). Investigation of the interaction between mucins and b -lactoglobulin under tribological stress. *Food Hydrocolloids*, 54, 57–65. https://doi.org/10.1016/j.foodhyd.2015.09.013

Çelebioğlu, H. Y., Lee, S., & Chronakis, I. S. (2019). Interactions of salivary mucins and saliva with food proteins : a review. *Critical Reviews in Food Science and Nutrition*, *0*(0), 1–20. https://doi.org/10.1080/10408398.2018.1512950

Centre, O. (2012). Measuring Surface Roughness Using Confocal Microscopy and ImageJ (or Fiji variant). Retrieved from https://www.otago.ac.nz/omni/otago684709.pdf

Chen, J., & Stokes, J. R. (2012). Rheology and tribology: Two distinctive regimes of food texture sensation. *Trends in Food Science and Technology*, *25*(1), 4–12. https://doi.org/10.1016/j.tifs.2011.11.006

Coles, J. M., Chang, D. P., & Zauscher, S. (2010). Molecular mechanisms of aqueous boundary lubrication by mucinous glycoproteins. *Current Opinion in Colloid & Interface Science, 15(6*), 406-416.

Cortese, B., Amone, S. D., Manca, M., Viola, I., Cingolani, R., & Gigli, G. (2008). Superhydrophobicity Due to the Hierarchical Scale Roughness of PDMS Surfaces, *(24)*, 2712–2718. https://doi.org/10.1021/la702764x

Demirel, M., & Kayan, B. (2012). Application of response surface methodology and central composite design for the optimization of textile dye degradation by wet air oxidation. *International Journal of Industrial Chemistry*.

Dinu, V., Liu, C., Ali, J., Ayed, C., Gershkovich, P., Adams, G. G., … Fisk, I. D. (2018). Analytical ultracentrifugation in saliva research : Impact of green tea astringency and its significance on the in-vivo aroma release. *Scientific Reports*, (August), 1–9. https://doi.org/10.1038/s41598-018-31625-w

Dresselhuis, D. M., Klok, H. J., Stuart, M. A. C., & Vries, R. J. De. (2007). Tribology of o / w Emulsions Under Mouth-like Conditions : Determinants of Friction, 158–171. https://doi.org/10.1007/s11483-007-9040-9

Ferrer-gallego, R., Hernández-hierro, J. M., Brás, N. F., Vale, N., Mateus, N., Freitas, V. De, … Escribano-bailon, M. T. (2017). INTERACTION BETWEEN WINE PHENOLIC ACIDS AND SALIVARY PROTEINS BY STD-NMR AND MOLECULAR-DYNAMIC SIMULATIONS. *Agricultural and Food Chemistry*. https://doi.org/10.1021/acs.jafc.6b05414

Gorji, S., & Bahram, M. (2010). Experimental design for the study and optimization of the effect of different surfactants on the spectrophotometric determination of sulfide based on phenothiazine dye production. *Analytical Methods*, 2(7), 948–953. https://doi.org/10.1039/c0ay00123f

Gudj, M., Chronakis, I. S., Lee, S., & Çelebio, H. Y. (2016). Investigation of the interaction between mucins and b -lactoglobulin under tribological stress, *54*, 57–65. https://doi.org/10.1016/j.foodhyd.2015.09.013

Jackson, R. (2016). Chapter 4-Taste and Mouth-Feel Sensations. In *Wine Tasting* (3rd editio).

Jiang, J. W., & Park, H. S. (2015). A Gaussian treatment for the friction issue of Lennard-Jones potential in layered materials: Application to friction between graphene, MoS2, and black phosphorus. *Journal of Applied Physics*, 117(12), 124304

Klapetek, P., Necas, D., & Anderson, C. (2019). Gwyddion user guide. Retrieved from http://gwyddion.net/download/user-guide/gwyddion-user-guide-en.pdf

Kontopidis, G., Holt, C., & Sawyer, L. (2004). Invited review: β-lactoglobulin: Binding properties, structure, and function. *Journal of Dairy Science*, *87*(4), 785–796. https://doi.org/10.3168/jds.S0022-0302(04)73222-1

Lamberti, A., Quaglio, M., Sacco, A., Cocuzza, M., & Pirri, C. F. (2012). Applied Surface Science Surface energy tailoring of glass by contact printed PDMS. *Applied Surface Science*, *258*(23), 9427–9431. https://doi.org/10.1016/j.apsusc.2011.12.117

Luck, P., Vårum, K. M., & Foegeding, E. A. (2015). Food Hydrocolloids Charge related astringency of chitosans. *Food Hydrocolloids*, *48*, 174–178. https://doi.org/10.1016/j.foodhyd.2015.02.024

Malone, M. E., Appelqvist, I. A. M., & Norton, I. T. (2003). Oral behaviour of food hydrocolloids and emulsions. Part 1. Lubrication and deposition considerations. *Food Hydrocolloids*, *17*(6), 763–773. https://doi.org/10.1016/S0268-005X(03)00097-3

Mason, R. L., Gunst, R. F., & Hess, J. L. (2003). *Statistical design and analysis of experiments: with applications to engineering and science* (2nd editio). John Wiley & Sons.

Miyoshi, E., & Nishinari, K. (1999). Non-Newtonian flow behaviour of gellan gum aqueous solutions. *Colloid and Polymer Science*, *277*(8), 727–734.

Peleg, H., Bodine, K. K., Noble, A. C., Morrisette, C., & Dan, M. (1998). Is® The Influence of Acid on Astringency of Alum and Phenolic Compounds, 371–378.

Penã-Neira, A. (2019). Management of Astringency in Red Wines, 257–272. https://doi.org/10.1016/B978-0-12-814399-5.00018-9

PYTKO-POLONCZYK1, J., JAKUBIK1, A., PRZEKLASA-BIEROWIEC1, A., & MUSZYNSKA, B. (2017). ARTIFICIAL SALIVA AND ITS USE IN BIOLOGICAL EXPERIMENTS. *JOURNAL OF PHYSIOLOGY AND PHARMACOLOGY*, 807–813.

Prakash, S., Dan, D., Tan, Y., & Chen, J. (2013). Applications of tribology in studying food oral processing and texture perception. *FRIN*, *54*(2), 1627–1635. https://doi.org/10.1016/j.foodres.2013.10.010

Ramos, O. L., Pereira, R. N., Rodrigues, R., Teixeira, J. A., Vicente, A. A., & Xavier Malcata, F. (2014). Physical effects upon whey protein aggregation for nano-coating production. *Food Research International*, *66*, 344–355. https://doi.org/10.1016/j.foodres.2014.09.036

Ramos, O. L., Pereira, R. N., Martins, A., Rodrigues, R., Teixeira, J. A., Pastrana, L., … Vicente, A. A. (2017). Design of whey protein nanostructures for incorporation and release of nutraceutical compounds in food. *Critical Reviews in Food Science and Nutrition*, *57*(7), 1377–1393. https://doi.org/10.1080/10408398.2014.993749

Ramos-Pineda, A. M., García-Estévez, I., Brás, N. F., Valle, E. M. M. del, Dueñas, M., & Bailón, M. T. E. (2017). Molecular Approach to the Synergistic E ff ect on Astringency Elicited by Mixtures of Flavanols. *Agricultural and Food Chemistry*. https://doi.org/10.1021/acs.jafc.7b01600

Rodrigues, R., Vicente, A. A., Ramos, O. L., Martins, A., Fuciños, C., Malcata, F. X., … Teixeira, J. A. (2015). Design of whey protein nanostructures for incorporation and release of nutraceutical compounds in food. *Critical Reviews in Food Science and Nutrition*, 57(7), 1377–1393. https://doi.org/10.1080/10408398.2014.993749

Sarkar, A., Andablo-reyes, E., Bryant, M., Dowson, D., & Neville, A. (2019). ScienceDirect Lubrication of soft oral surfaces. *Current Opinion in Colloid & Interface Science*, *39*, 61–75. https://doi.org/10.1016/j.cocis.2019.01.008

Scollary, G. R., Pásti, G., Kállay, M., Blackman, J., & Clark, A. C. (2012). Astringency response of red wines: Potential role of molecular assembly. *Trends in Food Science and Technology*, *27*(1), 25–36. https://doi.org/10.1016/j.tifs.2012.05.002

Singh, A., Vanga, S. K., Orsat, V., & Raghavan, V. (2018). Application of molecular dynamic simulation to study food proteins: A review. *Critical Reviews in Food Science and Nutrition*, 58(16), 2779–2789. https://doi.org/10.1080/10408398.2017.1341864

Siqueira, C., Picone, F., & Lopes, R. (2010). Food Hydrocolloids Interactions between milk proteins and gellan gum in acidified gels. *Food Hydrocolloids*, *24*(5), 502–511. https://doi.org/10.1016/j.foodhyd.2009.12.007

Stading, M., & Hermansson, A. (1990). Viscoelastic behaviour of 13-lactoglobulin gel structures. *Food Hydrocolloids*, *4*(2), 121–135. https://doi.org/10.1016/S0268-005X(09)80013-1

Torres, O., Yamada, A., Rigby, N. M., Hanawa, T., Kawano, Y., & Sarkar, A. (2019). Gellan gum: A new member in the dysphagia thickener family. *Biotribology*, 17, 8-18.

Turgeon, S. L., Beaulieu, M., Schmitt, C., & Sanchez, C. (2003). Protein–polysaccharide interactions: phase-ordering kinetics, thermodynamic and structural aspects. https://doi.org/10.1002/humu.20397

Upadhyay, R., Brossard, N., & Chen, J. (2016). Mechanisms underlying astringency: Introduction to an oral tribology approach. *Journal of Physics D: Applied Physics*, *49*(10), 104003. https://doi.org/10.1088/0022-3727/49/10/104003

Ur-rehman, A., Khan, N. M., Ali, F., Khan, H., Khan, Z. I. A. U., Jan, A. K., ... Al, A. U. E. T. (2015). KINETICS STUDY OF BIOPOLYMERS MIXTURE WITH THE HELP OF CONFOCAL LASER SCANNING MICROSCOPY, 1–9. https://doi.org/10.1111/jfpe.12245

Vakis, A. I., Yastrebov, V. A., Scheibert, J., Nicola, L., Dini, D., Minfray, C., ... Guarino, R. (2018). Tribology International Modeling and simulation in tribology across scales : An overview. *Tribology International*, *125*(November 2017), 169–199. https://doi.org/10.1016/j.triboint.2018.02.005

Vale, N., Gomes, P., Mateus, N., Freitas, V. De, & Heredia, F. J. (2017). Interaction between Wine Phenolic Acids and Salivary Proteins by Saturation-Transfer Di ff erence Nuclear Magnetic Resonance Spectroscopy (STD-NMR) and Molecular Dynamics Simulations. https://doi.org/10.1021/acs.jafc.6b05414

Valentová, H., & Panovská, Z. (2003). SENSORY EVALUATION | Taste. In *Encyclopedia of Food Sciences and Nutrition* (2nd Editio).

Vardhanabhuti, B., Cox, P. W., Norton, I. T., & Foegeding, E. A. (2011). Lubricating properties of human whole saliva as affected by β-lactoglobulin. *Food Hydrocolloids*, *25*(6), 1499–1506. https://doi.org/10.1016/j.foodhyd.2011.02.021

Vardhanabhuti, B., & Foegeding, E. A. (2009). Evidence of interactions between whey proteins and mucin: their implication on the astringency mechanism of whey proteins at low pH. *In Gums and Stabilisers for the Food Industry*, *15*, 137–146.

Vidal, S., Courcoux, P., Francis, L., Kwiatkowski, M., Gawel, R., Williams, P., & Waters, E. (2004). Use of an experimental design approach for evaluation of key wine components on mouth-feel perception. *Food Quality and Preference*, 15, 209–217. https://doi.org/10.1016/S0950-3293(03)00059-4

Wijk, R. A. de, & Prinz, J. F. (2005). The role of friction in perceived oral texture, *16*, 121–129. https://doi.org/10.1016/j.foodqual.2004.03.002

Xiong, L., Chen, P., & Zhou, Q. (2014). Adhesion promotion between PDMS and glass by oxygen plasma pre-treatment. *Journal of Adhesion Science and Technology*.

# CHAPTER V: Conclusion

This work reported how sensory perception plays an important role in food intake, comprising several mechanisms, techniques and interactions between the food and the oral processing, which emphasizes the astringency mouthfeel. The main conclusions drawn from this study are indicated in the following:

- After preparing the literature review it was possible to conclude that sensory perception and astringency are very complex phenomena, which have had some research attention, but none that was really complete. Thus, it was important to highlight in the review the existence of many combined mechanisms of astringency. We also considered the several methodologies as sensory analysis, molecular dynamics simulations and tribology to unravel the astringency mechanisms and/or to predict the astringency sensations elicited by different foods and beverages;
- Food-inks based on whey protein and gellan gum were successfully produced and tribologically tested against hydrophobic PDMS and hydrophilic commercial glass, using a ball-on-disk contact geometry;
- DOE allow to observe the impact of interactions between the variables in friction behaviour. DOE showed that the interaction of WPI with mucin resulted in a positive synergism in the Static regime (for initial speeds), Dynamic regime (10 mm/s) and Hydrodynamic regime (300 mm/s). On the other hand, the interaction of GG with mucin resulted in a positive synergism in the Hydrodynamic regime (300 mm/s). The DOE also points out that the lowest COF values corresponds to highest WPI concentrations.
- Classical MD simulation model chosen was the sample containing 7.75% of whey protein, 1.25% of gellan gum and 0.175% of mucins. Tribological assessment and molecular dynamics modelling showed that is possible to stablish a correlation between different scales. The discrepancies observed could be attributed to one or more of the following reasons: prevalence of distinct friction mechanisms at the different time and length scales considered; approximations assumed in the modelled tribosystem for the MD simulations; adequate choice and parametrization for the force fields used to model intermolecular interactions.

# CHAPTER VI: Appendix

## 6.1 Supplementary information

**Chapter VI - Table I -** Friction coefficients at different velocities after tribological experiments for DOE solutions.

| EXPERIMENTAL DESIGN | COF (Kinetic cof) | | | | | | |
|---|---|---|---|---|---|---|---|
| | Boundary Regime | | | Mixed Regime | | | Hydrodynamic Regime |
| Sliding speed | 0,1 mm/s | 1 mm/s | 10 mm/s | 30 mm/s | 50mm/s | 100 mm/s | 300 mm/s |
| **B1_1:** 5.5%WPI + 1%GG+ 0.1%Mucin | 0.027 | 0.025 | 0.038 | 0.023 | 0.018 | 0.022 | 0.032 |
| **B1_2:** 5.5%WPI + 1.5%GG+ 0.25%Mucin | 0.058 | 0.056 | 0.186 | 0.09 | 0.068 | 0.048 | 0.044 |
| **B1_3:** 10%WPI + 1%GG+ 0.25%Mucin | 0.06 | 0.071 | 0.072 | 0.06 | 0.052 | 0.043 | 0.038 |
| **B1_4:** 10%WPI + 1.5%GG+ 0.1%Mucin | 0.026 | 0.027 | 0.087 | 0.051 | 0.053 | 0.068 | 0.051 |
| **B1_5:7.75%WPI + 1.25%GG+ 0.175%Mucin** | **0.058** | 0.06 | 0.15 | 0.05 | 0.050 | 0.04 | **0.03** |
| **B2_1:** 5.5%WPI + 1%GG+ 0.25%Mucin | 0.347 | 0.351 | 0.540 | 0.270 | 0.220 | 0.114 | 0.049 |
| **B2_2:** 5.5%WPI + 1.5%GG+ 0.1%Mucin | 0.089 | 0.080 | 0.077 | 0.059 | 0.053 | 0.053 | 0.055 |
| **B2_3:** 10%WPI + 1%GG+ 0.1%Mucin | 0.047 | 0.041 | 0.031 | 0.040 | 0.037 | 0.050 | 0.037 |
| **B2_4:** 10%WPI + 1.5%GG+ 0.25%Mucin | 0.037 | 0.038 | 0.030 | 0.035 | 0.027 | 0.040 | 0.036 |
| **B2_5:7.75%WPI + 1.25%GG+ 0.175%Mucin** | **0.034** | 0.045 | 0.038 | 0.040 | 0.028 | 0.028 | **0.015** |
| **B3_1:** 3.98%WPI + 1.25%GG+ 0.175%Mucin | 0.127 | 0.136 | 0.401 | 0.069 | 0.055 | 0.052 | 0.037 |
| **B3_2:** 11.515%WPI + 1.25%GG+0.175%Mucin | 0.023 | 0.028 | 0.065 | 0.053 | 0.048 | 0.059 | 0.052 |
| **B3_3:** 7.75%WPI +0.831 %GG+ 0.175%Mucin | 0.026 | 0.023 | 0.029 | 0.015 | 0.012 | 0.014 | 0.025 |
| **B3_4**: 7.75%WPI + 1.668%GG+ 0.175%Mucin | 0.025 | 0.021 | 0.143 | 0.109 | 0.098 | 0.029 | 0.016 |
| **B3_5**:7.75%WPI + 1.25%GG+ 0.049%Mucin | 0.309 | 0.313 | 0.428 | 0.074 | 0.062 | 0.050 | 0.036 |
| **B3_6:**7.75%WPI +1.25 %GG+ 0.300%Mucin | 0.034 | 0.036 | 0.296 | 0.057 | 0.05 | 0.059 | 0.046 |
| **B3_7:7.75%WPI +1.25 %GG+ 0.175%Mucin** | **0.061** | 0.061 | 0.368 | 0.041 | 0.006 | 0.054 | **0.024** |

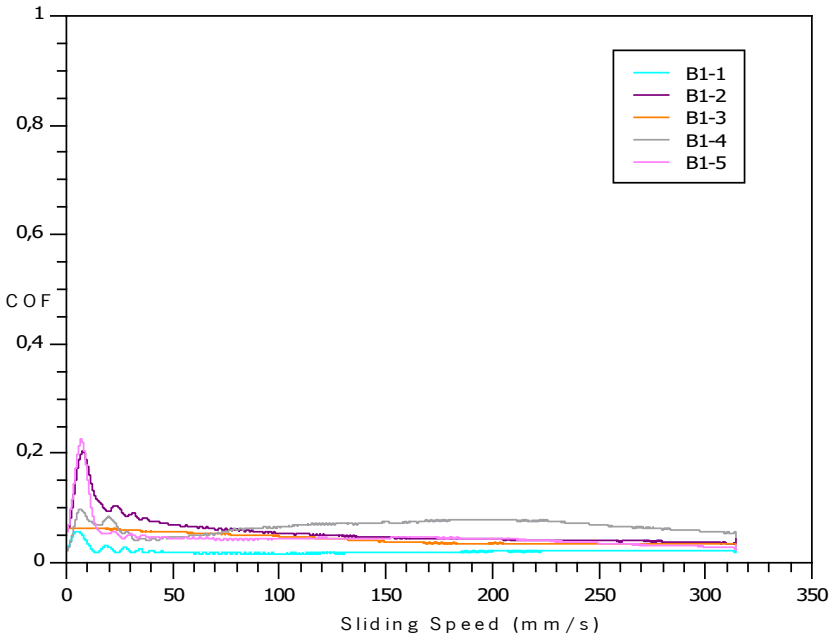


**Chapter VI - Figure 1**-Friction coefficient over a sliding speed ramp of the smoothed curves of WPI, GG and Mucins of the Block 1 of the DOE.

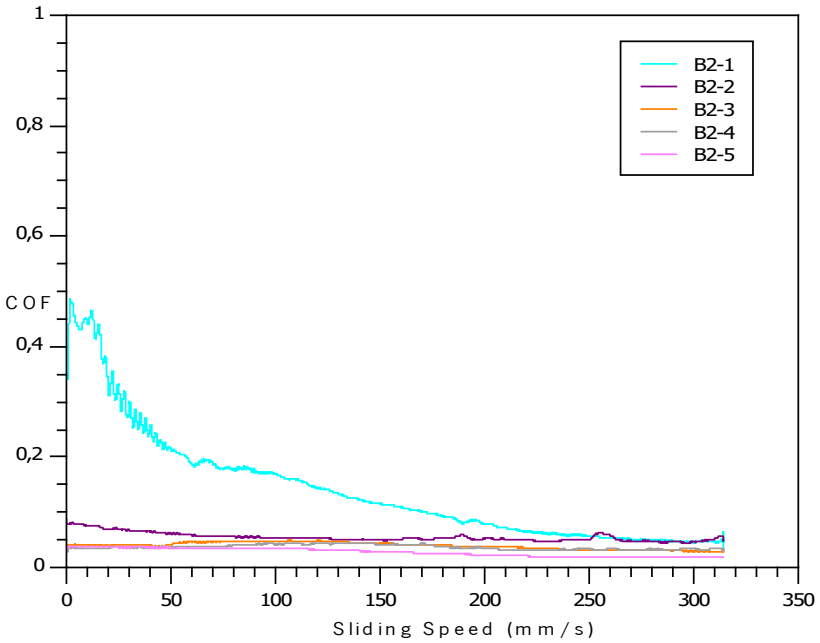


**Chapter VI - Figure 2**- Friction coefficient over a sliding speed ramp of the smoothed curves of WPI, GG and Mucins of the Block 2 of the DOE.

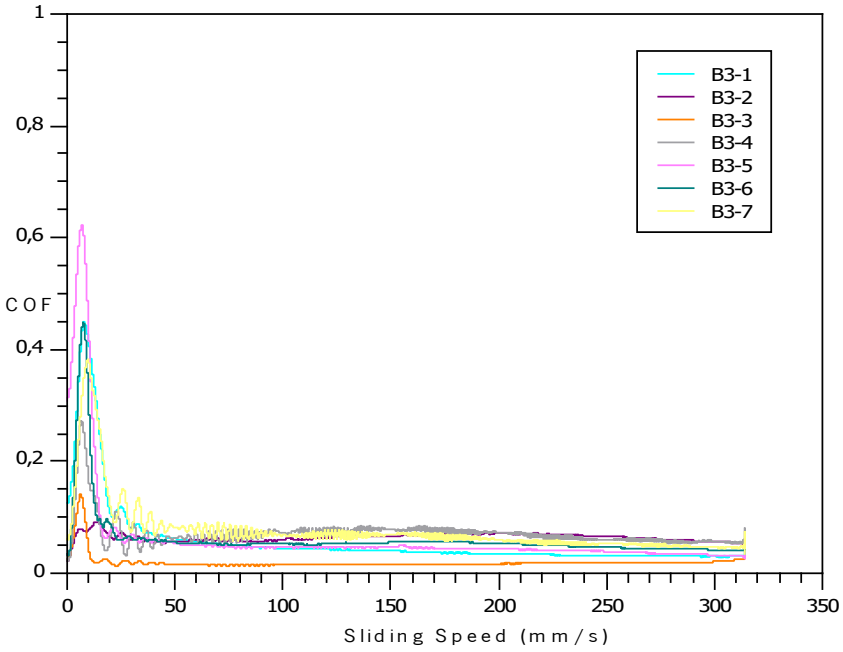


**Chapter VI - Figure 3**- Friction coefficient over a sliding speed ramp of the smoothed curves of WPI, GG and Mucins of the Block 3 of the DOE.

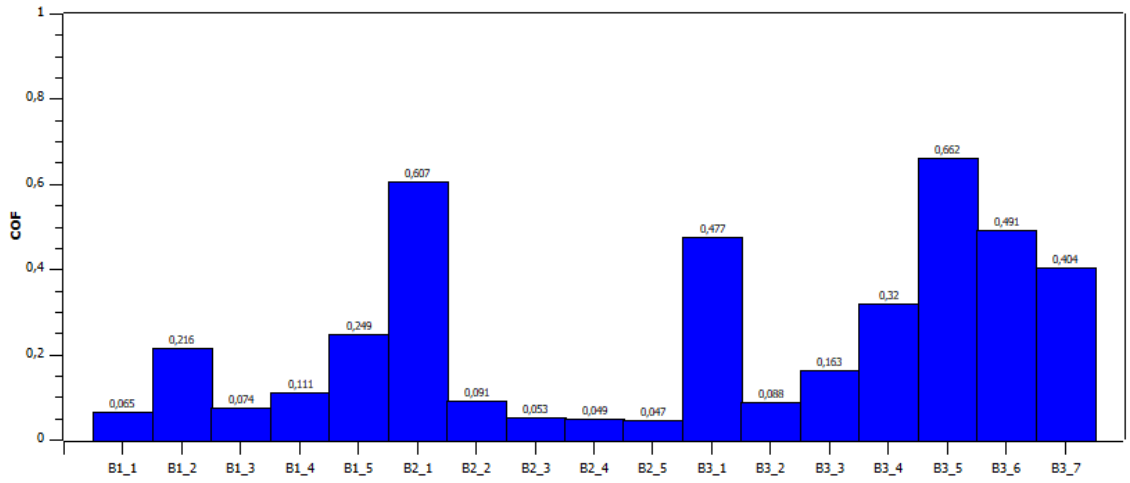


**Chapter VI - Figure 4**- Maximum Static Friction coefficient of the DOE.

**Chapter VI - Table II -** Force Field parameters MD simulation.

| ATOM (2Q2M - BETALACT) | Possible correspondence (FFGromos 43A1)* | C6 | C12 |
|---|---|---|---|
| N | N | 0.2436409E-02 | 0.1692601E-05 |
| C | C | 0.2340624E-02 | 0.3374569E-05 |
| O | O | 0.2261953E-02 | 0.7414932E-06 |
| CA | CA2+ | 0.1004890E-02 | 0.4980125E-06 |

| | | | |
|---|---|---|---|
| **NE(1,2)** | NE | 0.2436409E-02 | 0.1692601E-05 |
| **SD** | S ; SDMSO | ? | ? |
| **NZ** | NZ | 0.2436409E-02 | 0.1692601E-05 |
| **CD(1,2)** | CR1 ; C | ? | ? |
| **CH2** | CH2 | 0.7468416E-02 | 0.3396559E-04 |
| **OH** | CHO;H;O | ? | |
| **NH(1,2)** | N;NT; NR;NZ;NE;NL; H | ? | ? |
| **CZ(2,3)** | CR1; C | ? | ? |
| **OE(1,2)** | OA; OM; OW; O | ? | ? |
| **CB** | CR1 ; C | ? | ? |
| **OD(1,2)** | OA; OM; OW; O | ? | ? |
| **CG(1,2)** | CR1 ; C | ? | ? |
| **CE(1,2,3)** | CR1 ; C | ? | ? |
| **SG** | S; SDMSO | ? | ? |
| **ND(1,2)** | NT; NR;NZ;NE;NL | ? | ? |
| **OG(1)** | OA; OM; OW; O | ? | ? |

**Chapter VI - Table III -** Effects estimated for the siding speed where the COF reaches the max value.

| Factor | Effect Estimates; Var.:Static COF; R-sqr=.70592; Adj:.57224 (Spreadsheet final) 3 factors, 3 Blocks, 17 Runs; MS Residual=.0187198 DV: Static COF | |
|---|---|---|
| | p | Coeff. |
| Mean/Interc. | 0.005676 | 0.155631 |
| Block(2) | 0.008415 | 0.143962 |
| (1)WPI (%)(L) | 0.022126 | -0.098744 |
| Mucin (%)(Q) | 0.037061 | 0.090688 |
| 1L by 3L | 0.094532 | -0.088500 |

| Fcal | F0.1, GL regressao (5), GL residuos (11) |
|---|---|
| 5.280906 | 2.45 |
| $R^2$ = 70.6% | Fcal > F tab |

**Chapter VI - Table IV** - Effects estimated for the siding speed of 10mm/s.

| Factor | Effect Estimates; Var.:10 mm/s; R-sqr=.68296; Adj:.49273 (Spreadsheet final) 3 factors, 3 Blocks, 17 Runs; MS Residual=.0140336 DV: 10 mm/s | |
|---|---|---|
| | p | Coeff. |
| Mean/Interc. | 0.000246 | 0.218185 |
| Block(2) | 0.062713 | 0.081495 |
| (1)WPI (%)(L) | 0.021993 | -0.087003 |

| | | |
|---|---|---|
| GG (%)(Q) | 0.075451 | -0.065672 |
| 1L by 3L | 0.090817 | -0.078375 |

| Fcal | F0.1, GL regressao (6), GL residuos (10) |
|---|---|
| 3.590252 | 2.46 |
| $R^2$ = 68.3% | Fcal > F tab |

**Chapter VI - Table V** - Effects estimated for the siding speed of 300mm/s.

| Factor | Effect Estimates; Var.:300 mm/s; R-sqr=.74893; Adj:.63481 (Spreadsheet final) 3 factors, 3 Blocks, 17 Runs; MS Residual=.0000532 DV: 300 mm/s | |
|---|---|---|
| | p | Coeff. |
| Mean/Interc. | 0.000013 | 0.023651 |
| WPI (%)(Q) | 0.001263 | 0.008992 |
| Mucin (%)(Q) | 0.003506 | 0.007742 |
| 2L by 3L | 0.056352 | -0.005500 |

| Fcal | F0.1, GL regressao (5), GL residuos (11) |
|---|---|
| 6.569915 | 2.45 |
| $R^2$ = 74.9% | Fcal > F tab |

**Chapter VI - Table VI –** The percentage of particles before and after tribological assessment and the balance between both for particles sizes of ≤1μm, ≤5μm, ≤10μm and ≥25μm.

| | | Before Tribological Assessment | | | | After Tribological Assessment | | | | Balance | | | |
|---|---|---|---|---|---|---|---|---|---|---|---|---|---|
| **WPI** | GG | % ≤1μm | %≤5μm | %≤10μm | %≥25μm | % ≤1μm | %≤5μm | %≤10μm | %≥25μm | % ≤1μm | %≤5μm | %≤10μm | %≥25μm |
| **5.5** | 1 | 0 | 62.857 | 88.571 | 0 | 0 | 55 | 85 | 0 | 0 | -12.5 | -4.032 | 0 |
| **5.5** | 1.5 | 0 | 62.5 | 92.5 | 0 | 0 | 40 | 92.5 | 0 | 0 | -36 | 0 | 0 |
| **10** | 1 | 0 | 46.667 | 73.333 | 6.667 | 0 | 65 | 77.5 | 2.5 | 0 | 39.285 | 5.681 | -62.5 |
| **10** | 1.5 | 5 | 50 | 72.5 | 7.5 | 0 | 32.5 | 75 | 5 | -100 | -35 | 3.448 | -33.333 |
| **7.75** | 1.25 | 0 | 26.667 | 72.222 | 0 | 0 | 31 | 87 | 1 | 0 | 16.25 | 20.461 | 0 |
| **7.75** | 1.66 | 0 | 55 | 95 | 0 | 0 | 100 | 100 | 0 | 0 | 81.818 | 5.263 | 0 |
| **7.75** | 0.831 | 0 | 50 | 50 | 50 | 0 | 0 | 28.571 | 28.571 | 0 | -100 | -42.857 | -42.857 |
| **3.98** | 1.25 | 0 | 90 | 100 | 0 | 0 | 20 | 55 | 5 | 0 | -77.778 | -45 | 0 |
| **11.51** | 1.25 | 0 | 40 | 55 | 0 | 0 | 100 | 100 | 0 | 0 | 150 | 81.818 | 0 |

```
#########################################################
#
# TIP4P water + Mucines (5B, 7) + BetaLg + GG
#
# Cristiano Abreu
# September 2019
#
# Obs: version with PDMS as a top layer in SiO2 susbtrate and
biomolecules concentration adjusted to macro tribotests
# uses fix rigid or fix rigid/small variants for biomolecules
#
#########################################################
variable dt equal 0.001 # timestep (fs)
variable Tdamp equal ${dt}*100 # damping factor in Langevin thermostat
#variable Tdamp equal 10
variable nRowsUp equal 128 # number rows PDMS
variable nColsUp equal 24 # number columns PDMS
variable pdmsHeight equal 175 # height of PDMS layer
# separation between PDMS molecules on 3 axes
variable pdms_pitchX equal 3.0
variable pdms_pitchY equal 6.0
variable pdms_pitchZ equal 6.0
variable hgtWater equal 12.0 # height of lower water blocks
variable nWaterBlck equal 10 # number of water blocks rows to form
lubricant layer
variable WaterBlckSize equal 37 # lateral dimensions of individual
water blocks
variable nBLGmol equal 4 # number of rows of beta-lg molecules (Obs.:
counter starts at 0)
variable blg_pitchX equal 65 # separation between neighbor beta-lg
molecules in X
variable blg_pitchY equal 110 # separation between neighbor beta-lg
molecules in Y
variable nRowGGmol equal 9 # number of rows GG molecules in
simulation, X direction (Obs.: counter starts at 0)
variable nColGGmol equal 9 # number of columns GG molecules in
simulation, Y direction (Obs.: counter starts at 0)
variable gg_pitchX equal 35 # separation between neighbor GG molecules
in X
variable gg_pitchY equal 25 # separation between neighbor GG molecules
in Y
variable T_depart equal 600 # initial temperature of PDMS


#external load (W) applied to upper specimen
# Obs.: F(Si) = W, F(O) = W * [m(O)/m(Si)], in order for both atoms to
have the same acceleration
variable load equal -37.93 # units: kcal/mole-Angstrom (6.9477E-2 nN)
units real # check units -> change to standard metal
dimension 3
boundary p p p
atom_style full
newton on on
processors * * * grid numa # NUMA style mapping: auto-detetects which
cores are running in which nodes
#region box block -30 374 -135 169 -53 210 units box # old settings
region box block -21 371 -136 169 -38 190 units box
create_box 70 box bond/types 12 angle/types 17 dihedral/types 19
extra/bond/per/atom 4 extra/angle/per/atom 6 extra/dihedral/per/atom
36
###############
```

```
# water layer
###############
# inser water molecules (blocks of 35x35x35 Angstrom)
label loop0
variable loopVar loop 1 ${nWaterBlck} pad # variable to loop through
all CNT rows
# lower blocks
read_data water.data add append shift $(-10+v_loopVar *
v_WaterBlckSize - 36) -18 $(v_hgtWater - v_WaterBlckSize)
read_data water.data add append shift $(-10+v_loopVar *
v_WaterBlckSize - 36) $(-18-v_WaterBlckSize) $(v_hgtWater -
v_WaterBlckSize)
read_data water.data add append shift $(-10+v_loopVar *
v_WaterBlckSize - 36) $(-18+v_WaterBlckSize) $(v_hgtWater -
v_WaterBlckSize)
read_data water.data add append shift $(-10+v_loopVar *
v_WaterBlckSize - 36) $(-18+2*v_WaterBlckSize) $(v_hgtWater -
v_WaterBlckSize)

read_data water.data add append shift $(-10+v_loopVar *
v_WaterBlckSize - 36) $(-18-2*v_WaterBlckSize) $(v_hgtWater -
v_WaterBlckSize)
read_data water.data add append shift $(-10+v_loopVar *
v_WaterBlckSize - 36) $(-18+3*v_WaterBlckSize) $(v_hgtWater -
v_WaterBlckSize)
read_data water.data add append shift $(-10+v_loopVar *
v_WaterBlckSize - 36) $(-18-3*v_WaterBlckSize) $(v_hgtWater -
v_WaterBlckSize)
read_data water.data add append shift $(-10+v_loopVar *
v_WaterBlckSize - 36) $(-18+4*v_WaterBlckSize) $(v_hgtWater -
v_WaterBlckSize)
# top blocks
read_data water.data add append shift $(-10+v_loopVar *
v_WaterBlckSize - 36) -18 $(v_hgtWater)
read_data water.data add append shift $(-10+v_loopVar *
v_WaterBlckSize - 36) $(-18-v_WaterBlckSize) $(v_hgtWater)
read_data water.data add append shift $(-10+v_loopVar *
v_WaterBlckSize - 36) $(-18+v_WaterBlckSize) $(v_hgtWater)
read_data water.data add append shift $(-10+v_loopVar *
v_WaterBlckSize - 36) $(-18+2*v_WaterBlckSize) $(v_hgtWater)
read_data water.data add append shift $(-10+v_loopVar *
v_WaterBlckSize - 36) $(-18-2*v_WaterBlckSize) $(v_hgtWater)
read_data water.data add append shift $(-10+v_loopVar *
v_WaterBlckSize - 36) $(-18+3*v_WaterBlckSize) $(v_hgtWater)
read_data water.data add append shift $(-10+v_loopVar *
v_WaterBlckSize - 36) $(-18-3*v_WaterBlckSize) $(v_hgtWater)
read_data water.data add append shift $(-10+v_loopVar *
v_WaterBlckSize - 36) $(-18+4*v_WaterBlckSize) $(v_hgtWater)
next loopVar
jump SELF loop0
variable loopVar delete
########################################
# Insert biomolecules in simulation
########################################
# mucines 5B and 7
#read_data mucin5b.data add append offset 2 1 1 0 0 shift 130 60 96
group muc5b
#read_data mucin7.data add append offset 34 2 1 0 0 shift 180 0 111
group muc7
read_data m5b_mol_ID.data add append offset 2 1 1 0 0 shift 130 60 96
group muc5b
```

```
read_data m7_mol_ID.data add append offset 34 2 1 0 0 shift 180 0 111
group muc7
# beta-lg
label loop1

variable loopVar loop 0 ${nBLGmol} pad # loop through all pretended
BLG molecules rows
#read_data betaLg.lmpdat add append offset 58 3 1 0 0 shift $(-
20+v_loopVar*v_blg_pitchX) 80 46 group blg
#read_data betaLg.lmpdat add append offset 58 3 1 0 0 shift $(-
20+v_loopVar*v_blg_pitchX) $(80-1*v_blg_pitchY) 46 group blg
#read_data betaLg.lmpdat add append offset 58 3 1 0 0 shift $(-
20+v_loopVar*v_blg_pitchX) $(80-2*v_blg_pitchY) 46 group blg
read_data blg_mol_ID.lmpdat add append offset 58 3 1 0 0 shift $(-
20+v_loopVar*v_blg_pitchX) 80 46 group blg
read_data blg_mol_ID.lmpdat add append offset 58 3 1 0 0 shift $(-
20+v_loopVar*v_blg_pitchX) $(80-1*v_blg_pitchY) 46 group blg
read_data blg_mol_ID.lmpdat add append offset 58 3 1 0 0 shift $(-
20+v_loopVar*v_blg_pitchX) $(80-2*v_blg_pitchY) 46 group blg
next loopVar
jump SELF loop1
variable loopVar delete
# introduce remaining beta-lg molecules to complete pretended
concentration
#read_data betaLg.lmpdat add append offset 58 3 1 0 0 shift 295 -90 46
group blg
#read_data betaLg.lmpdat add append offset 58 3 1 0 0 shift 295 60 46
group blg
read_data blg_mol_ID.lmpdat add append offset 58 3 1 0 0 shift 295 -90
46 group blg
read_data blg_mol_ID.lmpdat add append offset 58 3 1 0 0 shift 295 60
46 group blg
# GG placement
label loop2a
variable loopVarOut loop 0 ${nRowGGmol} pad # loop through all GG
molecules rows
label loop2b
variable loopVarIn loop 0 ${nColGGmol} pad # loop through all GG
molecules columns
# OBS: Implement "MOLoffset" to add append to introduce a molecule ID
offset to be used in fix rigid/small
#read_data gellangum.lmpdat add append offset 62 8 11 15 0 shift
$(5+v_loopVarOut*v_gg_pitchX) $(-100+v_loopVarIn*v_gg_pitchY) 148
group gg
read_data gg_mol_ID.lmpdat add append offset 62 8 11 15 0 shift
$(5+v_loopVarOut*v_gg_pitchX) $(-100+v_loopVarIn*v_gg_pitchY) 148
group gg # MOLoffset = 37044
next loopVarIn
jump SELF loop2b
variable loopVarIn delete

next loopVarOut
jump SELF loop2a
variable loopVarOut delete
# complete remaining GG molecules to reach target concentration
label loop2c
variable loopVar loop 0 5 pad
#read_data gellangum.lmpdat add append offset 62 8 11 15 0 shift 355
$(-60+v_loopVar*v_gg_pitchY) 148 group gg
read_data gg_mol_ID.lmpdat add append offset 62 8 11 15 0 shift 355
$(-60+v_loopVar*v_gg_pitchY) 148 group gg
```

```
next loopVar
jump SELF loop2c
variable loopVar delete
########################################
# Insert upper PDMS specimen in simulation
########################################
label loop3
variable loopVarOut loop 0 ${nRowsUp} pad # loop through all PDMS rows
label loop4
variable loopVarIn loop 0 ${nColsUp} pad # loop through all PDMS
columns
# 1st layer
#read_data pdms.lmpdat add append offset 65 10 14 18 0 shift $(-
18.0+v_loopVarOut*v_pdms_pitchX) $(20.0+v_loopVarIn*v_pdms_pitchY)
$(v_pdmsHeight) group pdms
#read_data pdms.lmpdat add append offset 65 10 14 18 0 shift $(-
18.0+v_loopVarOut*v_pdms_pitchX) $(20.0-1*v_pdms_pitchY-
1*v_loopVarIn*v_pdms_pitchY) $(v_pdmsHeight) group pdms
# 2nd layer
read_data pdms.lmpdat add append offset 65 10 14 18 0 shift $(-
18.0+v_loopVarOut*v_pdms_pitchX) $(20.0+v_loopVarIn*v_pdms_pitchY)
$(v_pdmsHeight+v_pdms_pitchZ) group pdms
read_data pdms.lmpdat add append offset 65 10 14 18 0 shift $(-
18.0+v_loopVarOut*v_pdms_pitchX) $(20.0-1*v_pdms_pitchY-
1*v_loopVarIn*v_pdms_pitchY) $(v_pdmsHeight+v_pdms_pitchZ) group pdms
next loopVarIn
jump SELF loop4
variable loopVarIn delete
next loopVarOut
jump SELF loop3

variable loopVarOut delete
################################
# SiO2 lower specimen structure
################################
# atom types: 69, 70
region lo-fixed block -20 370 -135 170 -37 -27 units box # define
region where to allocate glass atoms, lower sample
region hi-fixed block -20 370 -135 170 184 189 units box # define
region where to allocate glass atoms, upper sample
lattice custom 1.0 &
a1 2.45670000 -4.25512922 .00000000 &
a2 2.45670000 4.25512922 .00000000 &
a3 .00000000 .00000000 5.40520000 &
basis .46990000 0.00000000 .66666667 &
basis 0.00000000 .46990000 .33333333 &
basis .46990000 .46990000 .00000000 &
basis .41410000 .26810000 .78540000 &
basis .26810000 .14600000 .45206667 &
basis .14600000 .41410000 .11873333 &
basis .26810000 .41410000 .78540000 &
basis .41410000 .14600000 .11873333 &
basis .14600000 .26810000 .45206667
create_atoms 2 region lo-fixed &
basis 1 69 &
basis 2 69 &
basis 3 69 &
basis 4 70 &
basis 5 70 &
basis 6 70 &
basis 7 70 &
```

```
basis 8 70 &
basis 9 70
create_atoms 2 region hi-fixed &
basis 1 69 &
basis 2 69 &
basis 3 69 &
basis 4 70 &
basis 5 70 &
basis 6 70 &
basis 7 70 &
basis 8 70 &
basis 9 70
mass 69 28.0855 # mass of Si atoms
mass 70 16.00 # mass of O atoms

group lo-fixed region lo-fixed # create group of atoms from lower
glass specimen
group hi-fixed region hi-fixed # create group of atoms from upper
glass specimen
#########################
# Force field parameters
#########################
# TIP4P water model, long-range Coulombic solver (pair_style +
kspace_style)
# lj/cut/tip4p/long args = otype htype btype atype qdist cutoff
(cutoff2)
# otype,htype = atom types for TIP4P O and H
# btype,atype = bond and angle types for TIP4P waters
# qdist = distance from O atom to massless charge (distance units)
# cutoff = global cutoff for LJ (and Coulombic if only 1 arg)
(distance units)
# cutoff2 = global cutoff for Coulombic (optional) (distance units)
#
# lj/cut/coul/long -> C-C, H-H, Si-C, Si-H interactions in PDMS
# lj/class2/coul/long -> Si-Si interactions in PDMS
#
# <- FIND ADEQUATE TYPE OF INTERMOLECULAR INTERACTIONS FOR EACH
BIOMOLECULES!!!
# lj/long/coul/long -> Mucine 5b/Mucine 7
# lj/cut mixed interactions PDMS/water, biomolecules/water
interactions
#
pair_style hybrid lj/cut/tip4p/long 1 2 1 1 0.1546 13.0 8.5
lj/cut/coul/long 13.0 8.5 lj/class2/coul/long 13.0 8.5
lj/long/coul/long cut long 13.0 8.5 lj/cut 3.0
# modify pair style
# "mix" keyword: apply arithmetic mixing rule formula for LJ
parameTers in cases of different atom types, i != j
# epsilon_ij = sqrt(epsilon_i * epsilon_j)
# sigma_ij = (sigma_i + sigma_j) / 2
# "tail" keyword: add a long-range VanderWaals tail correction to
energy and pressure
pair_modify tail yes mix arithmetic
# use harmonic potential, E = K(r - r0)^2, for bond style
# K, r0 values defined bellow in bond_coeff
#bond_style harmonic
bond_style hybrid harmonic class2 # PDMS/Water
# use harmonic potential, E = K(theta - theta0)^2, for angle style

# K, theta0 values defined bellow in angle_coeff
#angle_style harmonic # water only
```

```
angle_style hybrid harmonic charmm # for H2O + biomolecules, Obs.:
needs adjusted coeffs. afterwards
#angle_style hybrid harmonic charmm class2 # for H2O + biomolecules +
PDMS, Obs.: needs adjusted coeffs. afterwards
#angle_style hybrid harmonic # for H2O/PDMS/Alginate
#kspace_style pppm/tip4p 1.0e-5 # arg: relative error in forces
kspace_style pppm/disp/tip4p 1.0e-5 # arg: relative error in forces
# TIP4P/2005 water model LJ coefficients (epsilon, sigma)
pair_coeff 1 1 lj/cut/tip4p/long 0.1852 3.1589 # O-O
pair_coeff 2 2 lj/cut/tip4p/long 0.0 0.0 # H-H
pair_coeff 1 2 lj/cut/tip4p/long 0.0 0.0 # O-H
# bond force field coefficients
# prefactor K, r0 -> equilibrium bond distance
#bond_coeff 1 0.0 0.9572 # H-O # bond
bond_coeff 1 harmonic 0.0 0.9572 # H-O # bond
# angle FF coefficients for water
# prefactor K, theta0 -> equilibrium angle
angle_coeff 1 harmonic 0.0 104.52 # H-O-H
# mixed interactions H2O/biomolecules <--- OPTIMIZE to adjuste
hydrophoic caracter of biomolecules !!!
#pair_coeff 1*2 3*65 lj/cut 1.0 2.0
pair_coeff 1*2 3*65 lj/cut 0.3 4.0
# parameters mixed interactions H2O/PDMS
pair_coeff 1*2 66 lj/cut 0.394360 4.39 # H2O-C interactions
pair_coeff 1*2 67 lj/cut 0.394360 4.39 # H2O-H
pair_coeff 1*2 68 lj/cut 0.323728 4.67 # H2O-Si
#pair_coeff 1*2 66*68 lj/cut 1.0 2.0 # generic values - Less
hydrophobe
# mixed interactions biomolecules/PDMS <--- OPTIMIZE!!!
#pair_coeff 3*65 66*68 lj/cut 1.0 2.0
#pair_coeff 3*65 66*68 lj/cut 0.3 3.5 # changed to decrease
interactions between biomolecules/PDMS
pair_coeff 3*65 66*68 lj/cut 0.3 4.5
# parameters for SiO2 glass
pair_coeff 69*70 69*70 lj/cut 1.0 2.0 # SiO2/SiO2
#pair_coeff 1*65 69*70 lj/cut 1.0 2.0 # SiO2/biomolecules and
SiO2/water
pair_coeff 1*65 69*70 lj/cut 0.3 3.5 # SiO2/biomolecules and
SiO2/water - More hydrophobe

#pair_coeff 66*68 69*70 lj/cut 1.0 2.0 # SiO2/glass
pair_coeff 66*68 69*70 lj/cut 4.0 0.5 # SiO2/glass
###################################
# Biomolecules and PDMS FF coeffs
###################################
# pair coeffs for biomolecules intramolecular interactions <---
OPTIMIZE!!!
pair_coeff 3*65 3*65 lj/long/coul/long 3.0 6.0
# pair coeffs for PDMS-PDMS interactions <--- OPTIMIZE!!!
pair_coeff 66*67 66*67 lj/cut/coul/long 0.1944 3.73 # C-C, H-H, C-H
interactions
pair_coeff 68 68 lj/class2/coul/long 0.1310 4.29 # Si-Si
pair_coeff 66*67 68 lj/cut/coul/long 0.1596 3.83 # Si-C, Si-H
# Set weighting coefficients for pairwise Energy/Force contributions
between pairs of atoms permanently bonded
# Non-bonded LJ or Coulombic interaction between pair of atoms should,
therefore, be excluded (or reduced by these weighting factor)
# set default weights of 0.0 0.0 0.0 for the 3 coeffs, which is normal
used in CHARMM force field
# Obs.: coeffs can be defined explicitly w/ other pair_styles and
pair-wise contributions calculated as part of CHARMM dihedral_style
```

```
special_bonds charmm
# Obs.: Dihedral coeffs ALL EQUAL <--- OPTIMIZE!!!
#dihedral_style hybrid harmonic
dihedral_style hybrid harmonic charmm class2 # include CLASS2 dihedral
style for PDMS. MUST CONFIRM !!!
#dihedral_coeff *18 charmm 0.2 1 180 0.5 # dihedral coeffs for BLG and
GG molecules <- GENERIC VALUES
dihedral_coeff *18 harmonic 8.0 1 2
# for PDMS, if using COMPASS class2 dihedral style. ADJUST GENERIC
COEFFS !!!
dihedral_coeff 19 class2 100 75 100 70 80 60
dihedral_coeff 19 class2 mbt 3.5945 0.1704 -0.5490 1.5228
dihedral_coeff 19 class2 ebt 0.3417 0.3264 -0.9036 0.1368 0.0 -0.8080
1.0119 1.1010
dihedral_coeff 19 class2 at 0.0 -0.1850 -0.7963 -2.0220 0.0 -0.3991
110.2453 105.1270
dihedral_coeff 19 class2 aat -13.5271 110.2453 105.1270
dihedral_coeff 19 class2 bb13 0.0 1.0119 1.1010

bond_coeff 2*10 harmonic 0.0 0.9572 # values for biomolecules
bond_coeff 11*12 class2 1.0 100.0 80.0 80.0 # values for PDMS
# <- GENERIC VALUES, SEARCH ADEQUATE VALUES AFTER for each molecule
type !!!
angle_coeff 2*17 harmonic 1.0 80.0 # angle coeffs for PDMS and
biomolecules
# for PDMS, if using COMPASS class2 angle style. ADJUST GENERIC COEFFS
!!!
#angle_coeff 15*17 75.0
#angle_coeff 15*17 bb 10.5872 1.0119 1.5228
#angle_coeff 15*17 ba 3.6551 24.895 1.0119 1.5228
# Adjust sizeshape of processor sub-domain within to correct
computational loads imbalance
# Needed to avoid that the simulation stalls due to interconnects
bottleneck!
# Perform static load balancing
balance 0.8 shift x 500 1.1 out balance_x.txt
balance 0.8 shift y 500 1.1 out balance_y.txt
balance 0.8 shift z 500 1.1 out balance_z.txt # obs: test if gives
better performance w/ just balance in Z
# Perform dynamic load balancing afterwards
fix loadbl all balance 2000 0.8 shift z 500 1.1
###################
# Groups / fixes
###################
group water type 1 2
# create groups of disctinct elements from upper glass specimen to
apply load
group Si_glass type 69 # C atoms in glass
group O_glass type 70 # O atoms in glass
group Si_hi intersect Si_glass hi-fixed
group O_hi intersect O_glass hi-fixed
# reset atom IDs for the system, including all the global IDs stored
for bond, angle, dihedral, improper topology data
# Useful if atoms are lost following delete_atoms
#reset_ids
#run 0 # temperature may not be T_depart. Insures all DOFs are
accounted properly before rescaling temps of rigid bodies
# Treat biomolecules as independent rigid bodies
# When using Langevin thermostat, Tdamp (damp factor - time of
teperature relaxation in dt units)
```

```
# is inversely proporcional to fluid viscosity
group rigidmol union muc5b muc7 blg gg
fix rgd rigidmol rigid/nve molecule langevin 300 300 ${Tdamp} 428984
#fix rgd rigidmol rigid/nve/small molecule langevin 300 300 ${Tdamp}
428984 # test which variant "fix rigid" or "fix rigid/small" is more
efficient for the simulation
fix 1a lo-fixed setforce 0.0 0.0 0.0 # reset forces in lower glass
fix 1b hi-fixed setforce 0.0 0.0 0.0 # reset forces in upper glass
###############
# Computes
###############
#velocity rigidmol create ${T_depart} 277387 loop local # set initial
temperature of all biomolecules w/ uniforme distribution
# compute temperatures of individual biomolecules
compute tpmuc5b muc5b temp
compute tpmuc7 muc7 temp
compute tpblg blg temp
compute tpgg gg temp
# thermostating of PDMS specimen
compute tempPDMS pdms temp/partial 0 1 1 # compute PDMS temperature,
excluding X-motion
# set velocity of atoms randomly from uniform distribution using
previous "temp/partial" compute
# loop = local, for each processor to loop over only its atoms to
produce velocities
# Random number seed is adjusted to give different sets of velocities
on each processor
velocity pdms create ${T_depart} 277387 temp tempPDMS loop local
# rescale temperature of PDMS for linear DOF only in YZ
fix ftempPDMS pdms temp/rescale 10 300 300 0.1 1
fix_modify ftempPDMS temp tempPDMS
# thermostating of upper glass specimen
compute tempHi hi-fixed temp/partial 0 1 1 # compute upper glass
temperature, excluding X-motion
velocity hi-fixed create ${T_depart} 277387 temp tempHi loop local
# correct temp for linear DOF only in YZ
fix ftempHi hi-fixed temp/rescale 10 300 300 0.1 1

fix_modify ftempHi temp tempHi
# thermostating of lower glass specimen
compute tempLo lo-fixed temp # compute lower glass temperature
velocity lo-fixed create ${T_depart} 277387 temp tempLo loop local
# readjuste temperature of lower glass to 300 K
fix ftempLo lo-fixed temp/rescale 10 300 300 0.1 1
fix_modify ftempLo temp tempLo
#neighbor 3.0 multi
neighbor 4.0 multi
#neighbor 3.0 bin
neigh_modify delay 0 every 1 check yes one 5000
neigh_modify exclude group lo-fixed lo-fixed check no # turn off
pairwise interactions in lower SiO2 atoms
compute tp water temp
variable T equal 300.0
variable P equal 1.0
variable ci equal 5 #correlation interval
variable si equal 2 #sample interval
variable ti equal ${ci}*${si} #total interval
variable th equal 100 #thermo interval
variable di equal 5000 #dump interval
#variable Pdamp equal ${dt}*1000
variable den equal density
```

```
timestep ${dt} # unit: femtosecond
thermo ${th}
thermo_style custom step temp c_tp c_tpmuc5b c_tpmuc7 c_tpblg c_tpgg
c_tempPDMS c_tempHi c_tempLo ke pe etotal vol press v_den
# freeze water molecules during minimization of biomolecules
# Obs: minimization results in biomolecules atoms overlap
fix 2 water setforce 0.0 0.0 0.0
fix 2a rigidmol setforce 0.0 0.0 0.0
min_style cg
minimize 1.0e-9 1.0e-10 200000 300000
min_modify line backtrack
unfix 2
unfix 2a
##############

# Dynamics
##############
fix pdmsnve pdms nve
# NVE dynamics with Langevin thermostat (Brownian Dynamics)
fix lgv water langevin ${T} ${T} ${Tdamp} 19930830
fix nv water nve
# hold bond lengths and angles fixed by SHAKE algorithm
# fix ID group-ID style tol iter N constraint values ... keyword value
...
# tol = accuracy tolerance of SHAKE solution
# iter = max # of iterations in each SHAKE solution
# N = print SHAKE statistics every this many timesteps (0 = never)
# one or more constraint/value pairs are appended
# constraint = b or a or t or m
fix shakeh2o water shake 0.0001 200 5000 b 1 a 1
#fix shakeh2o water shake 0.001 200 5000 b 1 a 1
thermo_modify lost warn flush yes # warn only if lost atoms
thermo_modify lost/bond warn flush yes
#thermo_modify lost ignore flush yes # ignore if lost atoms
#dump 1 all atom/gz 10 dump.debug.lammpstrj.gz # for debug purposes
run 1000 # simulation speed assessment
#undump 1
dump 2 all atom/gz ${di} dump.muc_blg_gg.lammpstrj.gz
# constrain water molecules to initial water box during thermostating
using fixed walls
# avoids crashing of simulation due to H2O molecules being outside of
walls when resizing water layer
fix wall_x water wall/lj126 xlo -12.0 0.5 3.0 2.5 xhi 362.0 0.5 3.0
2.5 pbc yes units box
fix wall_y water wall/lj126 ylo -131.0 0.5 3.0 2.5 yhi 168.0 0.5 3.0
2.5 pbc yes units box
fix wall_z water wall/lj126 zlo -28.0 0.5 3.0 2.5 zhi 49.0 0.5 3.0 2.5
pbc yes units box
run 20000 # initial thermostating of full simulation
restart 1000 muc_blg_gg.restart1 muc_blg_gg.restart2 # write cyclic
restart files
#########################################################################
##########################################

# readjust Langevin thermostat to Tdamp = 0.1 for faster adjustment to
300 K for both water and biomolecules
#########################################################################
##########################################
unfix lgv
#fix lgv water langevin ${T} ${T} 0.1 19930830
fix lgv water langevin ${T} ${T} 100 19930830
```

```
fix glassnve hi-fixed nve # NVE integration of upper glass atoms to
mix biomolecules in water
# approach rapidely upper sample to mix biomolecules into water
fix apprhispec hi-fixed move linear 0.0 0.0 -0.5 units box
fix apprpdms pdms move linear 0.0 0.0 -0.5 units box
fix apprblg blg move linear 0.0 0.0 -0.5 units box
fix apprmuc5b muc5b move linear 0.0 0.0 -0.5 units box
fix apprmuc7 muc7 move linear 0.0 0.0 -0.5 units box
fix apprgg gg move linear 0.0 0.0 -0.5 units box
run 145000
unfix apprblg
run 70000
unfix apprmuc5b
unfix apprmuc7
run 40000
# remove approach velocities to avoid biased dynamics
unfix apprhispec
unfix apprpdms
unfix apprgg
write_restart biomol_water_mixed.restart # write restart file for
stage after biomolecules have been mixed with water
# Apply normal force on upper glass specimen
fix load1 Si_hi addforce 0.0 0.0 $(v_load) # apply external force to
fixed Si atoms
fix load2 O_hi addforce 0.0 0.0 $(v_load*16.00/28.0855) # apply
external force to fixed Oxyg atoms
# save temperatures of various molecules to data files
fix f_h2o_av_time water ave/time 10 10 100 c_tp file
temp_h2o_av.W${load}.txt
fix f_muc5b_av_time muc5b ave/time 10 10 100 c_tpmuc5b file
temp_muc5b_av.W${load}.txt
fix f_muc7_av_time muc7 ave/time 10 10 100 c_tpmuc7 file
temp_muc7_av.W${load}.txt

fix f_blg_av_time blg ave/time 10 10 100 c_tpblg file
temp_blg_av.W${load}.txt
fix f_gg_av_time gg ave/time 10 10 100 c_tpgg file
temp_gg_av.W${load}.txt
fix f_pdms_av_time pdms ave/time 10 10 100 c_tempPDMS file
temp_PDMS_av.W${load}.txt
# time averages of total forces on upper glass specimen, over longer
time steps
fix f_av_time_lo lo-fixed ave/time 10 10 100 f_1a[*] file f_glass-
lo.W${load}.txt
fix f_av_time_hi hi-fixed ave/time 10 10 100 f_1b[*] file f_glass-
hi.W${load}.txt
unfix glassnve # remove NVE integration of upper glass atoms to avoid
double integration w/ "fix move"
# move upper specimen w/ constant speed
fix 4 hi-fixed move linear 1E-1 NULL NULL units box
# apply gradual ramping of velocity, v = tanh(t/A), to upper asperity
to reduce oscilations
# increase gradually the velocity to 1 A/ps = 100 m/s
#variable VX equal (exp(step/45000)-exp(-
step/45000))/(exp(step/45000)+exp(-step/45000)) # Smaller size
structures
#variable VX equal (exp(step/30000)-exp(-
step/30000))/(exp(step/30000)+exp(-step/30000)) # Bigger size
structures
#fix 4 hi-fixed move variable NULL NULL NULL v_VX NULL NULL
# save to file velocity of upper glass sample
```

```
dump vel hi-fixed custom/gz 10000 v_glass.txt.gz vx vy vz
run 400000
write_restart muc_blg_gg_dynamics.restart
undump 2
undump vel
```